MATHEMATICAL MODELS BASED ON SPLINE FUNCTIONS

FOR

INDUSTRIAL APPLICATIONS

by

Eduardo Horacio Enrique

A thesis

presented to the University of Waterloo

in fulfilment of the

thesis requirement for the degree of

Doctor of Philosophy

in

Electrical and Computer Engineering

Waterloo, Ontario, Canada, 2000

The University of Waterloo requires the signatures of all persons using or photocopying this thesis. Please sign below, and give address and date.

ABSTRACT

There are several instances where samples of the controlled variable are the only data available to describe a process. In order to determine the performance of a plant, digital techniques are used to analyze the data. Then, the set of samples conforms the plant model. The main disadvantage of this approach is the poor predictive properties that the model has when changes in the process occur.

Spline functions are the tool of choice for the analytical representation of a plant based on the sampled data from a process. Once a plant model is described in spline form, the spline coefficients become the model parameters. These parameters are used for the adaptation of sample-based models.

Two practical applications are considered in this study: non-parametric plant models and systems excited with non-sinusoidal waveforms. Classical adaptive control techniques, such as projection algorithm and least square, can be used when non-parametric plant models are approximated by spline functions. Additionally, the spline approximation techniques extend the applicability of the non-parametric models to the area of multirate sampling control. The spline approximation of voltage and current signals is used in this work to predict the behavior of a nonlinear circuit at a different operating point. Instantaneous phasors are used in combination with spline functions to create a hybrid technique that takes advantage of both classical methods and spline models. Sampled data from electric arc furnaces are used to test the spline-base signal approximation techniques.

ACKNOWLEDGMENTS

I would like to thank my supervisor and mentor, Professor H. Quintana for his guidance and encouragement throughout the research and development of this thesis.

I gratefully acknowledge the contribution of Les Toth from the Electrical Department at Slater Steel in Hamilton, Ontario, Canada, for the provision of the electric arc furnace test unit and the on-site support.

I also acknowledge the contribution of James Wikston from the Corporate Operations - Electrical Department at Hatch Associates Ltd. in Mississauga, Ontario, Canada, for the provision of field data.

DEDICATION

To Pablo, Patricia and the memory of María Nicole.

TABLE OF CONTENTS

LIST OF ILLUSTRATIONS

Chapter 1

1. INTRODUCTION

1.1 Motivation and the main concepts

The problem of optimal recovery is that of approximating as effectively as possible a given map of any function known to belong to certain class from limited, and possible error-contaminated, information about it (Micchelli and Rivlin, 1976). In the process industry, it is common to find information about the plant to be controlled in the form of sampled data. These sampled data are, in most cases, the best description of the process that we can expect. The construction of models based on sampled data is the main object of study of this work. A new technique is developed to obtain plant models with a broader applicability in industrial processes. The characteristics of these models are described and their performance are compared to those models based on more traditional techniques like non-parametric models (NPMs).

In this work, spline and b-spline functions are the tools of choice for the interpolation of the sampled data. In recent years, some researchers have introduced splines and b-splines for the approximation of convolution systems (Rohal - Ilkiv, 1998; Guy and Karny, 2000). In their work, splines are used as a framework for the analysis of control systems; therefore, the control action is synthesized in the form of a spline polynomial. Although their approach is rigorous from the mathematical viewpoint, the applicability of their findings requires the use of a special type of controller with high sampling rate. Contrary to the line of research initiated by Rohal - Ilkiv and Guy and Karny, in this work the application of splines and b-splines addresses the solution of process control problems

in the time domain using traditional well-proven techniques currently used in industry. Therefore, this thesis is focused mainly on the enhancement of existing methods used in process control.

In this thesis, we focus on models for deterministic dynamical systems. By deterministic in this context, we refer to models that provide a complete description of the system response. This approach contrasts with stochastic models, where the response of the system contains a random component defined on some probability space.

In the present dissertation, the benefits of using the theory of spline functions are shown in two areas: process control and power system analysis. In the area of process control, more specifically chemical process control, a non-parametric convolution model is approximated by interpolating splines. The result is a model of lower dimension that is simple to use in systems that require model identification and adaptive control. For power systems analysis, the theory of splines is used for the approximation of voltage and current waveforms with pronounced distortion. The analytical expressions of these signals are used to optimize the power delivered to a nonlinear load.

1.2 The need for an adaptive non-parametric model

Model predictive control (MPC) is currently one of the most successful strategies for industrial process control. Qin and Badgwell (1997) reported over 2200 applications on a survey of MPC applications, the majority of them in the area of refining. It is traditionally developed for linear non-parametric process models, such as finite impulse response (FIR) or finite step response (FSR) models.

Model predictive control emerged into process industries during the late 1970s, and is commonplace in today's computer aided process control technologies. It has found

numerous applications in the chemical and petrochemical industries, the pulp and paper industries and the food industry (Prett and Garcia, 1988). It is the only methodology that can handle constraints in a systematic way during the design and implementation of the controller. Process input and output constraints are included directly in the problem formulation so that future constraint violations are anticipated and prevented (Qin and Badgwell, 1997).

Of the numerous variations of the MPC algorithms, Dynamic Matrix Control (DMC), described by Cutler and Ramaker (1979), and Model Algorithmic Control (MAC), described by Rouhani and Mehra (1982), are the most widely used in the process industry. A survey of the most representatives companies that control the global market in the current state of the art MPC technology, shows that 26 % of the applications use DMC techniques (Camacho and Bordons, 1999).

In the DMC and MAC frame work, model uncertainties and process disturbances are computed as the difference between the process measurement and the model prediction at the current time step. This difference is added to the model prediction for the next step. For sequential predictions, all future disturbances are considered equal to the current disturbance. Although the DMC and MAC formulations are simple, their models lack the flexibility that frequency domain models have when it comes to model identification. Changes in the dynamic of a process may be caused by the time varying nature of the process as well as by the process nonlinearities. These changes affect the prediction performance of the DMC and MAC methods.

One solution to the practical difficulty mentioned above is the use of Volterra series models in their discrete form (Isermann et al., 1992). To compensate for the large number of coefficients that the solution of the discrete Volterra kernel requires, several approaches

have been proposed. Nikolaou and Vulhandam (1998) demonstrated that parsimonious re-parametrization can be obtained by compressing the underlying FIR kernel using wavelets. This approach has been extended to the case of second-order discrete-time Volterra models (Mantha, 1998).

Although the current research trend in the development of more precise models is very promising, the proposed techniques lack the simplicity and proven reliability of more traditional algorithms like DMC and MAC.

1.3 Spline and b-spline models

The central idea of this work is the approximation of FIR by a set of interpolating splines. Due to the fact that only a limited number of sampled data is required for the construction of the interpolating splines, the resulting model has less parameters. At the same time, the reduction of the number of parameters allows the application of classical adaptive techniques for process identification. The result is a method that preserves the simplicity of a traditional MPC and expands its application to a larger class of processes.

In addition to the added adaptation properties, the models based on spline polynomials can be used in processes with multirate sampling. Several researchers have addressed the analysis of asynchronous and multirate sampling. These studies have shown that the sampling rate can be modified to improve system performance (Owens, 1986, 1996; Owens and Hong, 1986; Owens and Wang, 1987; Schumann *et al.*, 1981; Voulgaris, 1994; among others). In addition to variations on the sampling rate to improve performance, some researchers have studied the problem of asynchronous sampling due to system constraints (Issakson and Kaul, 1996; Sheen and Tsai, 1998). The spline model developed in this thesis deals with multirate sampling systems in a systematic way.

An alternative approach for the approximation of a NPM is the use of b-spline functions. Compared to the spline polynomials, the b-spline approximation of a NPM has a simpler formulation particularly for models with adaptive dead time. This feature is important due to the fact that in most industrial processes it is possible to find a dead time in the control loop. An overview of the contributions of this thesis in the area of process control is shown in Figure 1.1.

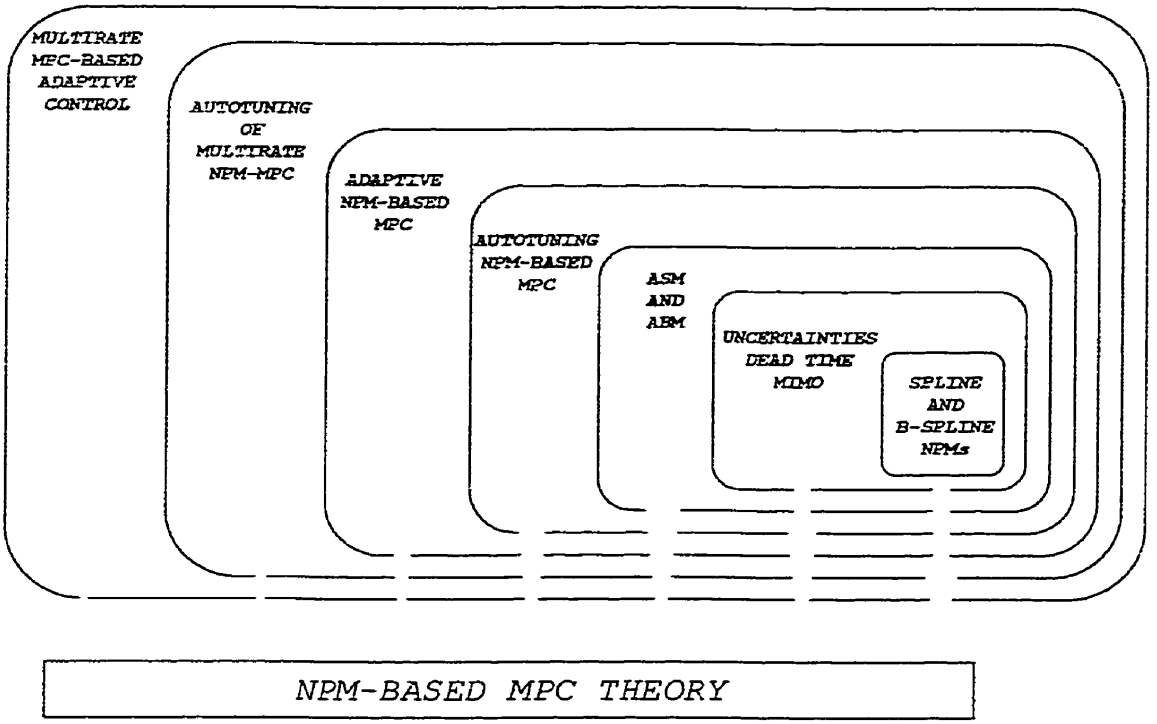

Figure 1.1: Contributions to the theory of MPCs based on NPMs.

1.3.1 Highlights of the benefits of using spline and b-spline techniques

One of the main advantages of the spline and b-spline techniques proposed in this work over the traditional techniques is the reduction of the model dimension. This reduction of

the model dimension is the starting point in the chain of contributions shown in Figure 1.1. The other important property unique to this techniques is the flexibility of the model-control system to adapt to a variable sampling environment.

As depicted in Figure 1.1, the development process can be interrupted at any point and still, a contribution to the theory of nonparametric models is made. This is an advantage of the proposed method compared to the traditional ones because it allows the integration of the partial contributions to controllers based on classical techniques.

As shown later in this thesis, the spline and b-spline techniques proposed in this work allows the development of simplified techniques for controller tuning. This a very important contribution when considering the practical connotation of the present dissertation.

1.4 Spline functions for power systems analysis

Traditionally, the analysis of circuits in the presence of harmonics is carried out in the frequency domain. Fourier techniques are used when voltage and current signals present distortions. The harmonic components of the signals are taken into account to estimate the active power at a load. The problem found with the use of Fourier techniques is that the analysis of the circuit is only valid for a given operating condition.

In this dissertation, the approximation of the signals by means of spline polynomials is used for the analysis of circuits in time domain. These spline polynomials are used to compute the average power and optimal operation conditions of an electric arc furnace (EAF). The application of this innovative approach to sampled data from a simulator and an EAF shows that the proposed method is an attractive alternative to the traditional

Fourier techniques. An overview of the contributions of this thesis in the area of power systems is shown in Figure 1.2.

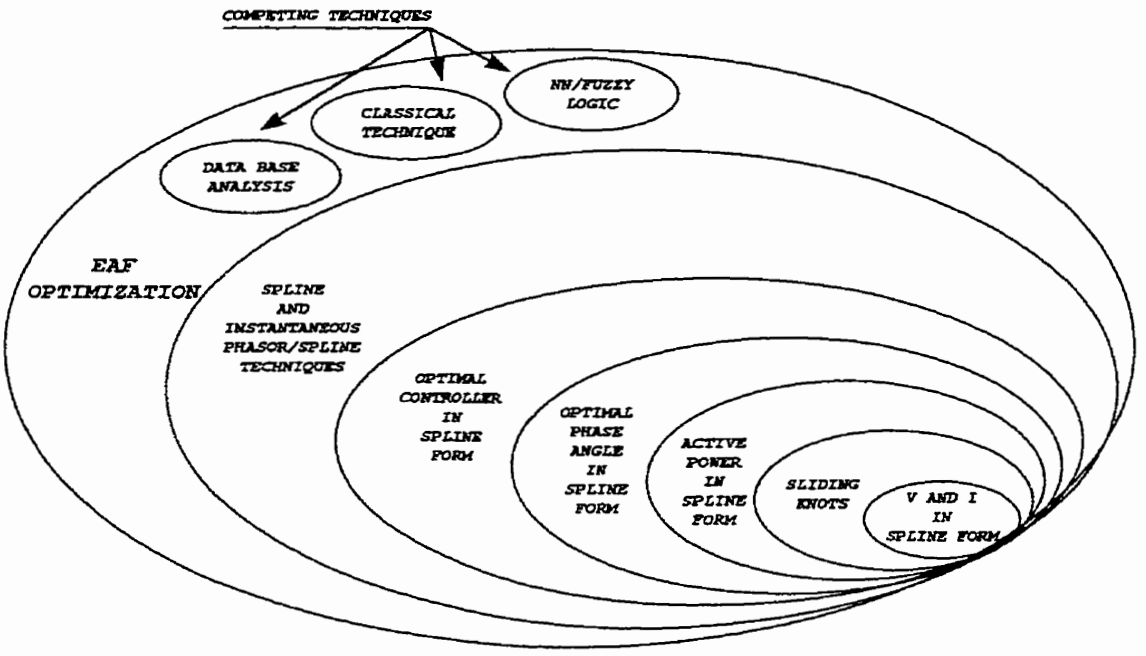

Figure 1.2: Contributions to the optimization of EAFs.

1.4.1 Highlights of the benefits of using spline functions techniques

The spline-based techniques developed for the optimization of the EAFs are immune to changes of the parameters of the network. Therefore, the optimization of a particular furnace depends only on the characteristics of the step-down transformer and furnace circuit. These circuit elements do not change during the course of a production batch. This is the main advantage that the spline function technique have compared to the competing techniques shown in Figure 1.2.

1.5 Thesis overview

Chapter 2 contains a review of the theory of spline and b-spline functions, together with the algorithms to compute the spline coefficients. In Chapter 3, some extensions to the theory of spline functions are presented. There is a brief discussion on the concept of relative versus absolute referencing for the expression of spline polynomials. The concept of sliding knots, proposed for the first time in this work, is introduced in this chapter. With the use of the sliding knots, the spline polynomials are extended outside their range of definition, allowing the application of splines in optimization methods. The analysis of the error introduced by sliding knots is presented in the form of a theorem at the end of this chapter.

In the first part of Chapter 4, there is a brief review of the DMC method. Following this, the topic of splines for the approximation of NPMs is presented. The concepts of pseudo inputs and pseudo parameters are described. The formulation of the projection algorithm (PA) for spline models follows right after. The analysis of model uncertainties and variable sampling time close this chapter.

The concept of b-spline models is introduced in Chapter 5. Similarly to the spline methods described in the previous chapter, b-splines are used to approximate NPMs. The advantages of the b-spline models compared to their spline counterparts are explained. The adaptive tuning of an MPC based on a b-spline model is presented in this chapter. A generalized version of adaptive tuning is derived for an MPC based on a standard NPM. The case of adaptive tuning of an MPC in a multirate sampling environment is analyzed in this chapter. At the end of Chapter 5, the identification of processes with dead time and the description of MIMO systems are explained. In Chapter 6, a series of examples

simulating a continuously stirred tank reactor (CSTR) are used to test the spline and b-spline techniques.

The approximation by spline functions of signals in power systems is developed in Chapter 7. Two techniques are described in this chapter: the first one is based on the total reconstruction of the voltage and current waveforms and the second one is based on the concept of instantaneous phasors. The proposed theories described in Chapter 7 are tested in Chapter 8. Data samples from simulators and an electrical arc furnace in operation are used to test the performance of the proposed techniques. The results are compared to a simplified electrical model of the furnace. A summary of the conclusions and suggestions for future research are presented in Chapter 9.

Chapter 2

2. THE THEORY OF SPLINE AND B-SPLINE FUNCTIONS

In this chapter, the fundamental concepts describing the spline and b-spline functions are provided. These techniques are used for the approximation of non-parametric models in Chapters 4 and 5 and the mathematical representation of signals in Chapter 7.

The developments and nomenclature of this chapter entirely follow the work of Cheney and Kincaid (1994).

2.1 Approximation by spline functions

2.1.1 First-degree spline

A spline function is a function consisting of polynomial pieces joined together with certain smoothness conditions explained later in this chapter. A simple example is the polygonal function (or spline of degree 1), whose pieces are linear polynomials joined together to achieve continuity, as in Figure 2.1.

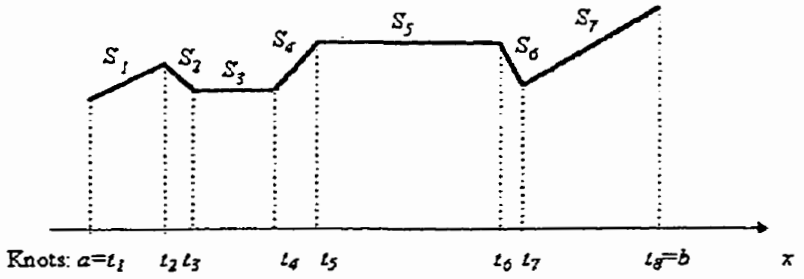

Figure 2.1: Interpolation with spline function of degree 1.

The points $t_1, t_2, \ldots, t_n$ at which the function changes its character are termed knots in the theory of splines. Thus the spline function shown in Figure 2.1 has eight knots. Such a function is somewhat complicated to define in explicit terms. We can mathematically define a spline as

$$S(x) = \begin{cases} S_1(x) & x \in [t_1, t_2] \\ S_2(x) & x \in [t_2, t_3] \\ \vdots & \\ S_{n-1}(x) & x \in [t_{n-1}, t_n] \end{cases} \qquad (2.1)$$

where

$$S_i(x) = c_i x + d_i \qquad (2.2)$$

Each piece of $S(x)$ is a linear polynomial. The function $S(x)$ is piece-wise linear. If the knots $t_1, t_2, \ldots, t_n$ were given and if the coefficients $c_1, d_1, c_2, d_2, \ldots, c_{n-1}, d_{n-1}$ were all known, the evaluation of $S(x)$ at a specific x would proceed by first determining the interval containing x and then using the appropriate linear function for that interval.

If the function S defined by Equation (2.1) is piece-wise continuous, we call it a spline of degree 1. It is characterized by the following three properties:

1. The domain of S is an interval $[a, b]$.
2. S is continuous on $[a, b]$.
3. There is a partitioning of the interval

$$a = t_1 < t_2 < \cdots < t_n = b \qquad (2.3)$$

such that S is a linear polynomial on each subinterval $[t_i, t_{i+1}]$.

Outside the interval $[a, b]$, $S(x)$ is usually defined to be the same function on the left of a as it is on the leftmost subinterval $[t_1, t_2]$ and the same on the right of b as it is on the rightmost subinterval $[t_{n-1}, t_n]$; namely, $S(x) = S_1(x)$ when $x < a$ and $S(x) = S_{n-1}(x)$ when $x > b$.

2.1.2 Second-degree splines

Interpolating splines of degree higher than 1 are more complex. We take up now the quadratic splines and show how to determine one that interpolates the samples in Table 2.1.

Table 2.1: Samples at the knots of a generic curve.

x	t_1	t_2	t_3	...	t_n
y	y_1	y_2	y_3	...	y_n

We shall assume that the points $t_1, t_2, \ldots, t_n$ serve also as the knots for our spline functions. Quadratic splines are not used in applications as often as natural cubic splines, which are developed in the next section. However, the derivations of quadratic and cubic splines are similar enough that an understanding of the simpler second-degree spline theory allows one to grasp easily the more complicated third-degree spline theory.

A function $S(x)$ is a spline of degree 2 if S is a piece-wise quadratic polynomial such that S and S' are continuous. A simple counting process shows us the number of conditions involved in defining such a quadratic spline. If there are n knots, then there are n -1 subintervals and n - 2 interior points. Since the spline $S(x)$ consists of quadratic polynomials of the form $c_i x^2 + d_i x + e_i$ over each subinterval $[t_i, t_{i+1}]$, there are 3 $(n - 1)$

coefficients. We then expect that 3 (n - 1) conditions fully define a quadratic spline function with n knots.

On each end of the subinterval $[t_i, t_{i-1}]$, the quadric spline function must satisfy the interpolation condition $S_i(t_i) = y_i$ and $S_i(t_{i+1}) = y_{i-1}$. Since there are n - 1 such subintervals, this imposes 2 (n - 1) conditions. The continuity of S does not add any additional conditions. However, the continuity of S ' at each of the interior knots gives n - 2 more conditions. Thus, we have 2 (n - 1) + n - 2 = 3 n - 4 conditions, or one condition short of the 3 n - 3 conditions required. There is a variety of ways to impose an additional condition.

2.1.3 Quadratic spline Q(x)

We now derive the equations for the interpolating quadratic spline, $Q(x)$. The value of $Q'(t_1)$ is prescribed as the additional condition. We seek a piece-wise quadratic function

$$Q(x) = \begin{cases} Q_1(x) & t_1 \le x \le t_2 \\ Q_2(x) & t_2 \le x \le t_3 \\ \vdots & \vdots \\ Q_{n-1}(x) & t_{n-1} \le x \le t_n \end{cases} \qquad (2.4)$$

which is continuously differentiable on the entire interval $[t_1, t_n]$ and which interpolates the data table; that is, $Q(t_i) = y_i$ for $1 \le i \le n$.

Since Q' is continuous, we can put $z_i \equiv Q'(t_i)$. At present, we do not know the correct values of z_i, but nevertheless the following must be the formula for Q_i:

$$Q_i(x) = \frac{z_{i+1} - z_i}{2(t_{i+1} - t_i)}(x - t_i)^2 + z_i(x - t_i) + y_i \qquad (2.5)$$

In order to see that this is correct, just verify that $Q_i(t_i) = y_i$, $Q_i'(t_i) = z_i$, and $Q_i'(t_{i+1}) = z_{i+1}$. These three conditions define the function Q_i uniquely on $[t_i, t_{i+1}]$ as given in Equation (2.5).

Now, in order for the quadratic spline function Q to be continuous and to interpolate the table of data, it is necessary and sufficient that $Q_i(t_{i+1}) = y_{i+1}$ for $i = 1, 2, \ldots, n\text{-}1$ in Equation (2.5) with z_1 arbitrary. When this equation is written out in detail and simplified, the result is:

$$z_{i+1} = -z_i + 2\left(\frac{y_{i+1} - y_i}{t_{i+1} - t_i}\right) \qquad 1 \le i \le n-1 \qquad (2.6)$$

This equation can be used to obtain the vector $[z_1, z_2, \ldots, z_n]^T$, starting with an arbitrary value for z_1.

2.1.3.1 Subbotin quadratic spline

A useful approximation process, first proposed by Subbotin (1967), consists of interpolation with quadratic splines, where the nodes for interpolation are chosen to be the first and last knot and the midpoints between knots. Remember that knots are defined as the points where the spline function is permitted to change in form from one polynomial to another. The nodes are the points where values of the spline are specified. In the Subbotin quadratic spline function, there are $n + 1$ interpolation conditions and 2 $(n - 2)$ conditions from the continuity of S and S'. Hence, we have the exact number of conditions needed, 3 n - 3, in order to define the quadratic spline function completely.

Suppose that knots $a = t_1 < t_2 < \ldots < t_n = b$ have been specified; let the nodes be the points

$$\begin{cases} \tau_o = t_1, \ \tau_n = t_n \\ \tau_i = \dfrac{1}{2}(t_i + t_{i+1}) \qquad 1 \le i \le n-1 \end{cases} \tag{2.7}$$

We seek a quadratic spline function S having the given knots and taking prescribed values at nodes:

$$S(\tau_i) = y_i \qquad 0 \le i \le n, \tag{2.8}$$

as shown in Figure 2.2.

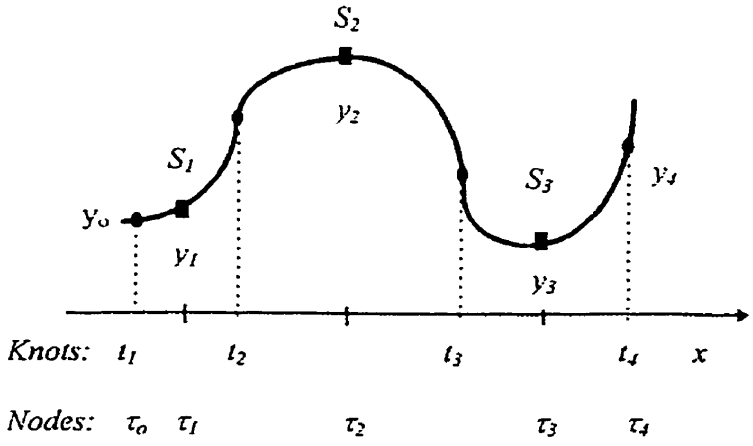

Figure 2.2: Second degree spline interpolation.

The knots create n - 1 subintervals, and in each of them S can be a different quadratic polynomial. Let us say that on $[t_i, t_{i-1}]$, S is equal to the quadratic polynomial S_i. Since S is a quadratic spline, it and its first derivative should be continuous. Thus $z_i \equiv S'(t_i)$ is well defined, although as yet we do not know its value. It is easy to see that on $[t_i, t_{i+1}]$, our quadratic polynomial can be represented in the form

$$S_i = y_i + \frac{1}{2}(z_i + 1 + z_i)(x - \tau_i) + \frac{1}{2h_i}(z_i + 1 - z_i)(x - \tau_i)^2 \qquad (2.9)$$

in which $h_i = t_{i+1} - t_i$. When the polynomial pieces $S_1, S_2, \ldots, S_{n-1}$ are joined together to form S, the result may be discontinuous. Hence, we impose continuity conditions at the interior knots

$$\lim_{x \to t_i^-} S_{i-1}(x) = \lim_{x \to t_i^-} S_i(x) \qquad 2 \le i \le n-1 \qquad (2.10)$$

Then, we obtain

$$h_{i-1}z_{i-1} + 3(h_{i-1} + h_i)z_i + h_i z_{i+1} = 8(y_i - y_{i-1}) \qquad 2 \le i \le n-1 \qquad (2.11)$$

The first and last interpolation conditions must also be imposed:

$$S(\tau_o) = y_o, \qquad S(\tau_n) = y_n \qquad (2.12)$$

These two equations lead to

$$\begin{aligned} 3h_1 z_1 + h_1 z_2 &= 8(y_1 - y_o) \\ 3h_{n-1}z_n + h_{n-1}z_{n-1} &= 8(y_n - y_{n-1}) \end{aligned} \qquad (2.13)$$

The system of equations governing the vector $z = [z_1, z_2, \ldots, z_n]^T$ then can be written in matrix form

$$\begin{bmatrix} 3h_1 & h_1 & & & & \\ h_1 & 3(h_1+h_2) & h_2 & & \mathrm{O} & \\ & h_2 & 3(h_2+h_3) & h_3 & & \\ & & \ddots & \ddots & \ddots & \\ & \mathrm{O} & & & 3(h_{n-2}+h_{n-1}) & h_{n-1} \\ & & & & h_{n-1} & 3h_{n-1} \end{bmatrix} \times \begin{bmatrix} z_1 \\ z_2 \\ z_3 \\ \vdots \\ z_{n-1} \\ z_n \end{bmatrix} = 8 \begin{bmatrix} y_1 - y_0 \\ y_2 - y_1 \\ y_3 - y_2 \\ \vdots \\ y_{n-1} - y_{n-2} \\ y_n - y_{n-1} \end{bmatrix} \quad (2.14)$$

After the z vector has been obtained, values of $S(x)$ can be computed from Equation (2.9).

2.1.4 Natural cubic splines

2.1.4.1 Introduction

The first- and second-degree splines discussed in the preceding section, although useful in certain applications, suffer an obvious imperfection: Their low-order derivatives are discontinuous. In the case of the first-degree spline (or polygonal line), this lack of smoothness is immediately evident, for the slope of the spline changes abruptly from one value to another at each knot. For the quadratic spline, the discontinuity is in the second derivative and it is, therefore, not so evident. But the curvature of the quadratic spline changes abruptly at each knot, and the curve is not pleasing to the eye.

A function S is called spline of degree k if

1. The domain of S is an interval $[a, b]$.
2. $S, S', S'', \ldots, S^{(k-1)}$ are all continuous functions on $[a, b]$.
3. There are points t_i (the knots of S) such that $a = t_1 < t_2 < \ldots < t_n = b$ and such that S is a polynomial of degree $\leq k$ on each subinterval $[t_i, t_{i-1}]$.

Higher-degree splines are used whenever more smoothness is needed in the approximating function. From the definition of a spline function of degree k, we see that such a function is continuous and have continuous derivatives S', S'', . . . , $S^{(k-1)}$ too. If we want the approximating spline to have a continuous m^{th} derivative, a spline of at least m + 1 is selected.

The choice of degree most frequently made for a spline function is 3. The resulting splines are, of course, termed cubic splines. In this case, we join cubic polynomials together in such a way that the resulting spline function has two continuous derivatives everywhere. At each knot three continuity conditions are imposed. Since S, S', and S'' are continuous, the graph of the function appears smooth to the eye. Discontinuities, of course, occur in the third derivative but cannot be detected visually, which is one reason for choosing degree 3. Experience has shown, moreover, that using splines of degree greater than 3 seldom yields any advantage. For technical reasons, odd-degree splines behave better than even-degree splines (when interpolating at the knots). Thus our emphasis upon the cubic splines is well justified.

2.1.4.2 Natural cubic spline

We turn next to interpolating a given table of function values by a cubic spline whose knots coincide with the values of the independent variable in the table. As was done earlier, we start with the data samples given in Table 2.2.

Table 2.2: Samples at the knots of a generic curve.

x	t_1	t_2	t_3	...	t_n
y	y_1	y_2	y_3	...	y_n

The t_i's are the knots and are assumed to be arranged in ascending order.

The function S that we wish to construct consists of n-1 cubic polynomial pieces,

$$\begin{cases} S_1(x) & t_1 \le x \le t_2 \\ S_2(x) & t_2 \le x \le t_3 \\ \vdots & \vdots \\ S_{n-1}(x) & t_{n-1} \le x \le t_n \end{cases} \qquad (2.15)$$

In this formula, S_i denotes the cubic polynomial that is used on the subinterval $[t_i, t_{i-1}]$. The interpolation conditions are

$$S(t_i) = y_i \qquad 1 \le i \le n \qquad (2.16)$$

The continuity conditions are imposed only at the *interior* knots $t_2, t_3, \ldots, t_{n-1}$. These conditions are written as

$$\lim_{x \to t_i^-} S^{(k)}(t_i) = \lim_{x \to t_i^+} S^{(k)}(t_i) \qquad k = 0,1,2 \qquad (2.17)$$

It turns out that two further conditions must be imposed in order to use all the available degrees of freedom. The choice that we make for these two extra conditions is

$$S''(t_1) = S''(t_n) = 0 \qquad (2.18)$$

The resulting spline function is then termed a natural cubic spline.

We now verify that the number of conditions imposed equals the number of coefficients needed. There are n knots and hence n - 1 subintervals. On each of these subintervals, we shall have a different cubic polynomial. Since a cubic polynomial has four coefficients, a total of 4 (n - 1) coefficients are available. As for conditions imposed, we have specified that within each interval the interpolating polynomial must go through two points, which gives 2 (n - 2) conditions. The continuity adds no additional conditions. The first and second derivatives must be continuous at the n - 2 interior points, for 2 (n - 2) more conditions. The second derivatives must vanish at the two endpoints for a total of 2 (n - 1) + 2 (n - 2) + 2 = 4 (n - 1) conditions.

2.1.4.3 Algorithm for natural cubic splines

We can develop a systematic procedure for determining the formula for a natural cubic spline, given a table of interpolating values.

Since S'' is continuous, the numbers

$$z_i \equiv S''(t_i) \qquad 1 \le i \le n \qquad (2.19)$$

are unambiguously defined. We do not yet know the values $z_2, z_3, \ldots, z_{n-1}$, but, of course, $z_1 = z_n = 0$ by Equation (2.18).

If the z_i's were known, we could construct S as described now. On the interval $[t_i, t_{i-1}]$, S'' is a linear polynomial taking the values z_i and z_{i+1} at the endpoints. Thus

$$S_i''(x) = \frac{z_{i+1}}{h_i}(x - t_i) + \frac{z_i}{h_i}(t_{i+1} - x) \qquad (2.20)$$

with $h_i = t_{i-1} - t_i$. Clearly, $S_i''(t_i) = z_i$, $S_i''(t_{i-1}) = z_{i-1}$, and S_i'' is linear in x. If this is integrated twice, we obtain S_i itself:

$$S_i(x) = \frac{z_{i+1}}{6h_i}(x - t_i)^3 + \frac{z_i}{6h_i}(t_i - x)^3 + cx + d \qquad (2.21)$$

where c and d are constants of integration. By adjusting the integration constants, we obtain a form for S_i that is easier to work with, namely,

$$S_i(x) = \frac{z_{i+1}}{6h_i}(x - t_i)^3 + \frac{z_i}{6h_i}(t_i - x)^3 + C(x - t_i) + D(t_{i+1} - x) \qquad (2.22)$$

where C and D are constants. If we differentiate Equation (2.22) twice, we obtain Equation (2.20).

The interpolation conditions $S_i(t_i) = y_i$ and $S_i(t_{i+1}) = y_{i+1}$ can be imposed now to determine the appropriate values of C and D, giving

$$S_i(x) = \frac{z_{i+1}}{6h_i}(x-t_i)^3 + \frac{z_i}{6h_i}(t_{i+1}-x)^3 + \left(\frac{y_{i+1}}{h_i} - \frac{h_i}{6}z_{i+1}\right)(x-t_i) + \left(\frac{y_i}{h_i} - \frac{h_i}{6}z_i\right)(t_{i+1}-x) \qquad (2.23)$$

When the values $z_1, z_2, \ldots, z_n$ have been determined, the spline function $S(x)$ is obtained from an equation of this form for $S_1(x), S_2(x), \ldots, S_{n-1}(x)$.

We now show how to determine the z_i's. One condition remains to be imposed, namely, the continuity of S'. At the interior knots t_i ($2 \le i \le n$ - 1), we must have $S'_{i-1}(t_i) = S_i'(t_i)$, as can be seen from Figure 2.3.

We have from Equation (2.23)

$$S_i' = \frac{z_{i+1}}{2h_i}(x-t_i)^2 - \frac{z_i}{2h_i}(t_{i+1}-x)^2 + \frac{y_{i+1}}{h_i} - \frac{h_i}{6}z_{i+1} - \frac{y_i}{h_i} + \frac{h_i}{6}z_i \qquad (2.24)$$

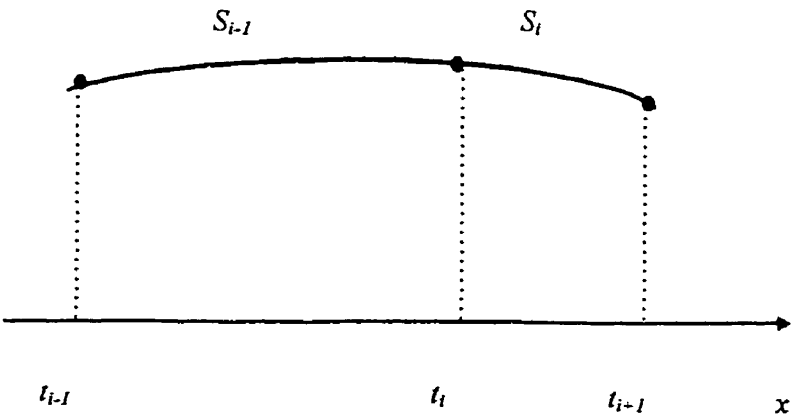

Figure 2.3: Natural cubic spline interpolation.

This gives

$$S_i'(t_i) = -\frac{h_i}{6} z_{i+1} - \frac{h_i}{3} z_i + b_i \qquad (2.25)$$

where

$$b_i = \frac{1}{h_i}(y_{i+1} - y_i) \qquad (2.26)$$

Analogously, we have

$$S'_{i-1}(t_i) = \frac{h_{i-1}}{6} z_{i-1} + \frac{h_{i-1}}{3} z_i + b_{i-1} \qquad (2.27)$$

When these are set equal to each other, the resulting equation can be arranged as

$$h_{i-1} z_{i-1} + 2(h_{i-1} + h_i) z_i + h_i z_{i+1} = 6(b_i - b_{i-1}) \qquad for \;\; 2 \le i \le n-1 \qquad (2.28)$$

By letting

$$u_i = 2(h_{i-1} + h_i) \qquad and \qquad v_i = 6(b_i - b_{i-1}), \qquad (2.29)$$

we obtain a tri-diagonal system of equations

$$\begin{cases} z_1 = 0 \\ h_{i-1}z_{i-1} + u_i z_i + h_i z_{i+1} = v_i & 2 \le i \le n-1 \\ z_n = 0 \end{cases} \qquad (2.30)$$

The System (2.30) is to be solved for the z_i's. The simplicity of the first and last equations is a result of the natural cubic spline conditions $S''(t_1) = S''(t_n) = 0$.

2.1.4.4 Example

Derive the equations of the natural cubic spline for the data samples of Table 2.3.

Table 2.3: Data samples.

x	-1	0	1
y	1	2	-1

Solution

First, we need to determine the tri-diagonal System (2.30). From the table, we have $h_1 = 1$, $h_2 = 1$, $b_1 = 1$, $b_2 = -3$, $u_2 = 4$, and $v_2 = -24$. The system is

$$\begin{cases} z_1 = 0 \\ z_1 + 4z_2 + z_3 = -24 \\ z_3 = 0 \end{cases} \qquad (2.31)$$

Thus, z_1=0, $z_2 = -6$, and $z_3 = 0$, and from (2.23) we have

$$\begin{cases} -(x+1)^3+3(x+1)-x & x\in[-1,0] \\ -(1-x)^3-x+3(1-x) & x\in[0,1] \end{cases} \qquad (2.32)$$

In general, writing system (2.31) in matrix form, we have

$$\begin{bmatrix} 1 & 0 & & & & \\ h_1 & u_2 & h_2 & & O & \\ & h_2 & u_3 & h_3 & & \\ & & \ddots & \ddots & \ddots & \\ & O & & h_{n-2} & u_{n-1} & h_{n-1} \\ & & & & 0 & 1 \end{bmatrix} \begin{bmatrix} z_1 \\ z_2 \\ z_3 \\ \vdots \\ z_{n-1} \\ z_n \end{bmatrix} = \begin{bmatrix} 0 \\ v_2 \\ v_3 \\ \vdots \\ v_{n-1} \\ 0 \end{bmatrix} \qquad (2.33)$$

On eliminating the first and last equations, we have

$$\begin{bmatrix} u_2 & h_2 & & & \\ h_2 & u_3 & h_3 & O & \\ & \ddots & \ddots & \ddots & \\ & O & h_{n-3} & u_{n-2} & h_{n-2} \\ & & & h_{n-2} & u_{n-1} \end{bmatrix} \begin{bmatrix} z_2 \\ z_3 \\ \vdots \\ z_{n-2} \\ z_{n-1} \end{bmatrix} = \begin{bmatrix} v_2 \\ v_3 \\ \vdots \\ v_{n-2} \\ v_{n-1} \end{bmatrix} \qquad (2.34)$$

which is a symmetric tri-diagonal system of order n - 2. We can develop an algorithm based on Gaussian elimination without pivoting, as follows:

$$\begin{cases} u_3 \leftarrow u_3 - \left(\dfrac{h_2}{u_2}\right) h_2 \\ v_3 \leftarrow v_3 - \left(\dfrac{h_2}{u_2}\right) v_2 \end{cases} \qquad (2.35)$$

$$\vdots$$

The general formulas are

$$\begin{cases} ui \leftarrow ui - \dfrac{h_{i-1}^2}{u_{i-1}} \\ vi \leftarrow vi - \dfrac{h_{i-1}v_{i-1}}{u_{i-1}} \end{cases} \qquad i = 3,4,\cdots,n-1 \tag{2.36}$$

The back substitution phase yields

$$\begin{aligned} z_{n-1} &\leftarrow \frac{v_{n-1}}{u_{n-1}} \\ z_{n-2} &\leftarrow \frac{v_{n-2} - h_{n-2}z_{n-1}}{u_{n-2}} \\ &\vdots \end{aligned} \tag{2.37}$$

The general formulae are

$$\begin{cases} z_{n-1} \leftarrow \dfrac{v_{n-1}}{u_{n-1}} \\ z_i \leftarrow \dfrac{v_i - h_i z_{i+1}}{u_i} \end{cases} \qquad i = n-2, n-3, \cdots, 2 \tag{2.38}$$

Putting all this together leads to the following algorithm.

2.1.4.5 Algorithm for solving the natural cubic spline tri-diagonal system directly

Given the interpolation points (t_i, y_i) for $i = 1, 2, \ldots, n$:

1. Compute for $i = 1, 2, \ldots, n - 1$

$$\begin{cases} h_i = t_{i+1} - t_i \\ b_i = \dfrac{1}{h_i}(y_{i+1} - y_i) \end{cases} \tag{2.39}$$

2. Set

$$\begin{cases} u_2 = 2(h_1 + h_2) \\ v_2 = 6(b_2 - b_1) \end{cases} \tag{2.40}$$

and compute inductively for $i = 3, 4, \ldots, n - 1$

$$\begin{cases} u_i = 2(h_i + h_{i-1}) - \dfrac{h_{i-1}^2}{u_{i-1}} \\ v_i = 6(b_i - b_{i-1}) - \dfrac{h_{i-1}v_{i-1}}{u_{i-1}} \end{cases} \tag{2.41}$$

3. Set

$$\begin{cases} z_n = 0 \\ z_1 = 0 \end{cases} \tag{2.42}$$

and compute inductively for $i = n - 1, n - 2, \ldots, 2$

$$z_i = \frac{v_i - h_i z_{i+1}}{u_i} \tag{2.43}$$

Finally, Equation (2.25) provides the value of $S'_i(t_i)$, which is

$$B_i = -\frac{h_i}{6} z_{i+1} - \frac{h_i}{3} z_i + \frac{1}{h_i}(y_{i+1} - y_i) \qquad (2.44)$$

Thus the nested form of $S_i(x)$ is

$$S_i(x) = y_i + (x - t_i)\left(B_i + (x - t_i)\left(\frac{z_i}{2} + \frac{1}{6h_i}(x - t_i)(z_{i+1} - z_i) \right) \right) \qquad (2.45)$$

2.1.4.6 Smoothness property

Why do spline functions serve the needs of data fitting better than ordinary polynomials? In order to answer this question, one should understand that interpolation by polynomials of high degree is often unsatisfactory because polynomials may exhibit wild *oscillations*. Polynomials are smooth in the technical sense of possessing continuous derivatives of all orders, whereas in this sense spline functions are not smooth.

Wild oscillations in a function can be attributed to its derivatives being very large. Consider the function whose graph is shown in Figure 2.4. The slope of the chord joining the points p and q is very large in magnitude. By the mean-value theorem, the slope of that chord is the value of the derivative at some point between p and q. Thus the derivative must attain large values. Indeed, somewhere on the curve between p and q there is a point where $f'(x)$ is large and negative. Similarly, between q and r there is a point where $f'(x)$ is large and positive. Hence there is a point on the curve between p and r

where $f''(x)$ is large. This reasoning can be continued to higher derivatives if there are more oscillations. This is the behavior that spline functions do not exhibit. In fact, the following results show that from a certain point of view, natural cubic splines are the best functions to employ for curve fitting.

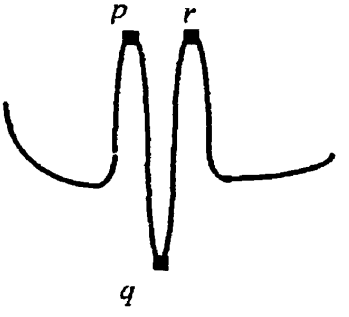

Figure 2.4: Interpolation of data points

2.1.4.7 Cubic spline smoothness property

The cubic spline smoothness property is taken into account when the degree of the interpolating spline polynomials is chosen. As shown in the following chapter, the sliding knots technique relies strongly in the smoothness of the spline polynomials at the knots.

If S is the natural cubic spline function that interpolates the twice-continuous function f at knots $a = t_1 < t_2 < \ldots < t_n = b$, then

$$\int_a^b [S''(x)]^2 dx \leq \int_a^b [f''(x)]^2 dx \qquad (2.46)$$

Proof

The interpretation of the integral inequality above is that the average value of $[S''(x)]^2$ on the interval $[a, b]$ is never larger than the average value of this expression with any twice-continuous function f that agrees with S at the knots. The quantity $[f''(x)]^2$ is related to the curvature of the function f. To verify the assertion about $[S''(x)]^2$, we let

$$g(x) = f(x) - S(x) \tag{2.47}$$

so that $g(t_i) = 0$ for $1 \le i \le n$, and $f'' = S'' + g''$. Now

$$\int_a^b (f'')^2 dx = \int_a^b (S'')^2 dx + \int_a^b (g'')^2 dx + 2\int_a^b S''g''dx \tag{2.48}$$

If the last integral were 0, we would be finished, for then

$$\int_a^b (f'')^2 dx = \int_a^b (S'')^2 dx + \int_a^b (g'')^2 dx \ge \int_a^b (S'')^2 dx \tag{2.49}$$

We apply the technique of the integration by parts to the integral in question to show that it is 0. We have

$$\int_a^b S''g''dx = S''g'\Big|_a^b - \int_a^b S'''g'dx = -\int_a^b S'''g'dx \tag{2.50}$$

Here, use has been made of the fact that S is a natural cubic spline, that is, $S''(a) = S''(b) = 0$. Continuing, we have

$$\int_a^b S'''g'dx = \sum_{i=1}^{n-1} \int_{t_i}^{t_{i+1}} S'''g'dx \tag{2.51}$$

Since S is a cubic polynomial in each interval $[t_i, t_{i-1}]$, its third derivative is a constant, say c_i. So

$$\int_a^b S'''g'dx = \sum_{i=1}^{n-1} c_i \int_{t_i}^{t_{i+1}} g'dx = \sum_{i=1}^{n-1} c_i \left[g(t_{i+1}) - g(t_i) \right] = 0 \tag{2.52}$$

since g vanishes at every knot.

2.2 B-splines

In this section we give an introduction to the theory of b-splines. These are special spline functions that are well adapted to numerical tasks and are being used more and more frequently in production-type programs for approximating data. The b-splines were so named because they formed a "basis" for the set of all splines. Throughout this section we suppose that an infinite set of knots has been prescribed in such a way that

$$\begin{cases} \cdots < t_{-2} < t_{-1} < t_0 < t_1 < t_2 < \cdots \\ \lim_{i \to \infty} t_i = \infty = -\lim_{i \to \infty} t_{-i} \end{cases} \tag{2.53}$$

The b-splines to be defined now depend on this set of knots, although the notation does not show this dependence. The b-splines of degree 0 are defined by

$$B_i^0(x) = \begin{cases} 1 & \text{if } t_i \le x < t_{i+1} \\ 0 & \text{otherwise} \end{cases} \qquad (2.54)$$

The graph of B_i^0 is shown in Figure 2.5.

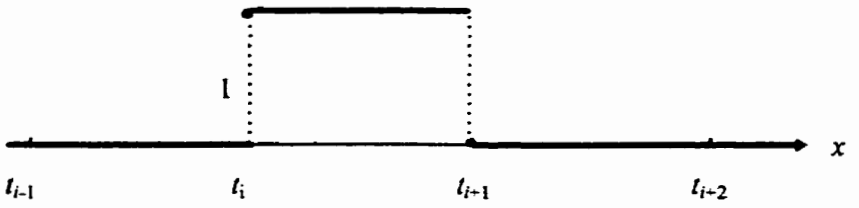

Figure 2.5: B-splines of degree 0.

Obviously, B_i^0 is discontinuous. However, it is continuous from the right at all points, even where the jumps occur as

$$\lim_{x \to t_i^+} B_i^0(x) = 1 = B_i^0(t_i) \quad \text{and} \quad \lim_{x \to t_{i+1}^-} B_i^0(x) = 0 = B_i^0(t_{i+1}) \qquad (2.55)$$

If the support of a function f is defined as the set of points x where $f(x) \neq 0$, then we can say that the support of B_i^0 is the half-open interval $[t_i, t_{i+1})$. Since B_i^0 is a piece-wise constant function, it is a spline of degree 0.

Two further observations can be made:

$$B_i^0(x) \geq 0 \text{ for all } x \text{ and for all } i \qquad (2.56)$$

$$\sum_{i=-\infty}^{\infty} B_i^0(x) = 1 \text{ for all } x \qquad (2.57)$$

Although the second of these assertions contains an infinite series, there is no question of convergence because for each x only one term in the series is different from 0. Indeed, for fixed x, there is a unique integer m such that $t_m \leq x < t_{m-1}$, and then

$$\sum_{i=-\infty}^{\infty} B_i^0(x) = B_m^0(x) = 1 \qquad (2.58)$$

Any spline of degree 0 that is continuous from the right and is based on the knots defined above can be expressed as a linear combination of the b-splines B_i^0. Indeed, if S is such a function, then it can be specified by a rule such as

$$S(x) = b_i \text{ if } t_i \leq x < t_{i+1} \qquad i = 0, \pm 1, \pm 2, \pm 3, \ldots \qquad (2.59)$$

Then S can be written as

$$S = \sum_{i=-\infty}^{\infty} b_i B_i^0 \qquad (2.60)$$

With the functions B_i^0 as a starting point, we now generate all the higher-degree b-splines by a simple recursive definition:

$$B_i^k(x) = \left(\frac{x - t_i}{t_{i+k} - t_i}\right) B_i^{k-1}(x) + \left(\frac{t_{i+k+1} - x}{t_{i+k+1} - t_{i+i}}\right) B_{i+1}^{k-1}(x) \qquad k \geq 1 \qquad (2.61)$$

Here $k = 1, 2, \ldots$ and $i = 0, \pm 1, \pm 2, \ldots$.

To illustrate the last equation, we show the graph of B_i^I in Figure 2.6.

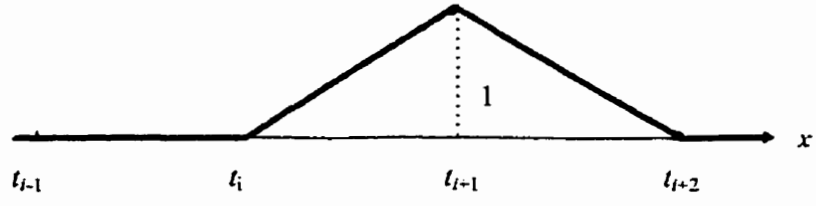

Figure 2.6: B-splines of degree 1.

The support of B_i^I is the open interval (t_i, t_i+2). It is true but perhaps not so obvious, that

$$\sum_{i=-\infty}^{\infty} B_i^1(x) = 1 \qquad \textit{for all } x \qquad (2.62)$$

and that every spline of degree 1 based on the knots defined in (2.53) is a linear combination of B_i^1.

The functions B_i^k as defined by Equation (2.61) are called b-splines of degree k. Since each B_i^k is obtained by applying linear factors to B_i^{k-1} and B_{i-1}^{k-1}, we see that the degrees actually rise by one at each step. So B_i^1 is piece-wise linear, B_i^2 is piece-wise quadratic, and so on.

It is also easily shown by induction that

$$B_i^k(x) = 0 \quad x \notin [t_i, t_{i-k+1}) k \geq 0 \tag{2.63}$$

and

$$B_i^k(x) > 0 \quad x \in [t_i, t_{i-k-1}) \; k \geq 0 \tag{2.64}$$

The principal use of the b-splines B_i^k ($i = 0, \pm 1, \pm 2, \ldots$) is as a basis for the set of all k^{th}-degree splines having the same knot sequence. Thus, linear combinations

$$\sum_{i=-\infty}^{\infty} c_i B_i^k \tag{2.65}$$

are important objects of study. We use c_i for fixed k and C_i^k to emphasize the degree k of the corresponding b-splines.

Our first task is to develop an efficient method to evaluate a function of the form

$$f(x) = \sum_{i=-\infty}^{\infty} C_i^k B_i^k(x) \qquad (2.66)$$

under the assumption that the coefficients C_i^k are given (as well as the knot sequence t_i). Using Equation (2.61) and some simple series manipulations, we have

$$f(x) = \sum_{i=-\infty}^{\infty} C_i^{k-1} B_i^{k-1}(x) \qquad (2.67)$$

where each C_i^{k-1} is defined to be appropriate coefficient. This algebraic manipulation shows how a linear combination of $B_i^k(x)$ can be expressed as a linear combination of $B_i^{k-1}(x)$. Repeating this process k - 1 times, we eventually express $f(x)$ in the form

$$f(x) = \sum_{i=-\infty}^{\infty} C_i^0 B_i^0(x) \qquad (2.68)$$

If $t_m \le x < t_{m-1}$, then $f(x) = C_m^0$. The formula by which the coefficients C_m^{j-1} are obtained is

$$C_1^{j-1} = \frac{C_i^j (x - t_i) + C_{i-1}^j (t_{+ji} - x)}{t_{i+j} - t_i} \qquad (2.69)$$

A nice feature of Equation (2.69) is that only the $k + 1$ coefficients C_m^k, C_{m-1}^k, . . . , C_{m-k}^k are needed to compute $f(x)$ if $t_m \le x < t_{m+1}$. Thus if f is defined by Equation (2.66) and we want to compute $f(x)$, we use Equation (2.69) to calculate the entries in the following triangular array:

$$\begin{array}{cccc} C_m^k & C_m^{k-1} & \cdots & C_m^0 \\ C_{m-1}^k & C_{m-1}^{k-1} & \cdots & \\ \vdots & \vdots & & \\ C_{m-k}^k & & & \end{array} \qquad (2.70)$$

Although our notation does not show it, the coefficients in Equation (2.66) are independent of x, whereas the C_i^{j-1}'s calculated subsequently by Equation (2.69) do depend on x. It is now simple to establish that

$$\sum_{i=-\infty}^{\infty} B_i^k(x) = 1 \quad \text{for all } x \text{ and all } k \ge 0 \qquad (2.71)$$

The smoothness of the b-splines B_i^k increases with the index k. In fact, we can show by induction that B_i^k has a continuous k - 1st derivative. The b-splines can be used as substitutes for complicated functions in many mathematical situations. Differentiation and integration are important examples. A basic result about the derivatives of b-splines is

$$\frac{d}{dx}B_i^k(x) = \left(\frac{k}{t_{i+k} - t_i}\right)B_i^{k-1}(x) - \left(\frac{k}{t_{i+k+1} - t_{i+1}}\right)B_{i+1}^{k-1}(x) \qquad (2.72)$$

This equation can be proven by induction, using the recursive Formula (2.61). Once (2.72) is established, we get the useful formula

$$\frac{d}{dx}\sum_{i=-\infty}^{\infty} c_i B_i^k(x) = \sum_{i=-\infty}^{\infty} d_i B_i^{k-1}(x) \quad \text{where} \quad d_i = k\left(\frac{c_i - c_{i-1}}{t_{i+k} - t_i}\right) \qquad (2.73)$$

For numerical integration, the b-splines are also recommended, especially for indefinite integration. Here is the basic result needed for integration.

$$\int_{-\infty}^{x} B_i^k(s)\,ds = \left(\frac{t_{i+k+1} - t_i}{k+1}\right)\sum_{j=i}^{\infty} B_j^{k+1}(x) \qquad (2.74)$$

The basic result (2.74) produces this useful formula:

$$\int_{-\infty}^{x} \sum_{i=-\infty}^{\infty} c_i B_i^k(s) \quad ds = \sum_{i=-\infty}^{\infty} e_i B_i^{k+1}(x) \tag{2.75}$$

where

$$e_i = \frac{1}{k+1} \sum_{j=-\infty}^{i} c_j (t_{j+k+1} - t_j) \tag{2.76}$$

It should be emphasized that this formula gives an indefinite integral (anti-derivative) of any function expressed as a linear combination of b-splines. Any definite integral can be obtained by selecting a specific value of x. For example, if x is a knot, say $x = t_m$, then

$$\int_{-\infty}^{t_m} \sum_{i=-\infty}^{\infty} c_i B_i^k(s) \quad ds = \sum_{i=-\infty}^{\infty} e_i B_i^{k+1}(t_m) = \sum_{i=m-k-1}^{m} e_i B_i^{k+1}(t_m) \tag{2.77}$$

2.2.1 *Interpolation and approximation by b-splines*

In the preceding section, we developed a number of properties of the b-splines and showed how b-splines are used in various numerical tasks. The problem of obtaining a b-spline representation of a given function was not discussed. Here we consider the problem of interpolating a table of data; later, a non-interpolatory method of approximation is described.

A basic question is how to determine the coefficients in the expression

$$S(x) = \sum_{i=-\infty}^{\infty} \mathrm{A}iB_{i-k}^{k}(x) \qquad (2.78)$$

so that the resulting spline function interpolates the prescribed Table 2.4.

Table 2.4: Sampled data.

x	t_1	t_2	t_3	...	t_n
y	y_1	y_2	y_3	...	y_n

We mean by "interpolate" that

$$S(t_i) = y_i \qquad 1 \le i \le n \qquad (2.79)$$

The natural starting point is with the simplest splines, corresponding to $k = 0$. Since

$$B_i^0(t_j) = \delta_{ij} = \begin{cases} 1, & i = j \\ 0, & i \neq j \end{cases} \tag{2.80}$$

the solution to the problem is immediate. Just set $A_i = y_i$ for $1 \leq i \leq n$. All other coefficients in (2.78) are arbitrary. In particular, they can be zero. We arrive then at the zero-degree b-spline

$$S(x) = \sum_{i=1}^{n} y_i B_i^0(x) \tag{2.81}$$

has the interpolation property

$$S(t_i) = y_i \qquad 1 \leq i \leq n \tag{2.82}$$

The next case, $k = 1$, also has a simple solution. We use the fact that

$$B_{i-1}^{1}(t_j) = \delta_{ij} \tag{2.83}$$

Hence, the following is true: The first-degree b-spline

$$S(x) = \sum_{i=1}^{n} y_i B_{i-1}^{1}(x) \tag{2.84}$$

has the interpolation property

$$S(t_i) = y_i \qquad 1 \le i \le n \tag{2.85}$$

If the table has four entries, for instance, we use B_0^1, B_1^1, B_2^1, and B_3^1. They, in turn, require for their definition knots $t_0, t_1, \ldots, t_5$. Knots t_0 and t_5 can be arbitrary. Figure 2.7 shows the graphs of the four splines. In such a problem, if t_0 and t_5 are not prescribed, it is natural to define them in such a way that t_1 is the midpoint of the interval $[t_0, t_2]$ and t_4 is the midpoint of the interval $[t_3, t_5]$. In both elementary cases considered, the unknown coefficients $A_1, A_2, \ldots, A_n$ in Equation (2.78) were uniquely determined by the interpolation conditions (2.79).

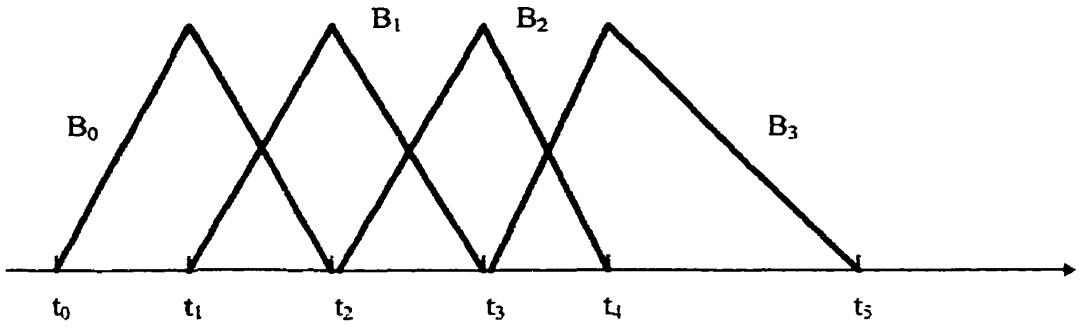

Figure 2.7: B-splines of degree 2.

If terms were present in Equation (2.78) corresponding to values of *i outside* the range (1, 2, . . . , n), they had no influence on the values of $S(x)$ at $t_1, t_2, \ldots, t_n$.

For higher-degree splines, we shall see that some arbitrariness exists in choosing the coefficients. In fact none of the coefficients are uniquely determined by the interpolation conditions. This fact can be advantageous if the other properties are desired for the solution. In the quadratic case, we begin with the equation

$$\sum_{i=-\infty}^{\infty} A_i B_{i-2}^2(t_j) = \frac{1}{t_{j+1} - t_{j-1}} \left[A_j (t_{j+1} - t_j) + A_{j+1} (t_j - t_{j-1}) \right] \qquad (2.86)$$

If the interpolation conditions (2.79) are now imposed, we obtain the following system of equations, which gives the necessary and sufficient conditions on the coefficients:

$$A_j(t_{j+1}-t_j)+A_{j+1}(t_j-t_{j-1})=y_j(t_{j+1}-t_{j-1}) \qquad 1\le j\le n \tag{2.87}$$

This is a system of n linear equations in $n+1$ unknowns $A_1, A_2, \ldots, A_{n-1}$.

One way to solve (2.87) is to assign any value to A_1 and then use (2.87) to solve for $A_2, A_3, \ldots, A_{n-1}$ recursively. For this purpose, the equations could be rewritten as

$$A_{j+1}=\alpha_j+\beta_j A_j \qquad 1\le j\le n \tag{2.88}$$

where the following abbreviations have been used:

$$\begin{cases} \alpha_j = y_j\left(\dfrac{t_{j+1}-t_{j-1}}{t_j-t_{j-1}}\right) \\ \beta_j = \dfrac{t_j-t_{j+1}}{t_j-t_{j-1}} \quad 1\le j\le n \end{cases} \tag{2.89}$$

In order to keep the coefficients small in magnitude, we recommend selecting A_1 so that the expression

$$\Phi = \sum_{i=1}^{n+1} A_i^2 \tag{2.90}$$

is a minimum. To determine this value of A_1, we proceed as follows. By successive substitution using Equation (2.88), we can show that

$$A_{j+1} = \gamma_j + \delta_j A_j \qquad 1 \le j \le n \tag{2.91}$$

where the coefficients γ_j and δ_j are obtained recursively by this algorithm:

$$\begin{cases} \gamma_1 = \alpha_1, & \delta_1 = \beta_1, \\ \gamma_j = \alpha_j + \beta_j \gamma_{j-1}, & \delta_j = \beta_j \delta_{j-1} \quad 2 \le j \le n \end{cases} \tag{2.92}$$

Then Φ is a quadratic function of A_1 as follows:

$$\begin{aligned}\Phi &= A_1^2 + A_2^2 + \cdots + A_{n+1}^2 \\ &= A_1^2 + (\gamma_1 + \delta_1 A_1)^2 + (\gamma_2 + \delta_2 A_1)^2 + \cdots + (\gamma_n + \delta_n A_1)^2\end{aligned} \tag{2.93}$$

To find the minimum of Φ, we take its derivative with respect to A_1 and set it equal to zero:

$$\frac{d\Phi}{dA_1} = 2A_1 + 2(\gamma_1 + \delta_1 A_1)\ \delta_1 + \cdots + 2(\gamma_n + \delta_n A_1)\ \delta_n = 0 \tag{2.94}$$

This is equivalent to $q A_1 + p = 0$, where

$$\begin{cases} q = 1 + \delta_1^2 + \delta_2^2 + \cdots + \delta_n^2 \\ p = \gamma_1 \delta_1 + \gamma_2 \delta_2 + \cdots + \gamma_n \delta_n \end{cases} \tag{2.95}$$

2.2.2 *Schoenberg's process*

An efficient process due to Schoenberg (1967) can also be used to obtain b-spline approximations to a given function. Its quadratic version is defined by

$$S(x) = \sum_{i=-\infty}^{\infty} f(\tau_i) B_i^2(x), \qquad \tau_i = \frac{1}{2}(t_{i+1} + t_{i+2}) \tag{2.96}$$

Here, of course, the knots are $\{t_i\}^{\infty}_{i=-\infty}$, and the points where f must be evaluated are midpoints between the knots.

Equation (2.96) is useful in producing a quadratic spline function that approximates f. The salient properties of this process are as follows:

1. If $f(x) = ax + b$, then $S(x) = f(x)$.

2. If $f(x) \geq 0$ everywhere, then $S(x) \geq 0$ everywhere.

3. $\max_x |S(x)| \leq \max_x |f(x)|$.

4. If f is continuous on $[a , b]$ and if $\delta = \max_i |t_{i-1} - t_i|$, then for x in $[a , b]$,

$$|S(x) - f(x)| \leq \frac{3}{2} \max_{a \leq u \leq v \leq u+\delta \leq b} |f(u) - f(v)|$$

5. the graph of S does not cross any line in a plane a greater number of times than does the graph of f.

Some of these properties are elementary; others are more complex. The significance of properties 4 and 5 should not be overlooked. Using 4, we can make the function S close to a continuous function f simply by making the "mesh size" δ small. This is because $f(u) - f(v)$ can be made as small as we wish by imposing the inequality $|u - v| \leq \delta$

(uniform continuity property). Property 5 can be interpreted as a shape-preserving attribute of the approximation process. In a crude interpretation, S should not exhibit more oscillations than f.

Chapter 3

3. SPLINE FUNCTIONS PROPERTIES

This chapter contains a description of the properties that stem from the theory of spline functions given in Chapter 2.

3.1 Absolute and relative reference

Spline functions can be expressed in absolute or relative reference form. Traditionally, the absolute reference has been used to define interpolating splines, that is, the origin of the independent variable x is the same for all the interpolating polynomials. When the absolute reference is used, the interpolating polynomial for a natural cubic spline has the form

$$S_i(x) = a_0 + a_1(x - t_i) + a_2(x - t_i)^2 + a_3(x - t_i)^3 \qquad (3.1)$$

When relative reference is used, the independent variable is defined as

$$x_r = x - t_i \qquad (3.2)$$

Then, the expression of the interpolating cubic spline becomes

$$S_i(x_r) = a_0 + a_1 x_r + a_2 x_r^2 + a_3 x_r^3 \qquad (3.3)$$

where

$$0 \le x_r \le t_{i+1} - t_i \tag{3.4}$$

The relative reference concept is visualised in Figure 3.1.

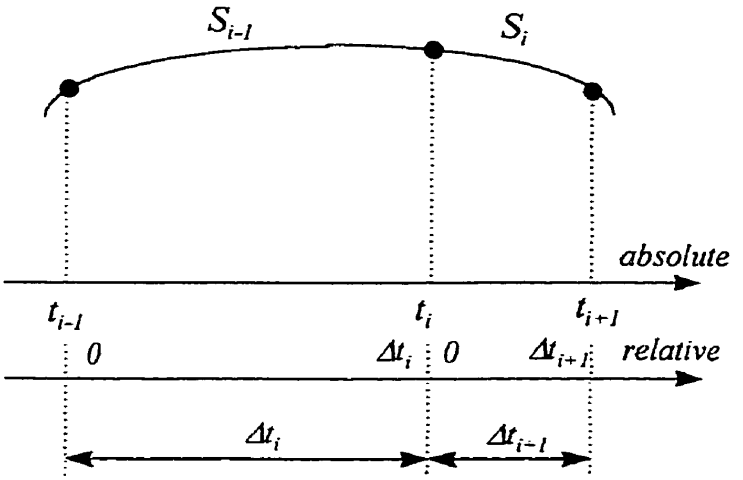

Figure 3.1: Absolute and relative references.

Notice that the polynomial coefficients remain unchanged. Relative referencing have some advantages over absolute referencing as shown in the following chapters.

3.1.1 Example

Using cubic splines, interpolate the data shown in Table 3.1 obtained from a magnetisation curve (Kraus, 1987) using absolute and relative referencing.

Table 3.1: Magnetisation curve samples.

H (kAm^{-1})	0	1	2	3	4	5	6	7	8	9	10
B (T)	0	0.2	0.6	1.2	1.5	1.6	1.65	1.7	1.73	1.76	1.78

Solution

We compute the spline function coefficients for each interval $[H_i, H_{i+1}]$ as described in Chapter 2. The form of the interpolating polynomial with absolute referencing is

$$B_i(H) = a_0 + a_1(H - H_i) + a_2(H - H_i)^2 + a_3(H - H_i)^3 \qquad (3.5)$$

and with relative referencing

$$B_i(H_r) = a_0 + a_1 H_r + a_2 H_r^{\,2} + a_3 H_r^{\,3} \qquad (3.6)$$

where

$$H_r = H - H_i \qquad (3.7)$$

Table 3.2 summarises the value of the polynomial coefficients.

Table 3.2: Coefficients of the interpolating cubic splines.

$H_i\ 10^3$	0	1	2	3	4	5	6	7	8	9
$a_0\ 10^0$	0	0.2	0.6	1.2	1.5	1.6	1.65	1.7	1.73	1.76
$a_1\ 10^{-3}$	0.165	0.268	0.559	0.494	0.161	0.059	0.050	0.040	0.028	0.026
$a_2\ 10^{-6}$	0	0.103	0.187	-0.251	-0.082	-0.019	0.009	-0.019	0.007	-0.009
$a_3\ 10^{-9}$	0.034	0.027	-0.146	0.056	0.021	0.009	-0.009	0.008	-0.005	0.003

Each of the spline polynomials is plotted together with the data points from Table 3.1. The following diagram shows the results:

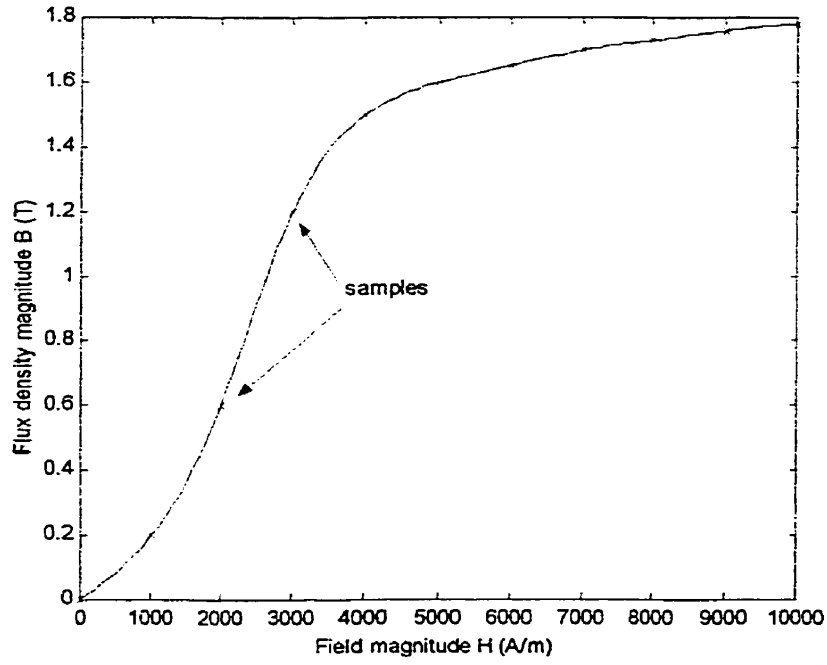

Figure 3.2: Interpolation of magnetisation curve by cubic splines.

3.2 Sliding knots technique

One of the contributions of this work is the technique called sliding knots. This technique is particularly important for the prediction of the plant output for variable sampling time, as shown in Chapter 4. Moreover, the sliding knots technique is thoroughly used for the optimization of power systems in time domain, as shown in Chapter 7.

3.2.1 Definition of sliding knots

We define as sliding knots the shifting of a knot pair x_i, x_{i-1} by Δx.

3.2.2 Effect of sliding knots over the spline polynomials

Let us consider now the possibility of introducing a shift Δx in the independent variable x in Equation (3.3), where relative referencing has been used for simplicity. The expression of the shifted polynomial is

$$S_i(x+\Delta x) = a_0 + a_1(x+\Delta x) + a_2(x+\Delta x)^2 + a_3(x+\Delta x)^3 \qquad (3.8)$$

Figure 3.3 shows a diagram where the shift forward due to Δx in $S_i(x)$ is indicated by a thicker line. The introduction of the shift forward Δx has the effect of extending the spline function $S_i(x)$ outside the range defined by the knots x_i, x_{i-1}.

The sliding knots technique relies on the cubic spline smoothness property demonstrated in Chapter 2. Given the fact that the natural cubic spline has a smooth transition at the knots, extrapolation using sliding knots is feasible in the vicinity of the intervals defined by the knots.

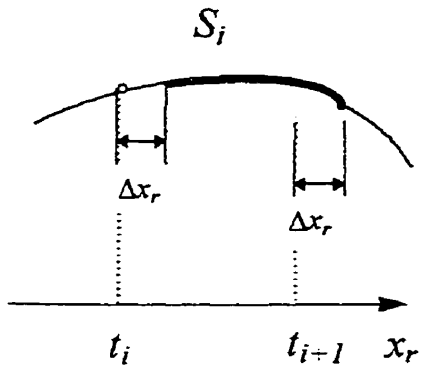

Figure 3.3: Curve showing the sliding knots.

The analysis of the sliding knots technique errors is addressed in the next subsection.

3.2.3 Sliding knots technique error analysis

Using the spline polynomials outside of their range of definition introduces errors. The validation of the sliding knots technique requires the analysis of these errors. This analysis is presented in the form of a theorem.

3.2.3.1 Theorem 3.1:

Let $t_i < t_{i+1} < t_{i+2}$ be a set of consecutive knots for which the spline polynomials S_i and S_{i+1} of order k are defined. Let these two spline polynomials be written as

$$S_i(x) = \sum_{h=0}^{k} a_h (x - t_i)^h \qquad t_i \le x \le t_{i+1} \tag{3.9}$$

and

$$S_{i+1}(x) = \sum_{h=0}^{k} b_h (x - t_{i+1})^h \qquad t_{i+1} \le x \le t_{i+2} \tag{3.10}$$

Let us also define the sliding knots error E_i, at any interval i delimited by $[t_i, t_{i+1}]$, as

$$E_i(x) = S_{i+1}(x) - S_i(x) \qquad t_{i+1} \le x \le t_{i+2} \tag{3.11}$$

where $x = t_{i+1} + \Delta x$. We say that the maximum absolute error E_{max} when sliding knots are used is given by

$$E_{max}(x) \le \max_i \left| (b_k - a_k)(x - t_{i+1})^k \right| \qquad x \in [t_{i+1}, t_{i+2}] \tag{3.12}$$

Proof:

From Expressions (3.9), (3.10) and (3.11) of the hypothesis we have

$$E_i = S_{i+1}(x) - S_i(x) = \sum_{h=0}^{k} b_h (x - t_{i+1})^h - \sum_{h=0}^{k} a_h (x - t_i)^h \tag{3.13}$$

By definition, a spline function of order k has k - 1 continuous derivatives at the knots. Taking knot t_i as a reference, we can express the coefficients of S_{i+1} as a function of those of S_i. The general expression for these coefficients is

$$b_h = \sum_{l=h}^{k} \frac{l!}{(l-h)!} a_l (t_{i+1} - t_i)^{l-h} \qquad h = 0, 1, \cdots, k-1 \tag{3.14}$$

Now, the sliding knots error $E_i(x)$ can be expressed as

$$E_i(x) = \sum_{h=0}^{k-1} \sum_{l=h}^{k} \frac{l!}{(l-h)!} a_l (t_{i+1} - t_i)^{l-h} (x - t_i)^h - \sum_{h=0}^{k} a_h (x - t_i)^h + b_k (x - t_{i+1})^k \tag{3.15}$$

After expanding the polynomials and using the following knots property

$$(x - t_i) - (x - t_{i+1}) = (t_{i+1} - t_i) \tag{3.16}$$

a Pascal's triangle arrangement of polynomial coefficients is identified. Then

$$E_i(x) = \sum_{h=0}^{k} a_h (x - t_i)^h - \sum_{h=0}^{k} a_h (x - t_i)^h - a_k (x - t_i)^k + b_k (x - t_i)^k \tag{3.17}$$

or

$$E_i(x) = (b_k - a_k)(x - t_{i+1})^k \qquad (3.18)$$

From Equations (3.9), (3.10) and (3.18) it is clear that the maximum error using the sliding knots technique occurs for the intervals $[t_i, t_{i+1}]$ and $[t_{i+1}, t_{i+2}]$ that have the largest difference b_k - a_k in the coefficients of their spline polynomials. Therefore, the following expression is true:

$$E_{max}(x) \le \max_i \left| (b_k - a_k)(x - t_{i+1})^k \right| \qquad x \in [t_{i+1}, t_{i+2}] \qquad (3.19)$$

□

Remark 3.1

The sliding knots technique error is given by those coefficients that are related to the k^{th} derivative of the spline polynomials of order k. From the expression of spline polynomial

$$S_i(x) = \sum_{h=0}^{k} a_h (x - t_i)^h \qquad (3.20)$$

the k^{th} derivative is

$$S^{(k)}(x) = k!\, a_k \qquad (3.21)$$

Notice that the coefficients related to the k^{th} derivative are the only coefficients of the interpolating splines that have no specifications in regards to their value at the knots. This may explain why they are the cause of errors when the spline polynomials are used outside the boundaries of definition.

Remark 3.2

The error from the sliding knot technique can be decreased by increasing the number of knots. The closer the knots are from each other, the smaller the difference between the coefficients of any two consecutive spline polynomials. From the analysis Equation (3.18) it is clear that a small difference in the spline coefficients reduces the error. In mathematical terms:

$$\lim_{t_{i-1}-t_i \to 0} b_k - a_k = 0 \qquad (3.22)$$

Then, from Equation (3.18)

$$\lim_{t_{i-1}-t_i \to 0} E_i(x) = 0 \qquad (3.23)$$

Chapter 4

4. SPLINE NON-PARAMETRIC MODELS

This chapter reviews the current methodology for output prediction based on non-parametric models as well as describes the development of models based on spline functions.

4.1 Introduction

Non-parametric models (NPMs), also known as convolution models, are based on sampled data from impulse or step time responses. These samples are called weighting factors and the number commonly required for the modeling of a plant ranges from 20 to 70 (Isermann 1981, Seborg et al. 1989). As reported by Muske and Rawlings (1993), over-parametrized models are one of the greatest limitations of the commercially available MPCs based on NPMs. For instance, a first order process can be described by a transfer function model using only three parameters (gain, time constant and deadtime) whilst an impulse response model will require more than 30 coefficients to describe the same dynamics. These coefficients are the samples of the impulse response at regular intervals. A minimum number of samples are required to approximate the continuous time convolution integral by a discrete version of this integral. As described by Isermann *et al.* (1992), the large number of parameters required to identify the NPMs affects the numerical stability of the estimation techniques.

The introduction of spline functions for the approximation of NPMs presented in this chapter, reduces the number of weighting factors, allowing the application of traditional adaptive techniques such as the projection algorithm (PA) or least squares (LS). The

objective is the development of an adaptive spline model (ASM) that extends the applicability of MPCs with linear NPMs to a larger class of processes, such as nonlinear time-invariant (NTI) or nonlinear time-variant (NTV) processes.

4.2 Non-parametric plant models

The construction of NPMs is an off-line, open-loop procedure. The plant is excited with a test signal and the output from the plant is recorded at regular intervals, given by the chosen sampling time *To*. Neglecting truncation errors, the process dynamics are approximated by means of an FIR model. Therefore, the model is inherently stable in the sense that, as long as the weight values are finite, the impulse response is bounded and of finite length.

The sampled data from the finite impulse response (FIR) of a plant are used as weighting coefficients for the prediction of the process output. The process output is predicted by solving the convolution sum

$$\hat{y}(t+To) = \sum_{k=0}^{N} g(kTo)\, u(t-kTo)\, To + n(t) \qquad (4.1)$$

where $\hat{y}$ is the predicted plant output; g, the unit impulse response of the plant (weighting factors); u, the plant input; n, a disturbance signal; and k denotes the time step.

Equation (4.1) is an open-loop prediction model in the sense that it does not provide any corrections for the influence of model errors or unmeasured load changes that may have occurred at any previous time step. To address this shortcoming, DMC and MAC techniques utilize a corrected prediction given by

$$\hat{y}(t+To) = \sum_{k=0}^{N} g(kTo)\, u(t-kTo)\, To + c(t) \qquad (4.2)$$

where

$$c(t) = y(t) - \sum_{k=0}^{N} g(kTo)\, u(t-kTo-To)\, To \qquad (4.3)$$

is the prediction correction and y is the actual plant output. This shift forward of the plant model correction is computed at every time step. Figure 4.1 shows a block diagram of the prediction-correction technique. The main drawback of this constant model mismatch assumption is the lack of adaptation to changes in the dynamics of the process. This is particularly important for nonlinear time-invariant (NTI) or linear time-variant (LTV) processes. During the development of the controller, the design algorithm is based on prior knowledge of the model and it is independent of it, but it is obvious that the benefits obtained from the simplicity of the formulation are affected by the discrepancies existing between the real process and the model used.

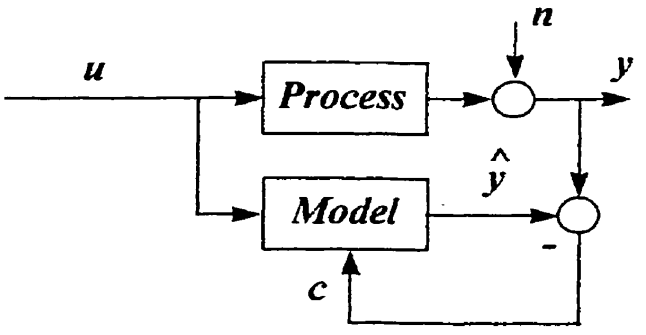

Figure 4.1: Block diagram of the model correction algorithm.

4.3 Plant model in spline form

The development of the spline model starts with the selection of a small set of samples obtained from the plant FIR at time instants called knots. This reduced number of samples resembles the parameters of the parametric models without the need of a transfer function, thereby allowing the application of classical adaptive techniques based on PA or LS.

4.3.1 Selection of the number and location of knots

The spline model of the plant requires the sampling of the impulse or step time responses in the same manner as in the classical NPM methods. Once the FIR of the plant is obtained, a decision is made on the number and location of the knots

4.3.1.1 Optimal number of knots

By conveniently selecting a reduced number of samples at the knots, a new set of weighting factors is generated. The lower the number of knots used for the spline model, the faster the convergence rate of the estimates during the adaptation process. On the other hand, if the number of knots is too small, it can result in a poor modeling of the plant.

The optimal number of knots is determined by the dynamic of the process shown in the FIR. In this thesis, the optimal number of knots is determined in an heuristic manner. This is similar to designing a model of the plant in frequency domain. Generally speaking, a reduced order model is preferred due to the faster convergence of the estimates.

The selection of the optimal number of knots in a more systematic and rigorous way is a topic for the future research.

4.3.1.2 Location of the knots

As described by Micchelli *et al.* (1976) and Gaffney and Powell (1976), the theory of splines provides the tools for the optimal location of the knots. These tools are valid only when the function that generates the data points is not time varying.

As described in Chapter 1, one of the main contributions of this work to the theory of MPCs is the reduction of the dimension of the NPMs. The reduction of the dimension of the NPMs allows the application of traditional adaptive techniques. The FIR used as the basis for the optimal location of the knots is not fixed in a time varying process. Therefore, the optimal location of the knots must be determined every time the dynamics of the process change.

In this work, a practical approach is used for the location of the knots. By analyzing the FIR and forecasting the behavior of the dynamics of the plant, a decision is made in regard to the best placement of the knots. Issues like variable deadtime and backslash must be considered when selecting the location of these knots.

4.3.2 Selection of the degree of the interpolating spline

The application of spline functions requires the selection of the degree of the interpolating polynomials. Cubic functions are best suited for this task mainly due to their superior interpolating properties as compared to other polynomials. This superiority demonstrated by the cubic spline smoothness property and the sliding knots technique described in Chapters 2 and 3 respectively. The selection of knots based on the FIR of a continuously stirred tank reactor (CSTR), is shown in Figure 4.2. The CSTR process is described in Chapter 6.

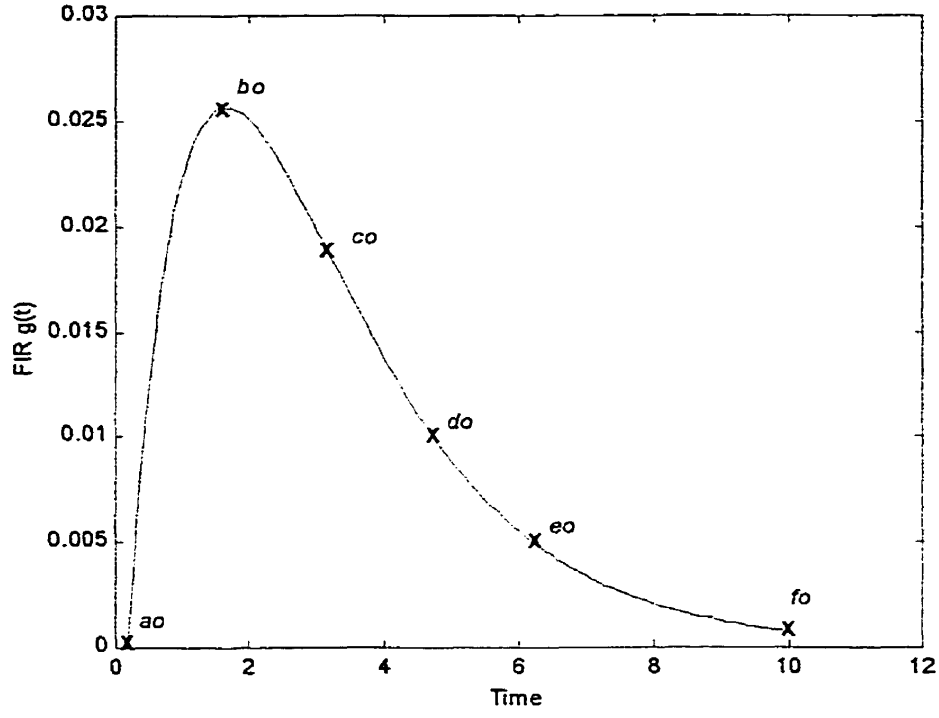

Figure 4.2: Selection of knots in a FIR of a CSTR.

Table 4.1: Sampled data at the knots.

knots	t_0	t_1	t_2	t_3	t_4	t_5
samples	a_0	b_0	c_0	d_0	e_0	f_0

The computation of the spline functions starts from the plant time response evaluated at the knots, as shown in Table 4.1 for a six-knot system. The coefficients of the interpolating polynomials are computed using the recursive algorithm described in Chapter 2. The cubic spline approximation of a FIR has the form

$$g(t) \approx \begin{cases} g_a(t) = a_0 + a_1 t + a_2 t^2 + a_3 t^3 & t \in [t_0, t_1] \\ g_b(t) = b_0 + b_1 t + b_2 t^2 + b_3 t^3 & t \in [t_1, t_2] \\ g_c(t) = c_0 + c_1 t + c_2 t^2 + c_3 t^3 & t \in [t_2, t_3] \\ g_d(t) = d_0 + d_1 t + d_2 t^2 + d_3 t^3 & t \in [t_3, t_4] \\ g_e(t) = e_0 + e_1 t + e_2 t^2 + e_3 t^3 & t \in [t_4, t_5] \end{cases} \qquad (4.4)$$

Once the spline functions are computed, the weighting factors of the non-parametric model are obtained by interpolation between knots. Notice that the spline polynomials g_a, g_b, g_c, g_d, and g_e are defined according to a relative reference convention, as described in Chapter 3.

4.4 Adaptive spline models

4.4.1 Reduction of the dimension of the model

The spline functions representation of the FIR that is given in Equation (4.4) is further simplified, thereby reducing the number of parameters describing the process. Let us define the following interpolating splines coefficient vectors:

$$\begin{aligned} A &= [a_0\ a_1\ a_2\ a_3] \\ B &= [b_0\ b_1\ b_2\ b_3] \\ C &= [c_0\ c_1\ c_2\ c_3] \\ D &= [d_0\ d_1\ d_2\ d_3] \\ E &= [e_0\ e_1\ e_2\ e_3] \end{aligned} \qquad (4.5)$$

Let us also define a vector of sampled data for a six-knot spline system

$$S_0 = [a_0\ b_0\ c_0\ d_0\ e_0\ f_0] \tag{4.6}$$

From the continuity conditions of the cubic splines described in Chapter 2, a transformation matrix T_R is defined such that the coefficients of the spline polynomials are expressed as a function of the samples at the knots. For a six-knots spline system, the relationship between coefficients of the spline polynomials and the samples at the knots is given by

$$[A\ B\ C\ D\ E]\ T_R = S_0\ I_T \tag{4.7}$$

where the transformation matrix T_R is defined as

$$T_R = \begin{bmatrix} L(t_1) & O & O & O & Ie \\ Id & L(t_2) & O & O & O \\ O & Id & L(t_3) & O & O \\ O & O & Id & L(t_4) & O \\ O & O & O & Id & F(t_5) \end{bmatrix} \tag{4.8}$$

with

$$L(t) = \begin{bmatrix} 1 & 1 & 0 & 0 \\ 0 & t & 1 & 0 \\ 0 & t^2 & 2t & 1 \\ 0 & t^3 & 3t^2 & 3t \end{bmatrix} \tag{4.9}$$

$$F(t)=\begin{bmatrix}1 & 1 & 0 & 0\\ 0 & t & 0 & 0\\ 0 & t^2 & 0 & 1\\ 0 & t^3 & 0 & 3t\end{bmatrix} \tag{4.10}$$

$$Id=\begin{bmatrix}0 & 0 & 0 & 0\\ 0 & 0 & -1 & 0\\ 0 & 0 & 0 & -1\\ 0 & 0 & 0 & 0\end{bmatrix} \tag{4.11}$$

$$Ie=\begin{bmatrix}0 & 0 & 0 & 0\\ 0 & 0 & 0 & 0\\ 0 & 0 & -1 & 0\\ 0 & 0 & 0 & 0\end{bmatrix} \tag{4.12}$$

and

$$I_T=\begin{bmatrix}1 & 0 & 0 & 0 & 0 & 0 & \cdots & 0 & 0 & 0 & 0\\ 0 & 1 & 0 & 0 & 1 & 0 & \cdots & 0 & 0 & 0 & 0\\ 0 & 0 & 0 & 0 & 0 & 1 & \cdots & 0 & 0 & 0 & 0\\ 0 & 0 & 0 & 0 & 0 & 0 & \cdots & 0 & 0 & 0 & 0\\ 0 & 0 & 0 & 0 & 0 & 0 & \cdots & 1 & 0 & 0 & 0\\ 0 & 0 & 0 & 0 & 0 & 0 & \cdots & 0 & 1 & 0 & 0\end{bmatrix} \tag{4.13}$$

Then, from Equation (4.7)

$$[A\ B\ C\ D\ E]=S_0\ I_T\ T_R^{-1} \tag{4.14}$$

To validate Expression (4.14), the non-singular characteristics of transformation matrix T_R must be proven.

4.4.1.1 Proposition 4.1:

The matrix T_R is always of full rank.

Proof

The proof of the above proposition requires that all the coefficients of the cubic spline interpolating polynomials are uniquely defined. Therefore, we need to verify that the number of conditions imposed equals the number of coefficients needed. Referring to the definition of spline functions described in the Chapter 2, there are n knots and hence n - 1 subintervals. Since a cubic polynomial has four coefficients, a total of 4 (n - 1) coefficients are available. As for the conditions imposed, we have specified that within each interval the interpolating polynomial must go through two points, which gives 2 (n - 2) conditions. The continuity adds no additional conditions. The first and second derivatives must be continuous at the n - 2 interior points, leading to 2 (n - 2) more conditions. The second derivatives must vanish at the two endpoints. Thus, a total of 2 (n - 1) + 2 (n - 2) + 2 = 4 (n - 1) conditions are required.

□

Remark 4.1

Matrices T_R and I_T can be used to compute the spline coefficients based on the samples at the knots. Observing Equation (4.14), the spline coefficients can be determined in a non-recursive manner using these two transformation matrices.

Remark 4.1

Due to the fact that the present work deals with process control where sampling times are generally larger than 100 ms, the presence of t, t^2 and t^3 in the elements of matrices (4.9) and (4.10) do not impose any numerical problems during the inversion of matrix T_R.

4.4.2 Plant output prediction

Having the plant model in spline form reduces the number of parameters to be estimated, because, only the samples at the knots need be updated. Based on Equation (4.1), and neglecting the disturbances modeled by n, the prediction of the plant output using the interpolating polynomials (4.4) takes the form

$$\begin{aligned} y(t+To) = & \sum_{i=0}^{t_1/To-1} g_a(iTo)\, u(t-iTo)To + \\ & \sum_{i=0}^{t_2-t_1/To-1} g_b(iTo)\, u(t-t_1-iTo)To + \\ & \sum_{i=0}^{t_3-t_2/To-1} g_c(iTo)\, u(t-t_2-iTo)To + \\ & \sum_{i=0}^{t_4-t_3/To-1} g_d(iTo)\, u(t-t_3-iTo)To + \\ & \sum_{i=0}^{t_5-t_4/To-1} g_e(iTo)\, u(t-t_4-iTo)To \end{aligned} \qquad (4.15)$$

4.4.3 *Pseudo input signal*

Let us define the following impulse control signal vectors:

$$\begin{aligned}
U_A^T(t) &= [u(t)\ u(t-To) \cdots u(t-t_1+To)] \\
U_B^T(t) &= [u(t-t_1)\ u(t-t_1-To) \cdots u(t-t_2+To)] \\
U_C^T(t) &= [u(t-t_2)\ u(t-t_2-To) \cdots u(t-t_3+To)] \\
U_D^T(t) &= [u(t-t_3)\ u(t-t_3-To) \cdots u(t-t_4+To)] \\
U_E^T(t) &= [u(t-t_4)\ u(t-t_4-To) \cdots u(t-t_5+To)]
\end{aligned} \tag{4.16}$$

representing the sequence of plant inputs that affect each of the spline functions intervals as shown in Expression (4.15). Further, let us define the following time sequence matrices:

$$Ta = \begin{bmatrix} 1 & To & To^2 & To^3 \\ 1 & 2To & (2To)^2 & (2To)^3 \\ \vdots & \vdots & \vdots & \vdots \\ 1 & t_1 & t_1^2 & t_1^3 \end{bmatrix} \tag{4.17}$$

$$Tb = \begin{bmatrix} 1 & To & To^2 & To^3 \\ 1 & 2To & (2To)^2 & (2To)^3 \\ \vdots & \vdots & \vdots & \vdots \\ 1 & t_2 & t_2^2 & t_2^3 \end{bmatrix} \tag{4.18}$$

and similarly for *Tc*, *Td*, and *Te*. We can now introduce the concept of pseudo input signal U_0, given by

$$U_o(t) = I_T\ T_R^{-1}\ T^T{}_{a-e} U_{A-E}(t) \tag{4.19}$$

where

$$U_{A-E}(t) = \left[U_A^T(t) \quad U_B^T(t) \quad U_C^T(t) \quad U_D^T(t) \quad U_E^T(t)\right]^T \tag{4.20}$$

and

$$T_{a-e} = \begin{bmatrix} Ta & O & O & O & O \\ O & Tb & O & O & O \\ O & O & Tc & O & O \\ O & O & O & Td & O \\ O & O & O & O & Te \end{bmatrix} \tag{4.21}$$

The pseudo input signal U_0 is expressed as a vector of pseudo input elements

$$U_0(t) = \begin{bmatrix} u_{a_0}(t) \\ u_{b_0}(t) \\ u_{c_0}(t) \\ u_{d_0}(t) \\ u_{e_0}(t) \end{bmatrix} \tag{4.22}$$

Finally, combining Equations (4.6), (4.15), (4.19) and (4.22), a compact expression for the plant output prediction (in matrix form) is given by

$$y(t+To) = S_0\, U_0(t)\, To \tag{4.23}$$

Comparing Equation (4.23) with Equation (4.1), we find the rationale behind the concept of pseudo inputs given by the elements of U_0 in Equation (4.22). Also, notice that the elements of vector S_0 are the spline coefficients at the beginning of each interval; thereby, they conform a set of pseudo parameters of the plant model.

4.4.4 Identification

Using the projection algorithm (PA) and the nomenclature given in Goodwin and Sin (1984), we obtain the estimates for the coefficients a_0, b_0, c_0, d_0, and e_0 at the knots of the FIR. The estimation of the spline parameters requires the computation of the following:

$$S_0(t+To) = S_0(t) + \frac{pU_0^T(t)}{q + U_0^T(t)\, U_0(t)}\, c(t) \tag{4.24}$$

where

$$0 < p < 2 \tag{4.25}$$

and

$$q > 0 \tag{4.26}$$

Equation (4.24), in its traditional form, would have $p = 1$ and $q = 0$. The addition of a small coefficient q prevents singularities (division by zero). Coefficient p determines the convergence rate of the estimates. If p is larger than or equal to 2, the convergence of the estimates is not guaranteed. For more complex formulations of the projection algorithm, p is made variable with time to include, for instance, a dead zone. Equation (4.24) is also known as normalized least-mean-squares, in which case, the choice of p is usually such that $0 < p \leq 1$.

Spline coefficients a_0 and f_0 are made equal to further reduce model dimension. These two last coefficients will determine the drifting effect that the plant undergoes in a time varying process. Notice that the prediction correction c defined by Expression (4.3) is now part of the expression of the PA.

4.5 Analysis of model uncertainties for robust control

The objective of robust control is to design controllers which preserve stability in spite of model uncertainties. The sources of model uncertainties are the simplifying assumptions that have to be made in regards to the plant. Nonlinearities are either unknown and hence unmodeled, or modeled and later ignored to simplify the analysis. Because the real environment may change with time, or operating conditions may vary, the control system must be able to withstand these variations.

The particular property that a control system must possess so that it operates in realistic situations is called robustness. Although the use of feedback contemplates the inaccuracies

of the model implicitly, the term robust control is used in literature for control systems that explicitly consider the discrepancies of the model and the real process.

The robust control analysis in this work focuses on the most important feature of convolution models, which is, to predict future values of the output variables. The uncertainties can be defined in terms of the prediction capabilities of the model.

4.5.1 Models uncertainties

As in the case of model predictive controller, convolution controllers are used to predict future trajectories. In this contexts, seems reasonable to describe models uncertainties by a family of models that may generate a band of trajectories in which the process trajectory will be included when the same input is applied in spite of model uncertainties.

4.5.1.1 FIR uncertainties

The natural way of considering non-parametric model uncertainties in the presence of truncated impulse responses is by assuming the weighting coefficients are not known exactly. The effect is compounded when the finite impulse response is approximated by spline functions. A general approach is to consider that the impulse response may be within a set defined by

$$\underline{g}_i \leq g_i \leq \overline{g}_i \qquad (4.27)$$

that is

$$g_i(\theta) = g_i + \theta_i \tag{4.28}$$

with θ defined by

$$gm_i - \bar{g}_i \le \theta_i \le \underline{g}_i - gm_i \tag{4.29}$$

where gm_i is the plant nominal response.

The dimension of the uncertainty parameter vector is $20 < N < 70$. The use of spline polynomials reduces substantially this dimension to just the number of knots as shown later in this section.

The predicted output can be computed as

$$\hat{y}(t + To) = \sum_{i=0}^{N-1} (gm_i + \theta_i) u(t - iTo)\ To \tag{4.30}$$

while the predicted nominal response is

$$\hat{y}m(t + To) = \sum_{i=0}^{N-1} gm_i u(t - iTo)\ To \tag{4.31}$$

The prediction band around the nominal response is then limited by:

$$\min_{\theta} \sum_{i=0}^{N-1} \theta_i u(t - iTo)\, To \quad and \quad \max_{\theta} \sum_{i=0}^{N-1} \theta_i u(t - iTo)\, To \tag{4.32}$$

4.5.1.2 Global uncertainties

As described in Camacho and Bordoms (1999), the plant is described by a family of models

$$y(t + To) = f(y(t), \cdots, y(t - nTo), u(t), \cdots, u(t - nTo)) + \theta(t) \tag{4.33}$$

For impulse response models, the prediction of the plant output at instant $t + To$ with parametric and temporal uncertainties description is given by

$$\hat{y}(t + To) = \sum_{i=0}^{N-1} (gm_i + \theta_i) u(t - iTo)\, To \tag{4.34}$$

$$\hat{y}(t + To) = \sum_{i=0}^{N-1} (gm_i) u(t - iTo)\, To + \theta_i(t + To) \tag{4.35}$$

then,

$$\theta(t + To) = \sum_{i=0}^{N-1} \theta_i u(t - iTo)\, To \tag{4.36}$$

and for bounded control signal u, which is generally the case in practical applications, the maximum and minimum limits for the plant output prediction uncertainty are

$$\underline{\theta} = \min_{u,\theta_i} \sum_{i=0}^{N-1} \theta_i u(t - iTo)\ To \tag{4.37}$$

$$\overline{\theta} = \max_{u,\theta_i} \sum_{i=0}^{N-1} \theta_i u(t - iTo)\ To \tag{4.38}$$

4.5.2 Global uncertainties for spline models

When the FIR is approximated by spline polynomials, the plant model parameters g become the samples at the knots and the control signal u becomes the pseudo control signal. As described earlier in this chapter, the predicted plant output as a function of the samples at the knots is given by,

$$y(t + To) = S_0\ U_0(t)\ To \tag{4.39}$$

Following the analysis of global uncertainties described for NPMs, it is possible to obtain an expression that relates the global uncertainties of the spline models as a function of the uncertainties of the samples at the knots.

4.5.2.1 Theorem 4.2:

Let the plant output prediction be given by Equation (4.39). Let the spline model So be expressed as a function of its uncertainty θ_{So} as follows:

$$S_0 = Sm_0 + \theta_{S_0} \qquad (4.40)$$

Then, the maximum and minimum of plant output prediction global uncertainties are

$$\underline{\theta} = \min_{U_0, \theta_{S_0}} \theta_{S_0} U_0(t)\ To \qquad (4.41)$$

and

$$\overline{\theta} = \max_{U_0, \theta_{S_0}} \theta_{S_0} U_0(t)\ To \qquad (4.42)$$

Proof

We prove this theorem by following the analysis of the global uncertainties for NPMs. By analogy, and using (4.40) of the hypothesis, Expressions (4.34) and (4.35) are transformed into the expressions of the output prediction with parametric and temporal uncertainties in spline form

$$\hat{y}(t + To) = (Sm_o + \theta_{S_o})\ Uo(t)\ To \qquad (4.43)$$

$$\hat{y}(t + To) = Sm_o\ Uo(t) + \theta(t + To) \qquad (4.44)$$

then,

$$\theta(t+To) = \theta_{So} Uo(t)\ To \tag{4.45}$$

and for bounded pseudo control signal Uo, what is general the case in practical applications, the maximum and minimum limits for the plant output prediction uncertainty in spline form are

$$\underline{\theta} = \min_{U_0 . \theta_{S_0}} \theta_{S_0} U_0(t)\ To \tag{4.46}$$

$$\overline{\theta} = \max_{U_0 . \theta_{S_0}} \theta_{S_0} U_0(t)\ To \tag{4.47}$$

□

4.6 Multirate sampling systems

In this subsection, the development of spline models for multirate sampling environments is presented.

There are two ways to address plant output prediction for variable sampling time: the first and more intuitive is based on the recovery of the weighting coefficients by means of the spline transform (Ostrander, 1971); the second is based on the concept of pseudo inputs and the sliding knots technique.

4.6.1 Recovery of the weighting coefficients

Once the plant is mathematically represented by spline polynomials, the weighting coefficients g_i are computed by the spline transform at the corresponding time instants. These coefficients are used in the convolution Expression (4.1).

4.6.2 Pseudo input approach

This method is recommended when model identification is intended. The concept of pseudo input is a key stone component of the proposed technique and is used in the transformation of the spline model into an asynchronous model.

The multirate sampling method based on the recovery of the weighting coefficients described in the previous subsection assumes the possibility of modifying the dimension of the vectors and matrices of the system model-controller. The pseudo input approach is recommended when the dimension of these vectors and matrices remain unchanged.

4.6.2.1 Time matrices

As shown earlier in this chapter, matrices *Ta* to *Te* are used to define the pseudo inputs in the spline model. These matrices are expressed in terms of the time instants at the sampled knots. Although the knots remain unchanged, the sampling time *To* is no longer constant. Then, time sequence matrices *Ta* to *Te* need to be modified. Let Δta_i be the duration of the control action u. In a variable sampling environment, the control signal vector U_A is given by

$$U_A(t) = [u(t)\Delta ta_1 \; u(t-\Delta ta_2)\Delta ta_2 \cdots u(t-t_1+\Delta ta_n)\Delta ta_n] \qquad (4.48)$$

Under these conditions, the time series matrix Ta is defined as

$$Ta = \begin{bmatrix} 1 & ta_1 & ta_1^2 & ta_1^3 \\ 1 & ta_2 & ta_2^2 & ta_2^3 \\ \vdots & \vdots & \vdots & \vdots \\ 1 & ta_n & ta_n^2 & ta_n h \end{bmatrix} \qquad (4.49)$$

with

$$ta_i = \sum_{n=1}^{i} \Delta ta_i \quad and \quad ta_i < t_2 \qquad (4.50)$$

Similar development should be followed for impulse vectors U_B to U_E and time sequence matrices Tb to Te.

Chapter 5

5. B-SPLINE NON-PARAMETRIC MODELS

5.1 Introduction

As indicated in Chapter 2, b-splines form the basis for all spline functions. In Chapter 4, the approximation of non-parametric models by means of spline polynomials has been developed. There is some similitude between the use of spline and b-spline functions for the approximation of non-parametric models. The most important one is the reduction of the models dimension, allowing the application of traditional adaptive techniques. The resulting adaptive b-spline model (ABM), however, differs in the way it handles the modeling of processes with deadtime. Additionally, the concepts of pseudo inputs and pseudo parameters have simplier and more compact formulation. For these reasons, the use of b-spline models have and advantage over their spline counterparts. The compact formulation of b-spline models make them suitable for the synthesis of MIMO models. Commercial processes like steam generators (Mehra et al., 1982), destillation columns (Richaelt et al., 1978), fluid catalytic cracking and hydrocrackers (Garcia and Prett, 1986 and Cutler and Hawlkins, 1988) and multi-effect evaporation systems (Ricker et al., 1986) are some of the applications most commonly found in industry that may benefit from MIMO b-spline models. Therefore, the development of models based on b-splines is a relevant practical topic.

One of the drawbacks of the MPC with NPM is the derivation of the control law when the process dynamic changes. The tuning of the controller parameters needs to be addressed every time the model is updated. As shown later in this chapter, the b-spline

model presents an alternative to on-line controller parameters tuning. This on-line adaptive tuning is generalized to any type of MPC with NPM, whether they are based on b-spline functions or not. The approach is extended to multirate sampled processes.

5.2 B-spline representation of the plant model

5.2.1 Plant model

The b-spline model of a plant requires the sampling of the impulse or step time response in the same manner as in the classical NPM methods. By conveniently selecting a reduced number of samples at time instants called knots, a set of b-splines are generated. As in the case of spline models, the lower the number of knots used for the b-spline model, the faster the convergence rate of the estimates during the adaptation process. On the other hand, if the number of knots is too small, it can result in a poor modeling of the plant.

The application of the proposed technique requires the selection of the degree of the basis formed by the b-splines. Second degree b-splines are best suited for this task mainly due to their superior approximation properties as compared to b-splines of lower order. Additionally, a higher order b-spline model reduces the need for a large number of knots. The b-splines comply with the mathematical properties described in Chapter 2. The approximation by means of b-splines of a the FIR of a CSTR plant, is shown in Figure 5.1.

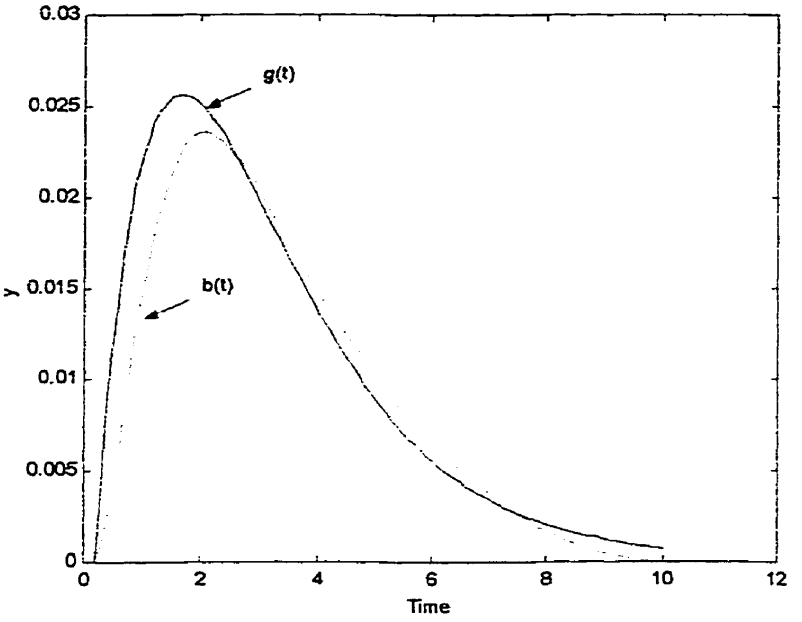

Figure 5.1: FIR of a CSTR given by $g(t)$ and its b-spline approximation, $b(t)$.

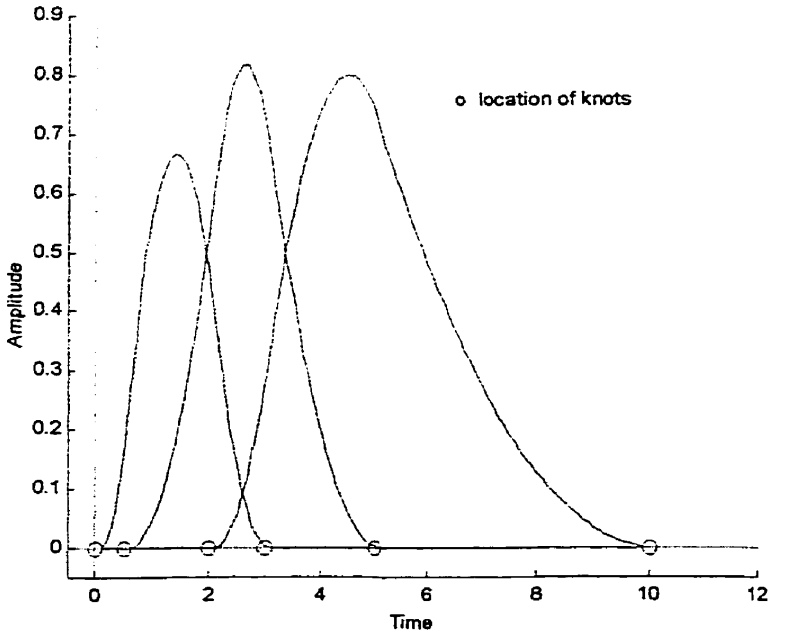

Figure 5.2: Set of b-splines that conforms the basis for $b(t)$.

The b-splines, knot sequences and basis used to approximate the NPM are shown in Figure 5.2. The b-spline basis of the model shown in the above figure remains unchanged throughout the development of the proposed method.

The development of the b-splines model starts from the location of the knots, as shown in Figure 5.2 for a six-knot system ($M = 6$). The set of b-splines are computed using the recursive algorithm described in Chapter 2. The coefficients for the linear combination of the b-splines are computed using the Schoenberg's process as described also in Chapter 2. The expression of the b-spline model of a FIR has the form

$$g(t) \approx b(t) = \sum_{i=-\infty}^{\infty} g(\tau_i) B_i^2(t), \quad \tau_i = \frac{1}{2}(t_{i+1} + t_{i+2}) \tag{5.1}$$

where $g(\tau_i)$ must be evaluated at the midpoints between knots.

Expression (5.1) indicates that the support of b is a basis of infinite b-splines B_i^2. Due to the fact that control theory deals with causal systems, the summation in Expression (5.1) is restricted to $0 \le i$. On the other hand, the NPM are based on a finite time response model, as it is the case of the FIR. Then

$$0 \le i \le M - 3 \tag{5.2}$$

These limitations explain the finite basis shown in Figure (5.2). The truncation of the b-spline basis is of fundamental importance for the proper modeling of plants with deadtime.

5.2.2 *Plant output prediction*

Having the plant model in b-spline form reduces the number of parameters to be estimated. Only the coefficients $g(\tau_i)$ given in Expression (5.1) need to be updated. As indicated earlier, only a limited number of b-splines are required as a basis for the approximation of g. Therefore, there are only M - 3 b-spline coefficients $g(\tau_i)$ to be computed. Based on Equation (4.1) from Chapter 4, and neglecting the disturbances modeled by n, the prediction of the plant output using the b-spline Expression (5.1) has the form

$$\hat{y}(t+To) = \sum_{k=0}^{N} \sum_{i=0}^{M-1} g(\tau_i) B_i^2(kTo)\, u(t-kTo)\, To \qquad (5.3)$$

5.3 Adaptive b-spline model

5.3.1 *Pseudo input signal*

The b-splines B_i^2 in Expression (5.3) are affected by the sequence of input signals u. Then, the plant prediction $\hat{y}$ is obtained by the cumulative effect of the input signal sequence u over each b-spline B_i^2. From Expression (5.3), the plant output prediction is computed as

$$\hat{y}(t+To) = \sum_{i=0}^{M-1} g(\tau_i) \sum_{k=0}^{N} B_i^2(kTo)\, u(t-kTo)\, To \qquad (5.4)$$

or, in compact form,

$$\hat{y}(t+To) = G(\tau)\ B^2\ U_p(t)\ To \tag{5.5}$$

with $G(\tau)$, a 1 by M - 3 vector of b-spline coefficients; B^2 , an M - 3 by N matrix of second order b-splines; and U_p, an N by 1 vector of present and past control actions. Let a pseudo input vector U^B be defined as

$$U^B(t) = B^2\ U_p(t) \tag{5.6}$$

where superscript B is used to highlight the fact that a b-spline basis has been used to define this vector. Then, the plant output prediction is computed as

$$y(t+To) = G(\tau)\ U^B(t)\ To \tag{5.7}$$

Expression (5.7) represents the plant output prediction based on the b-spline model. The b-spline model represented by vector $G(\tau)$ is called the adaptive b-spline model (ABM). It has a dimension equal to M - 3 equal to the number of b-splines that support the approximation of g. Notice that the elements of vector $G(\tau)$ are the samples of g at the mid-point between the knots; thereby, they conform a set of pseudo parameters of the b-spline model.

5.3.2 *Identification*

Using the projection algorithm (PA) and the nomenclature given in Goodwin and Sin (1984), we can obtain estimates of the elements of $G(\tau_t)$. The estimation process requires the computation of the following:

$$G(t+To) = G(t) + \frac{p\,[U^B(t)]^T}{q + U^{B^T}(t)\,U^B(t)}\,c(t) \tag{5.8}$$

where

$$0 < p < 2 \tag{5.9}$$

and

$$q > 0 \tag{5.10}$$

Coefficient p determines the convergence rate, whereas coefficient q is required to avoid singularities during computation.

5.4 Controller design method

The design of a model predictive controller is based on the future behavior of the process over the prediction horizon. The design includes a number of parameters which are adjusted to give the desired response as well as an appropriated amount of controller

effort. When the process dynamic changes, it is necessary to retune the controller parameters. In theory, every time the internal model is updated, the controller must be tuned to achieve a constant performance. The tuning of a predictive controller requires computational effort, creating the need for a systematic approach to reduce this computation.

5.4.1 *Criteria for controller design*

The primary objective of the controller is to determine the sequence of control actions that minimize the sum of the square deviations of the predictive output from the reference trajectory, as well as the control effort. This objective is mathematically expressed as

$$J(U) = E(t)^T W_E E(t) + U(t)^T W_U U(t) \qquad (5.11)$$

where E, is a vector of predicted errors over the prediction horizon; U, a vector of future control sequence over the control horizon; W_E, a weighting matrix for predicted errors and W_U, a weighting matrix for future control moves. Neglecting the model-process mismatch, the error vector E is expressed as

$$E(t) = R(t) - \hat{Y}(t) \qquad (5.12)$$

with R, a vector of future references and $\hat{Y}$, a vector of predicted outputs. Then, the performance criterion (5.11) as a function of the reference trajectory is given by

$$J(U) = (R - \hat{Y})^T W_E (R - \hat{Y}) + U^T W_U U \qquad (5.13)$$

Minimization of the performance criterion (5.13) leads to an expression for the optimal control law (see for instance Seborg *et al.*, 1989). Weighting matrices W_E and W_U are diagonal and, in practice, one of them is kept fixed while the other is tuned to obtain the desired response.

5.4.2 B-spline adaptive predictive controller

The performance criterion (5.13) is valid for any reference trajectory. In particular, it is valid for $R = O$. In this particular case, Expression (5.13) becomes

$$J(U)\big|_{R=O} = \hat{Y}(t)^T W_E \hat{Y}(t) + U(t)^T W_U U(t) \qquad (5.14)$$

The plant output prediction vector $\hat{Y}$ is expressed in terms of the b-spline model $G(\tau)$ and the pseudo inputs U^B as described earlier in this chapter. Based on Expression (5.5), the following augmented matrices are defined:

$$\Gamma = \begin{bmatrix} G(\tau) & O & \cdots & O \\ O & G(\tau) & \cdots & O \\ \vdots & \vdots & \ddots & O \\ O & O & O & G(\tau) \end{bmatrix} \qquad (5.15)$$

a N_P by $N_P \times M$ matrix with N_P equal to the prediction horizon; and

$$\mathrm{B}=\begin{bmatrix} B^2 & \mathrm{O} & \cdots & \mathrm{O} \\ \mathrm{O} & B^2 & \cdots & \mathrm{O} \\ \vdots & \vdots & \ddots & \mathrm{O} \\ \mathrm{O} & \mathrm{O} & \mathrm{O} & B^2 \end{bmatrix} \qquad (5.16)$$

a $N_r \cdot x\ M$ by $N + N_r \cdot - 1$ matrix of b-spline basis functions, with N equal to the model NPM dimension (FIR). Then, Expression (5.14) is transformed into

$$J(U)\big|_{R=\mathrm{O}} = (\Gamma \mathrm{B} U(t) To)^T W_E (\Gamma \mathrm{B} U(t) To) + U(t)^T W_U U(t) \qquad (5.17)$$

By manipulation of the transpose operator, (5.17) is expressed as follows:

$$J(U)\big|_{R=\mathrm{O}} = To U(t)^T \mathrm{B}^T (\Gamma^T W_E \Gamma) \mathrm{B} U(t) To + U(t)^T W_U U(t) \qquad (5.18)$$

Expression (5.18) is the adaptive version of the performance criterion (5.14). The weighting matrix W_{E} is affected by the b-spline coefficients that will adapt to changes of the process dynamic.

5.4.2.1 Weighting matrix adaptation

Let us consider a time-variant process at two different time instances t_1 and t_2. Form the controller standpoint, we are in the presence of different plants. Let Γ_1 and Γ_2 be the matrices of b-spline model coefficients at t_1 and t_2 respectively. It is interesting to show how the weighting matrices W_E and W_U of a predictive controller have to be modified in order to maintain the same performance. To this end, the process response to a step reference is analyzed at these two time instants.

Let $\hat{Y}_1$ and $\hat{Y}_2$ be the vectors of the plant output predictions for the process with the dynamics at time t_1 and t_2 respectively, subject to the same control action U. Figure 5.3 shows a schematic representation of the time response for a step reference with final plant output value equal to zero.

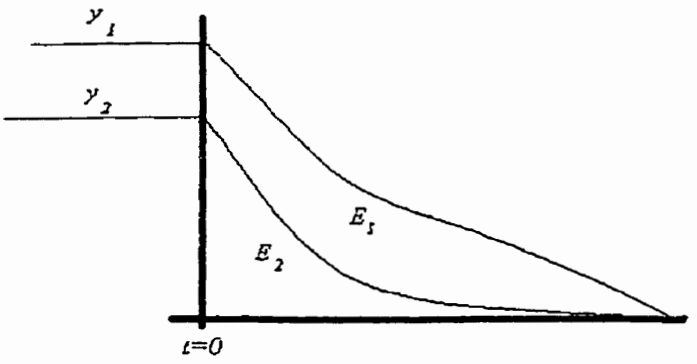

Figure 5.3: Step time responses of the same process with changed dynamics.

Figure 5.3 shows that the difference in time responses result in different sequence of tracking errors given by E_t. Equal performance of the controller at times t_1 and t_2 requires that the performance criterion $J(U)$ remains constant. Due to the fact that the same sequence of control moves U is applied to both plants, obtaining a constant performance requires that W_E and W_U must be modified. In practice, only one matrix is changed at a time, therefore, the elements of W_E are chosen as the tuning parameters.

Denoting as $J_1(U)$ and $J_2(U)$ the performance criteria for instants t_1 and t_2, the adaptive tuning of the controller requires that

$$J_1(U)\big|_{R=0} = J_2(U)\big|_{R=0} \qquad (5.19)$$

for equal U. Then, the following condition is derived

$$\Gamma_1^T W_{E1} \Gamma_1 = \Gamma_2^T W_{E2} \Gamma_2 \qquad (5.20)$$

Assuming that the controller is tuned at instant t_1, W_{E2} is expressed as a function of the W_{E1} as follows:

$$W_{E2} = (\Gamma_2 \Gamma_2^T)^{-1} \Gamma_2 \Gamma_1^T W_{E1} \Gamma_1 \Gamma_2^T (\Gamma_2 \Gamma_2^T)^{-1} \qquad (5.21)$$

where the concept of pseudo-inverse matrix introduced by Penrose (1956) has been used. Further reduction of the Expression (5.21) is achieved by considering that

$$(\Gamma_2\Gamma_2^T)^{-1} = \frac{I}{\sum_{i=1}^{M-3}(g_2(\tau_i))^2} \qquad (5.22)$$

and

$$\Gamma_1\Gamma_2^T = I\sum_{i=1}^{M-3} g_2(\tau_i)g_1(\tau_i) \qquad (5.23)$$

where I is the identity matrix of dimension M - 3 by M - 3 and $g(\tau_i)$ are the b-spline coefficients defined in Expression (5.1). Finally, the adaptive tuning law is written as

$$W_{E2} = \left(\frac{\sum_{i=1}^{M-3} g_1(\tau_i)g_2(\tau_i)}{\sum_{i=1}^{M-3} g_2(\tau_i)^2}\right)^2 W_{E1} \qquad (5.24)$$

or

$$W_{E2} = K_E{}^2 W_{E1} \qquad (5.25)$$

Notice that the dimension M - 3 is given by the number of b-spline functions that form the basis of the plant model.

5.4.3 *Generalized weighting matrix adaptation*

The concept of weighting matrix adaptation developed in the above subsection is a particular case of a technique that includes a larger class of models.

Let a NPM be represented by its FIR given by g of dimension N. This NPM can be approximated by a b-spline model. Let $G(\tau)$ be the vector of coefficients of the b-spline basis. According to the Schoenberg's process reviewed in Chapter 2, the elements of $G(\tau)$ are given by g evaluated at the midpoints between the knots. It is feasible to assign the value of the weighting coefficients of g to the elements of $G(\tau)$, resulting in a b-spline coefficients vector of dimension N. These coefficients are, in terms, associated to the b-spline basis that is the support for the approximation of g. Each b-spline requires the selection of knots that, for consistency with the elements of $G(\tau)$ defined above, should be arbitrarily positioned around each sample of g. Figure 5.4 shows a schematic representation of the steps followed in the generation of this b-spline basis.

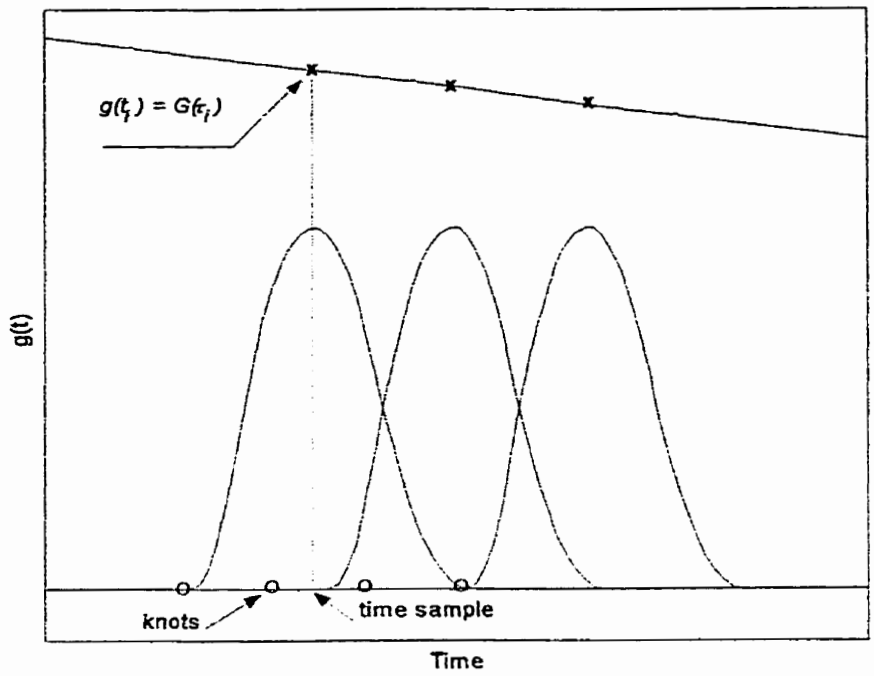

Figure 5.4: B-spline basis and FIR sampled data.

Under the conditions described above, the adaptive tuning law given by Expression (5.24) is generalized as

$$W_{E2} = \left(\frac{\sum_{i=1}^{N} g_1(t_i) g_2(t_i)}{\sum_{i=1}^{N} g_2(t_i)^2} \right)^2 W_{E1} \qquad (5.26)$$

where the coefficients of the b-spline model have been replaced by the samples of the FIR. Notice that the generalized weighting matrix adaptation is independent of the b-spline basis, therefore, it is valid for both b-spline models and non-b-spline models alike.

5.4.4 Multirate sampling environment

The case of multirate sampling environment was first introduced in Chapter 4. When the plant FIR model is approximated by b-slpines, the weighting coefficients can be recovered by interpolation. It is critical to address, however, the tuning of weighting matrices W_E and W_U after a change in the control sampling time.

When the controller is initially tuned for the nominal sampling time T_0, a decision is made in regards to the control and prediction horizons. These horizons play an important role in the performance of the predictive controller as reported in Seborg et al.,(1989) and Isermann *et al.*,(1992). In general terms, the horizons are tuning parameters that relate the effect of the control actions and the plant output predictions with respect to the open-loop time response. Therefore, the nominal FIR of the nominal plant (i.e. the FIR of the plant with sampling time T_0) is the sampling time invariant used as a reference to determine the new horizons when the sampling time is changed. From the analysis of Expression (5.11), it is clear that vectors E and U as well as matrices W_E and W_U will change dimensions when the sampling time is changed.

At first glance, it can be stated that the re-tuning of the weighting matrices W_E and W_U only requires the truncation of the columns and rows beyond the new control and predictions horizons. The justification for this statement is that the change of sampling time does not change the dynamic of the plant. However, one of the motivations for the

change of sampling time is the reduction of the control action. Then, the validity of the assumption of the truncation of the weighting matrices remains to be proven.

5.4.4.1 Proposition 5.1

Let the weighting matrices W_E and U_E of the criterion performance

$$J(U) = E^T W_E E + U^T W_U U \qquad (5.27)$$

be diagonal and of equal elements w_E and w_U respectively. Let two distinct sampling times T_0 and T_1, produce two performance criteria $J_0(U)$ and $J_1(U)$. Let also N_{Y0} and N_{Y1} be integer numbers representing the prediction horizons of the plant output for each sampling time. Similarly, let N_{U0} and N_{U1} be integer numbers representing the control actions horizons for each sampling time. Let us impose the following conditions to the sampling time and horizons:

$$N_{Y1} = \frac{T_1}{T_0} N_{Y0} \quad and \quad N_{U1} = \frac{T_1}{T_0} N_{U0} \qquad (5.28)$$

Then, equal performance criteria for both sampling times requires that

$$\frac{w_{E0}}{w_{E1}} = \frac{w_{U0}}{w_{U1}} \qquad (5.29)$$

Proof

In regards to the expression for the performance criterion (5.27), it is possible to evaluate $J(U)$ for the case that the plant and controller are in steady state with two different sampling times. Given the fact that the sampling time does not affect the response of the system controller-plant in steady state, the same mismatch occurs between the reference trajectory and the plant output for sampling times T_0 or T_1. Then, the elements the error the vector E are constant and equal for both sampling times. Additionally, the control actions given by the elements of U are also constant and equal for both sampling times. Therefore, the performance criteria for the controller with sampling times T_0 and T_1 in steady state are given by

$$J_0(U)\big|_{R=const.} = \sum_{i=1}^{N_{E0}} e_i^{\,2} w_{E0i} + \sum_{i=1}^{N_{U0}} u_i^{\,2} w_{U0i} \qquad (5.30)$$

and

$$J_1(U)\big|_{R=const.} = \sum_{i=1}^{N_{E1}} e_i^{\,2} w_{E1i} + \sum_{i=1}^{N_{U1}} u_i^{\,2} w_{U1i} \qquad (5.31)$$

Expressions (5.26) and (5.27) are simplified as follows:

$$J_0(U)\big|_{R=const.} = N_{E0} e^2 w_{E0} + N_{U0} u^2 w_{U0} \qquad (5.32)$$

and

$$J_1(U)\big|_{R=const.} = N_{U1}e^2 w_{E1} + N_{U1}u^2 w_{U1} \qquad (5.33)$$

The horizons of the plant output prediction and the control actions for each sampling time are related by Expression (5.28) of the hypothesis. For equal performance criteria $J_0(U)$ and $J_1(U)$, the combination of Expressions (5.28), (5.32) and (5.33) results in

$$\frac{w_{E0}}{w_{E1}} = \frac{w_{U0}}{w_{U1}} \qquad (5.34)$$

□

5.4.4.2 Corollary 5.2

Expression (5.34) shows that the re-tuning of the controller weighting matrices W_E and W_U is possible by changing their dimensions. This conclusion stems from the fact that only the relative weight between the elements of w_E and w_U is relevant in the minimization of Expression (5.27). Then, imposing the condition $w_{U0} = w_{U1}$ to the elements of the control action weighting matrix determines that $w_{E0} = w_{E1}$ for equally tuned controllers. Therefore, the change of the dimension of W_E and W_U does not affect the performance of the controller for different sampling times.

Remark 5.1

When condition (5.28) does not apply, that is

$$\frac{T_1}{T_0}N_{V0} \quad and \quad \frac{T_1}{T_0}N_{U0} \tag{5.35}$$

are not integers, Expression (5.34) gives only approximated controller performances.

5.5 Processes with deadtime

5.5.1 Introduction

Deadtime estimation is a critical factor during the development of a plant model. Errors in the estimation of the deadtime generate structured uncertainties that affect overall performance of the controller. Results from simulations (Camacho and Bordons, 1999) have shown that for small plant deadtimes, the stability of the system controller-plant is guaranteed for models with large deadtime errors. However, for processes with deadtimes in the order of ten time steps only a model error of one step is allowed. It can be said, that good deadtime estimation is fundamental because, for errors larger than one time step unit, the system can become unstable if the deadtime is high.

From the point of view of the robust analysis (Morari and Zafiriou, 1989), the robust stability is affected only by the deadtime error but not by the absolute value of the deadtime. On the other hand, for robust performance, both, the deadtime error and the absolute value have to be considered.

5.5.2 B-spline models with deadtime

The representation of non-parametric models by b-splines allows the adaptation of the model to changes of the process deadtime. Conveniently selecting the set of knots that define the location of the b-spline basis, the deadtime is estimated as a parameter. In Chapter 6, the performance of the ABM for a plant with variable deadtime is studied.

5.6 Global uncertainties for b-spline models

The impact of model uncertainties in the plant output prediction is analyzed in this section. The methodology followed in Chapter 4 is used here to obtain an expression for the global uncertainties in the presence of b-splines models.

Based on Expression (4.41), the prediction of the plant output using b-splines when model uncertainties are considered takes the form

$$\hat{y}(t+To) = G(\tau)\, U^{B}(t)\, To + \theta(t+To) \tag{5.36}$$

By making the analogy to the spline model uncertainties given in Expressions (4.42) and (4.43), the b-spline model uncertainties are determined by computing the following expressions:

$$\underline{\theta} = \min_{u.\theta_G} \theta_G U^{B}(t) \tag{5.37}$$

$$\overline{\theta} = \max_{u.\theta_G} \theta_G\, U^{B}(t) \tag{5.38}$$

where θ_G denotes the uncertainties in the evaluation of the b-spline coefficients.

5.7 B-spline models for MIMO systems

The results obtained in this chapter for the approximation of NPM using b-splines are extended to multiple-input multiple-output (MIMO) systems, by using the principle of superposition (Seborg et al., 1989). For a system having two inputs and two outputs, the b-spline MIMO model becomes

$$\begin{bmatrix} \hat{y}_1(t+To) \\ \hat{y}_2(t+To) \end{bmatrix} = \begin{bmatrix} G_{11}(\tau) & G_{12}(\tau) \\ G_{21}(\tau) & G_{22}(\tau) \end{bmatrix} \begin{bmatrix} B^2 & O \\ O & B^2 \end{bmatrix} \begin{bmatrix} u_1(t) \\ u_2(t) \end{bmatrix} \qquad (5.39)$$

where $\hat{y}_1$ and $\hat{y}_2$ denote the prediction of the plant outputs; u_1 and u_2, the plant inputs and $G_{ij}(\tau)$ the b-spline coefficient sub-matrices. Notice that in this particular case, the same b-spline basis is used for both input signals, that is, they share the same knots sequence.

Chapter 6

6. SIMULATION OF A CSTR

In this chapter, the spline and b-spline techniques are tested. The process chosen for the simulation is a continuously stirred tank reactor (CSTR).

6.1 Continuous stirred tank reactor

To illustrate the performance of the proposed adaptive techniques, let us consider the first-order, exothermic, irreversible reaction A→B that is carried out in a well mixed CSTR (Uppal *et al*, 1974) shown in Figure 6.1.

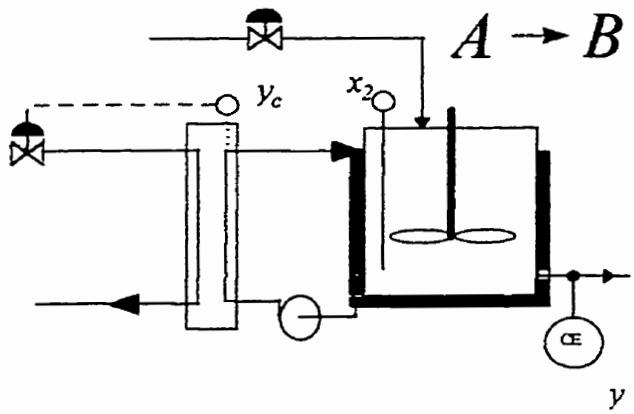

Figure 6.1: Simplified diagram of a CSTR.

The system consists of a constant-volume reactor that is cooled by a single coolant stream. The objective is to control the effluent concentration from the tank by manipulating the cooling jacket temperature. The process model consists of two nonlinear ordinary

differential equations (NDE), describing the material and energy balances. These equations are

$$\frac{dy}{dt} = -y + Da(1-y)\exp\left(\frac{x_2}{1+\frac{x_2}{\gamma}}\right) \qquad (6.1)$$

$$\frac{dx_2}{dt} = -x_2 + BDa(1-y)\exp\left(\frac{x_2}{1+\frac{x_2}{\gamma}}\right) + \beta(yc - x_2) \qquad (6.2)$$

The state y stands for the composition, and x_2 denotes the temperature. The manipulated variable is the cooling jacket temperature y_c. As opposed to the case study reported by Piovoso *et al.* (1992), the composition y is assumed measurable.

6.1.1 Plant parameters

The parameters used in the simulation are: $D_a = 0.072$, $\gamma = 20.0$, $B = 8.0$, and $\beta = 0.3$. These parameters are dimensionless variables described by Uppal *et al* (1974) and they are related to the material and energy coefficients of the CSTR. The value selected for these parameters coincide with those chosen by Henson and Seborg (1997).

6.2 Non-parametric model

For the present analysis, a sampling time *To* of 0.1 time units is selected. The CSTR impulse time response is obtained by increasing the cooling jacket temperature y_c in 10

units during one sample. Solving simultaneously Equations (6.1) and (6.2) we arrive to the FIR that is shown in Figure 6.2, for two different values of the Damköhler number (D_a).

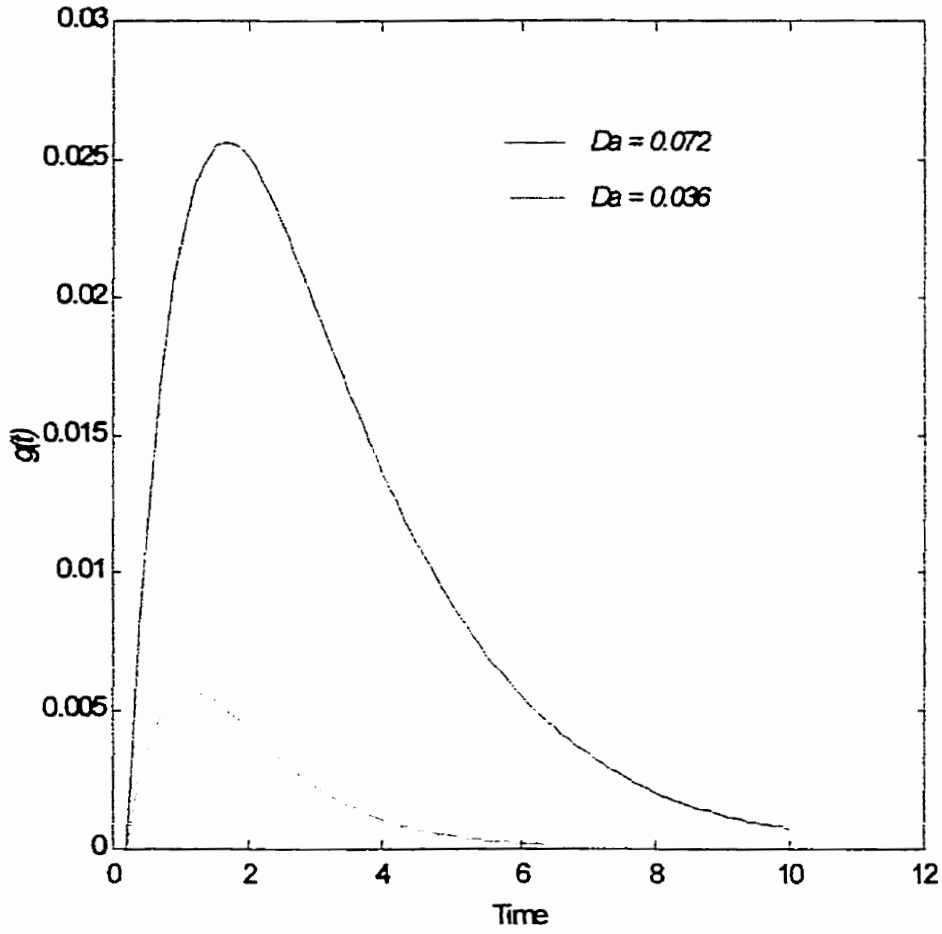

Figure 6.2: CSTR FIR for two different Damköhler numbers (D_a).

Table 6.1 shows the convolution model coefficients (g_i) for $0 \leq t \leq 10$ and $To = 0.1$.

Table 6.1: Impulse response coefficients for To = 0.1.

Sampling instant	FIR coefficients (10^{-3})	Sampling instant	FIR coefficients (10^{-3})	Sampling instant	FIR coefficients (10^{-3})	Sampling instant	FIR coefficients (10^{-3})
0.1	0	2.6	2.8172	5.1	0.3795	7.6	0.0372
0.2	1.5070	2.7	2.6310	5.2	0.3473	7.7	0.0337
0.3	2.7022	2.8	2.4535	5.3	0.3177	7.8	0.0306
0.4	3.6347	2.9	2.2848	5.4	0.2905	7.9	0.0278
0.5	4.3465	3.0	2.1249	5.5	0.2655	8.0	0.0252
0.6	4.8736	3.1	1.9739	5.6	0.2426	8.1	0.0229
0.7	5.2466	3.2	1.8315	5.7	0.2215	8.2	0.0207
0.8	5.4920	3.3	1.6975	5.8	0.2023	8.3	0.0188
0.9	5.6323	3.4	1.5718	5.9	0.1846	8.4	0.0170
1.0	5.6864	3.5	1.4541	6.0	0.1684	8.5	0.0154
1.1	5.6707	3.6	1.3439	6.1	0.1536	8.6	0.0140
1.2	5.5989	3.7	1.2410	6.2	0.1400	8.7	0.0127
1.3	5.4829	3.8	1.1451	6.3	0.1276	8.8	0.0115
1.4	5.3322	3.9	1.0558	6.4	0.1162	8.9	0.0104
1.5	5.1554	4.0	0.9728	6.5	0.1059	9.0	0.0094
1.6	4.9592	4.1	0.8956	6.6	0.0964	9.1	0.0085
1.7	4.7495	4.2	0.8240	6.7	0.0878	9.2	0.0077
1.8	4.5311	4.3	0.7577	6.8	0.0799	9.3	0.0070
1.9	4.3079	4.4	0.6963	6.9	0.0726	9.4	0.0063
2.0	4.0832	4.5	0.6395	7.0	0.0661	9.5	0.0057
2.1	3.8596	4.6	0.5870	7.1	0.0601	9.6	0.0051
2.2	3.6391	4.7	0.5385	7.2	0.0546	9.7	0.0047
.23	3.4235	4.8	0.4937	7.3	0.0496	9.8	0.0042
2.4	3.2140	4.9	0.4525	7.4	0.0451	9.9	0.0038
2.5	3.0117	5.0	0.4145	7.5	0.0409	10	0.0034

6.3 Spline plant model

In this section, a spline functions based model of the CSTR is developed using the guidelines detailed in Chapter 4. The plant model in spline form is obtained by sampling the FIR that is shown in Figure 6.2 ($D_a = 0.072$). The knots and the samples of the FIR at these knots are listed in Table 6.2. The interpolating polynomials coefficients are listed in Table 6.3.

Table 6.2: CSTR - FIR samples at the knots

Knots	0	2.0	4.0	6.0	8.0	10
Samples	0.0000	0.0250	0.0137	0.0056	0.0021	0.0007

Table 6.3: Interpolating splines coefficients

	Coefficients				
Sub-index	*a*	*b*	*c*	*d*	*e*
0	0.0000	0.0250	0.0137	0.0056	0.0021
1	0.0181	0.0033	-0.0082	-0.0021	-0.0013
2	0.0000	-0.0078	0.0020	0.0002	0.0002
3	-0.0014	0.0016	-0.0002	0.0000	0.0000

6.3.1 Plant output prediction

In order to compare the performance of the traditional NPM and the ASM a series of tests are performed for different plant conditions.

6.3.1.1 Non-linear time invariant case (NTI)

The CSTR is excited with a train of cooling jacket step references. The performance of the non-parametric model (NPM) and the spline adaptive model (ASM) are compared in Figure 6.3. From this figure, it becomes clear that both, the NPM and ASM, have good performance for one step ahead prediction and there are no distinguishable differences.

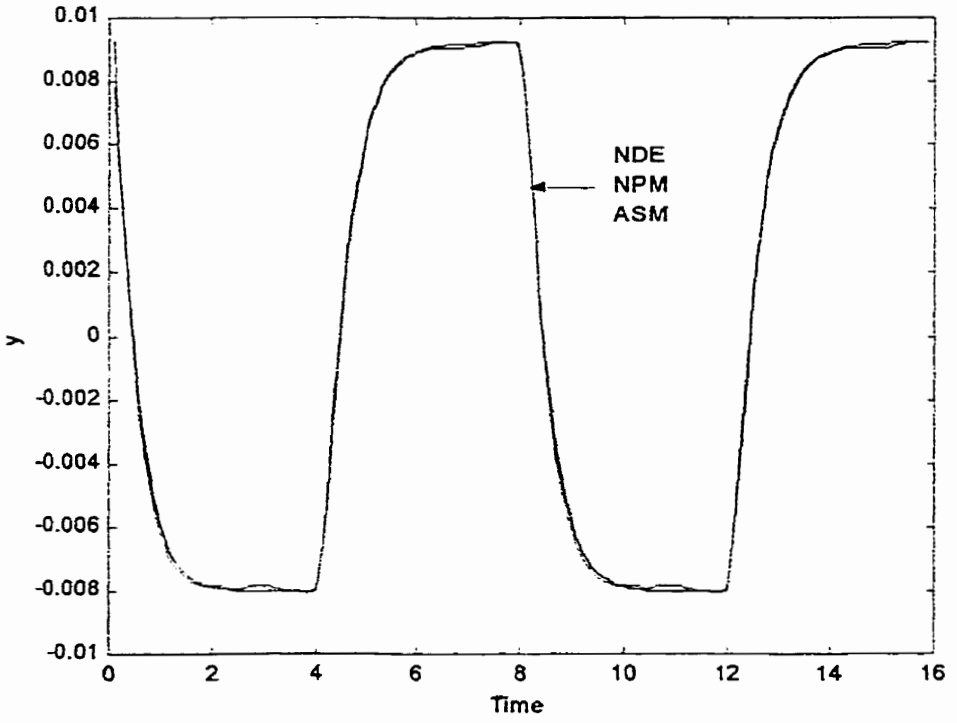

Figure 6.3: Plant output prediction of NPM and ASM compared to the NDE for a sequence of cooling jacket temperature changes (± 10%).

To determine the correction effort made by both models, Equation (4.3) is evaluated at every time step and the results are plotted. The results are visualized in Figure 6.4, from where we conclude that the correction effort due to model mismatch is larger for the NPM than the ASM, which is practically zero.

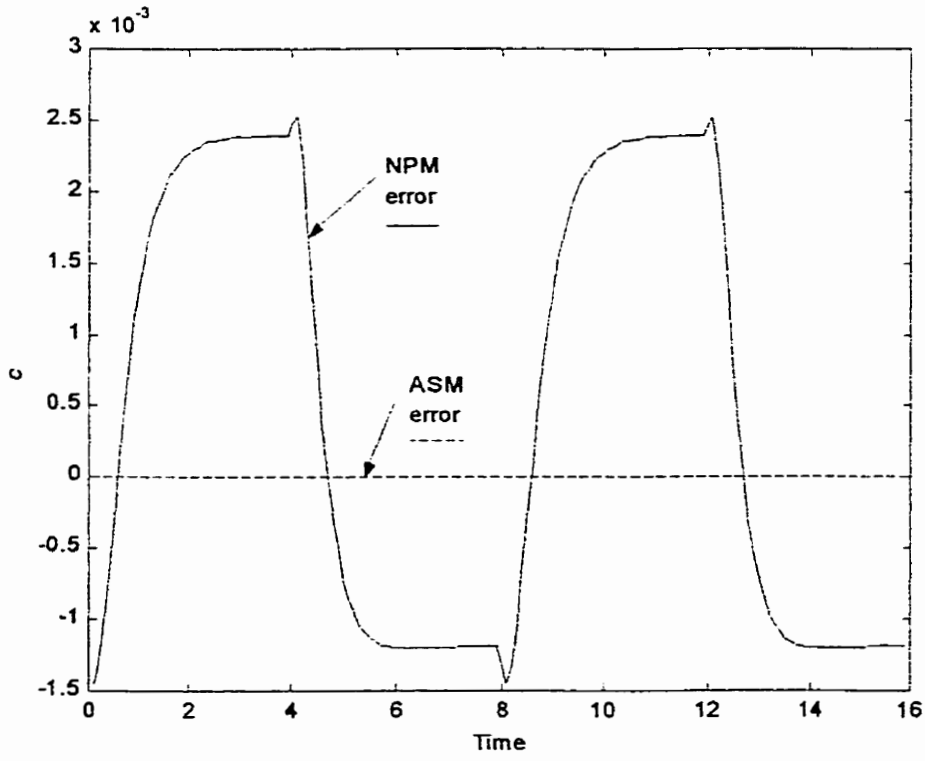

Figure 6.4: Correction effort made by both, the NPM and ASM for one step ahead prediction.

The model-process mismatch affects long-term prediction for multiple steps horizons. Therefore, the ASM proves to have superior prediction capabilities in this case of NTI processes. Notice that the model requires asymmetric prediction correction for the NPM; this is the result of the nonlinear behavior of the CSTR. The smaller correction effort of the ASM, as compared to the NPM, is due to the adaptation of the so called pseudo parameters. The time variation of these pseudo parameters is shown in Figure 6.5.

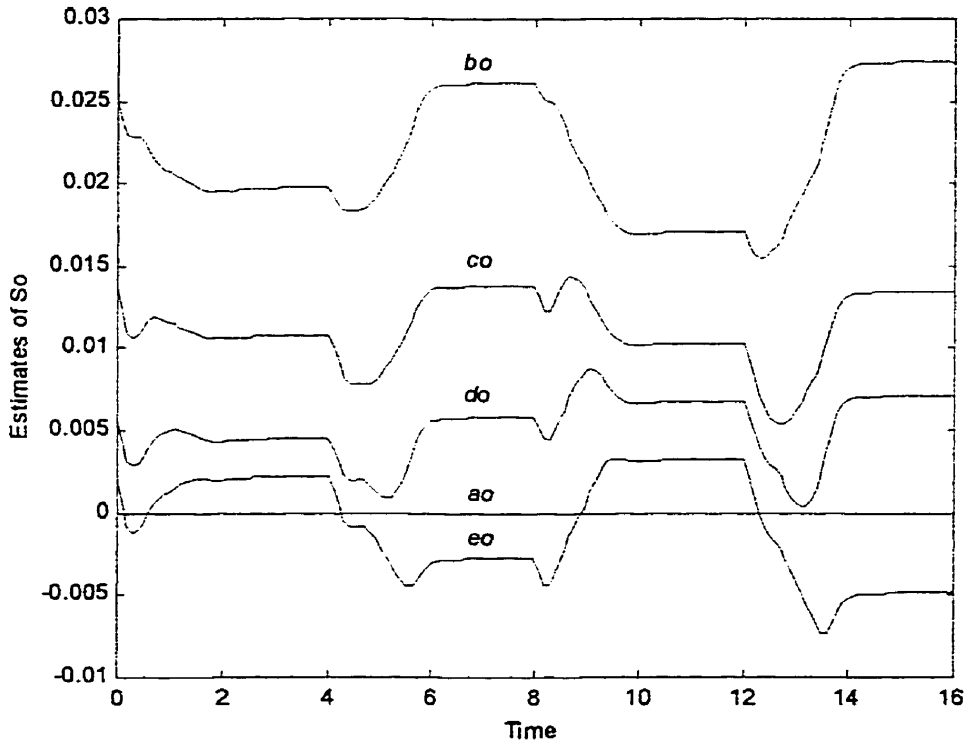

Figure 6.5: Estimation of the spline coefficients or pseudo parameters of the ASM for a NTI process.

As described in Chapter 4, the rate of convergence and sensitivity of the adaptation process is determined by the coefficient p. Convergence of the estimates on the ASM is subject to the limitations imposed to the PA for classical models (Miller 1997).

6.3.1.2 Non-linear time variant case (NTV)

The CSTR is excited with a sequence of changes in the jacket cooling temperature; this time, however, the Damköhler number D_a is slowly reduced at a rate of 0.1% per sample. The prediction capability of the ASM, as compared to the NPM, for a total reduction of 50% in the Damköhler number D_a is shown in Figure 6.6.

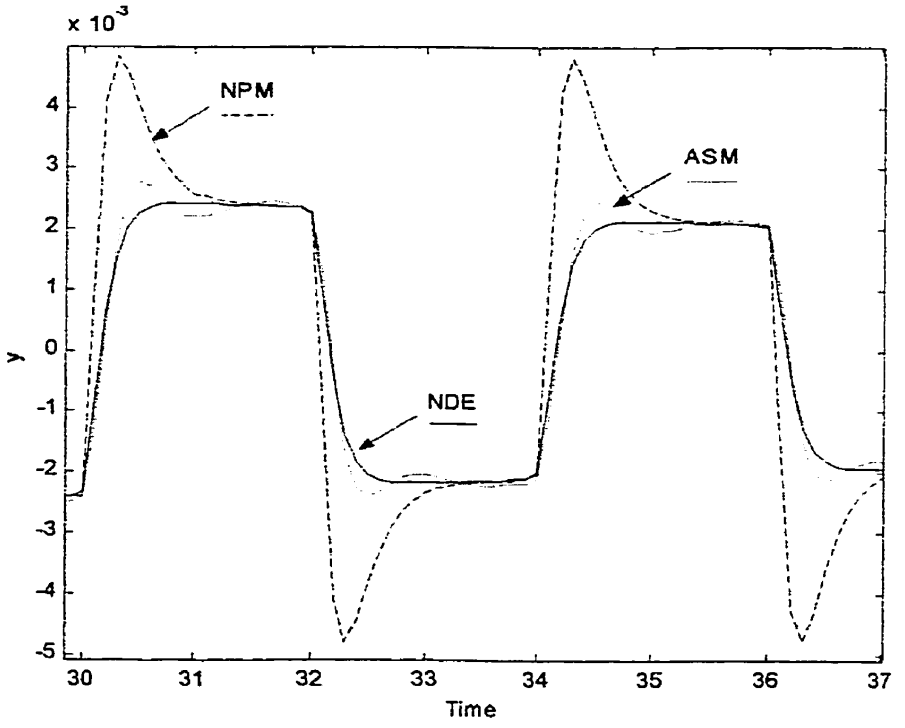

Figure 6.6: Plant output prediction of NPM and ASM compared to the NDE, for a sequence of cooling jacket temperature changes and a slow change of the Damköhler number D_a.

It becomes clear from Figure 6.6 that the model mismatch of the NPM degrades the prediction capabilities when sudden changes occur in the control variable. However, the prediction capabilities reappear once the process is in steady state. An explanation of this phenomenon is that the prediction correction of the NPM given by Expression (4.3) addresses model offsets but ignores dynamic mismatches. This is the trade-off to be considered when the simplicity of the NPM is preferred as opposed to more complex methods. Notice that the reduction of the Damköhler number D_a affects the amplitude of the plant step response. This explains why Figures 6.3 and 5.6 differ in the amplitude of the plant output time response.

The adaptation of the pseudo parameters (samples at the knots) of the ASM is shown in Figure 6.7. This adaptation allows the superior prediction performance of the ASM as compared to the NPM.

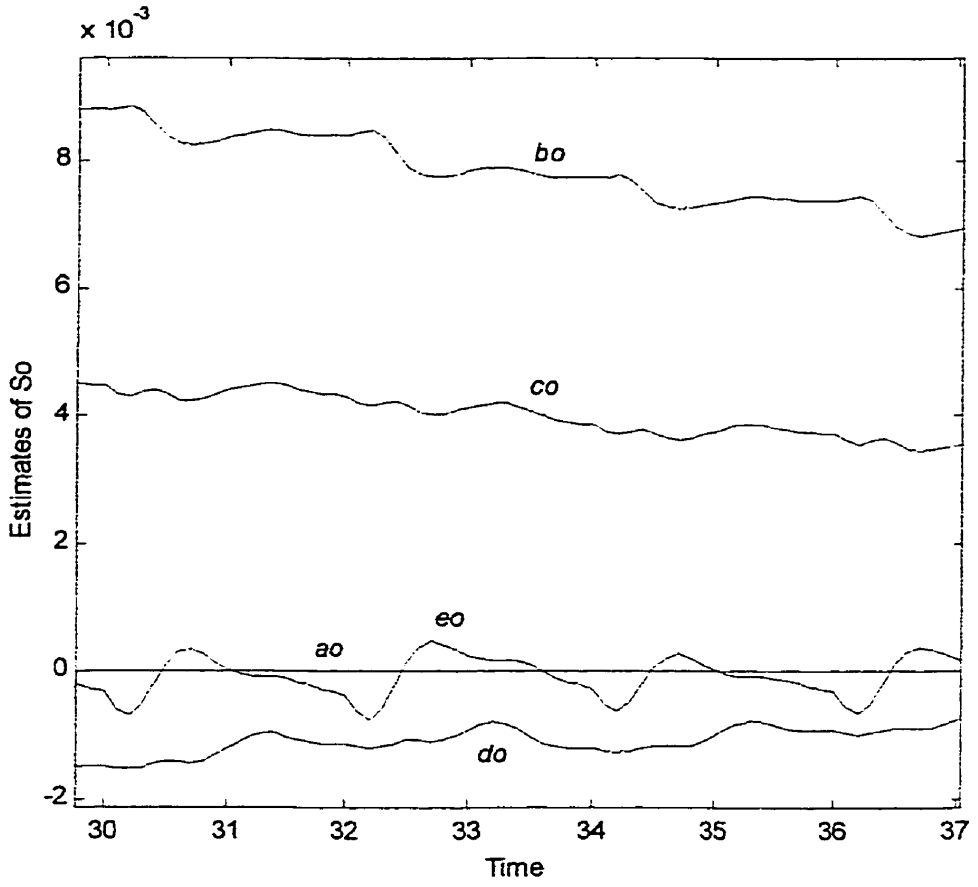

Figure 6.7: Convergence of the estimates of the spline coefficients or pseudo parameters of the ASM for a NTV plant.

6.4 B-spline plant model

The b-spline model of the plant is obtained by sampling the FIR of the CSTR shown in Figures 6.2 ($D_a = 0.072$) and following the steps described in Chapter 5. The results are shown in Figure 6.8 and listed in Table 6.4.

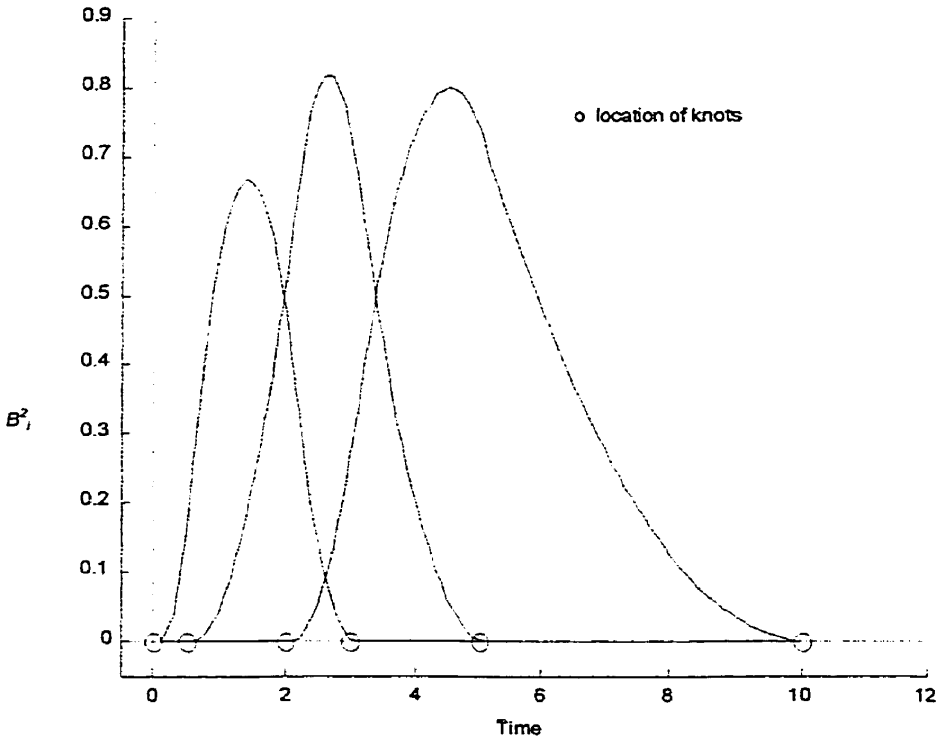

Figure 6.8: Set of B-splines that conforms the basis for $b(t)$.

Table 6.4: Knots sequence and b-spline coefficients.

t_i	0	0.5	2.0	3.0	5.0	10
$g(\tau_i)$	0	0.0247	0.0228	0.0137	0	

6.4.1 Plant output prediction

6.4.1.1 Non-linear time invariant case (NTI)

The CSTR is excited with a train of cooling jacket step references. The performance of the non-parametric model (NPM) and the b-spline adaptive model (ABM) are compared in Figure 5.9. From this figure, it becomes clear that both, the NPM and ABM, have good prediction performance for one step ahead in the time sequence and there is no distinguishable differences between them.

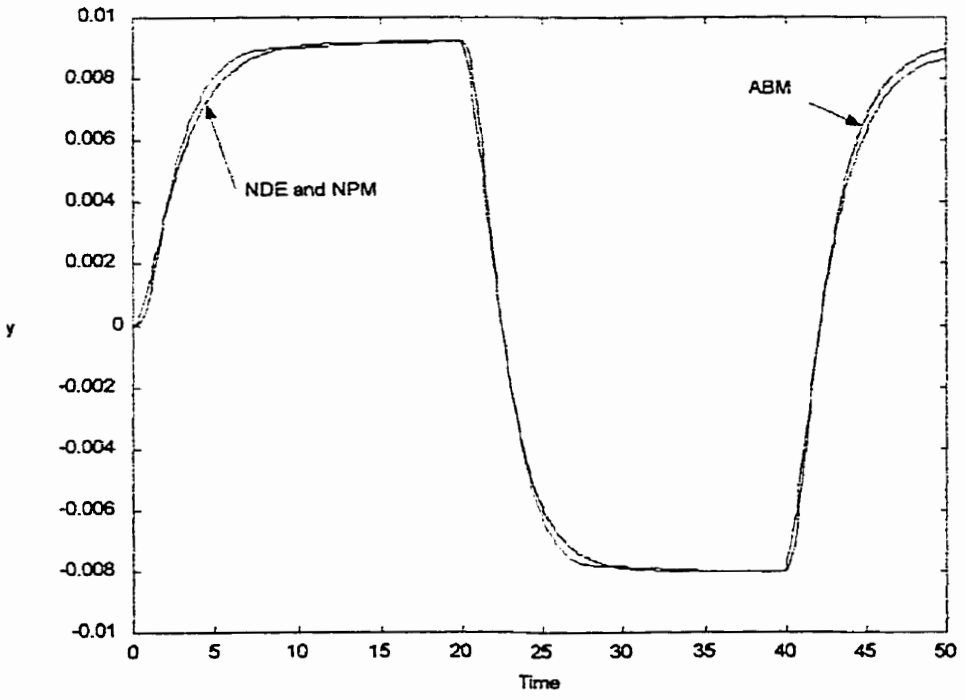

Figure 6.9: Plant output y (NDE) compared to plant output prediction $\hat{y}$ (NPM and ABM).

6.4.1.2 Non-linear time variant case (NTV)

The CSTR is excited with a sequence of changes in the jacket cooling temperature; this time, however, the Damköhler number D_a is reduced in 80% of its original value. The prediction capability of the ABM, as compared to the NPM, for a reduced Damköhler number D_a is shown in Figure 6.10. This figure shows that the ABM predicts the plant output with minimum error, having superior performance than the NPM.

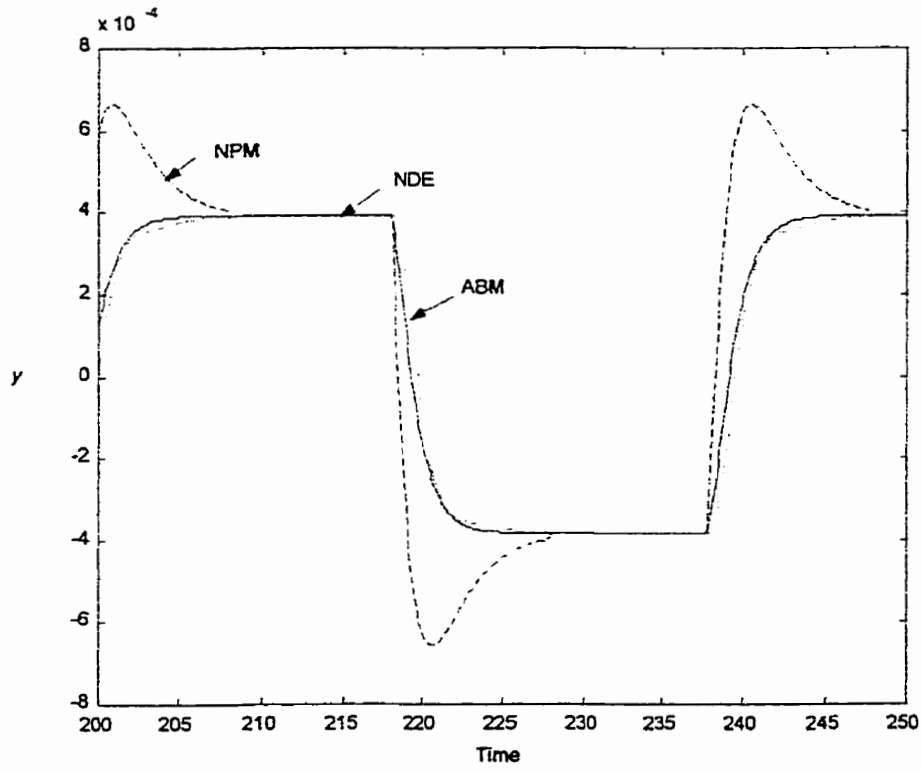

Figure 6.10: Plant output prediction performance for 80% reduction of D_a.

6.4.2 *Plant with deadtime*

A deadtime of five times *To* is introduced in the simulated CSTR plant. When the identification of the plant is initiated, the ABM undergoes a parameter adaptation process that results in a shifting of the FIR as shown in Figure 6.11.

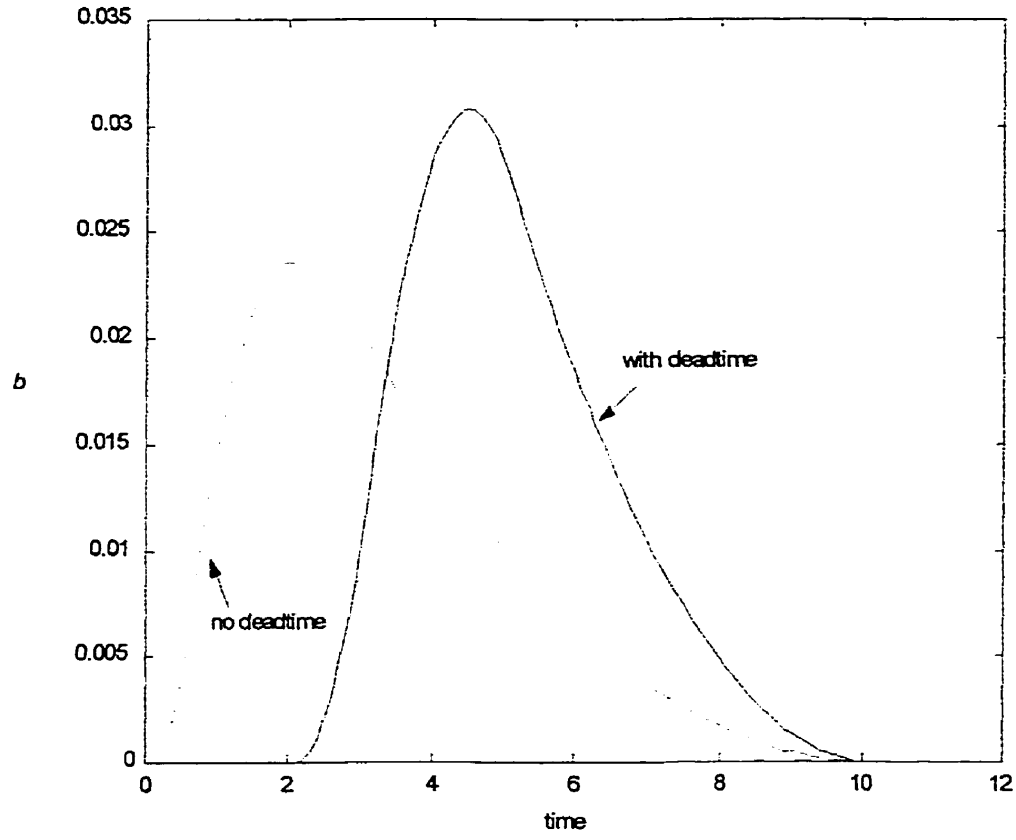

Figure 6.11: Deadtime identification by the ABM model.

We see in Figure 6.11 the ability of the model to adjust to the new environment with process deadtime. The b-spline coefficients undergo the transformation depicted in Figure 6.12.

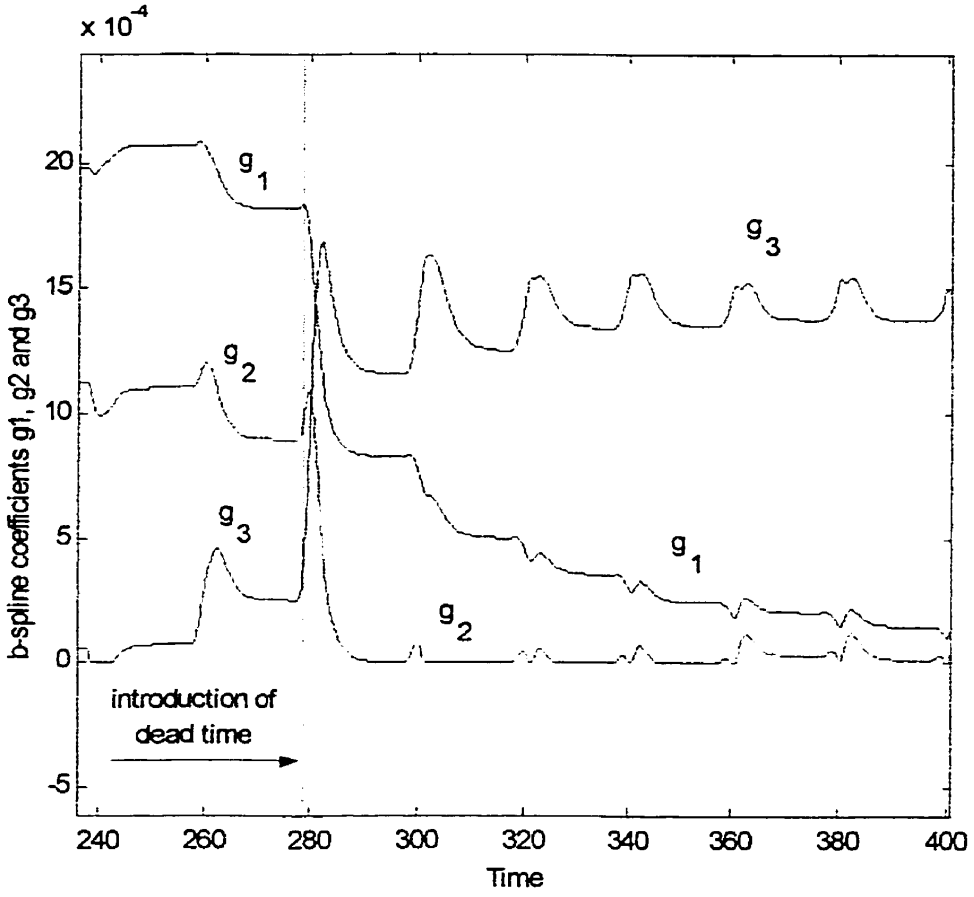

Figure 6.12: Convergence of the estimates when a process deadtime is introduced.

It becomes clear from Figures 6.11 and 6.12 that the proper selection of the knots as well as the number of b-spline basis is a critical issue.

Figure 6.13 shows the improved performance of the ABM model compared to the NPM when the plant presents variations on the deadtime and the coefficient D_a simultaneously.

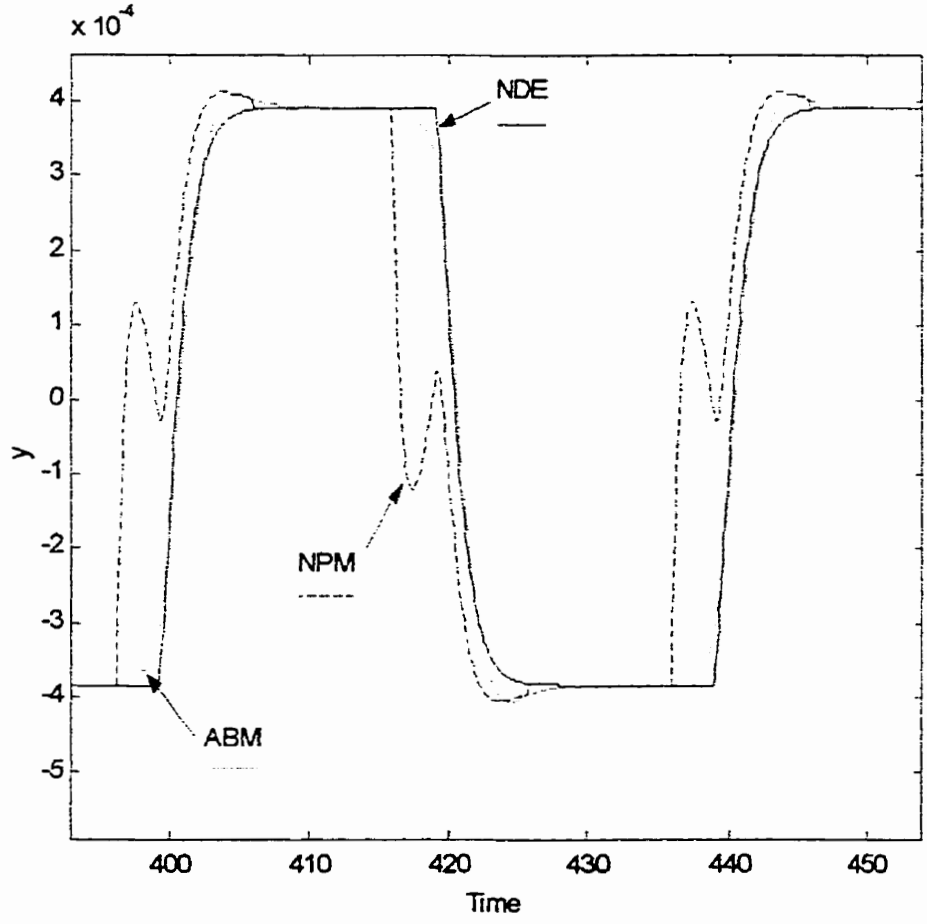

Figure 6.13: NDE, NPM and ABM performances after the introduction of a deadtime in the CSTR model and a change of the D_a.

Figure 6.13 clearly shows how the presence of process deadtime seriously affects the prediction performance of the NPM. On the other hand, the ABM closely predicts the plant output (NDE).

6.5 B-spline adaptive predictive controller

In this simulation, the theory of the b-spline adaptive predictive controller is tested. The controller is initially tuned with the set of parameters listed in Table 6.5. An integral action is also added to the controller to complete the design.

Table 6.5: Predictive controller parameters.

Parameter	Setting
N_U	1
N_Y	10
W_E	I : identity matrix
W_U	0.02 I

6.5.1 Control of a time varying process

The simulation of the plant-predictive controller system for Da = 0.072 result in the tracking time response shown in Figure 6.14. When the Damköhler number is set at 80% of its original value, the tracking capabilities of the predictive controller are significantly degraded as concluded from the analysis of Figure 6.15. The change in the process

dynamics captured by the controller internal model (a b-spline model in this case), substantially affects the performance of the controller. Figure 6.16 shows the improved performance of the plant-predictive controller system when a b-spline adaptive predictive controller is used. In this case, the weighting matrix of the prediction errors W_E is re-tuned from $W_E = I$ to $W_E = 4.8\, I$.

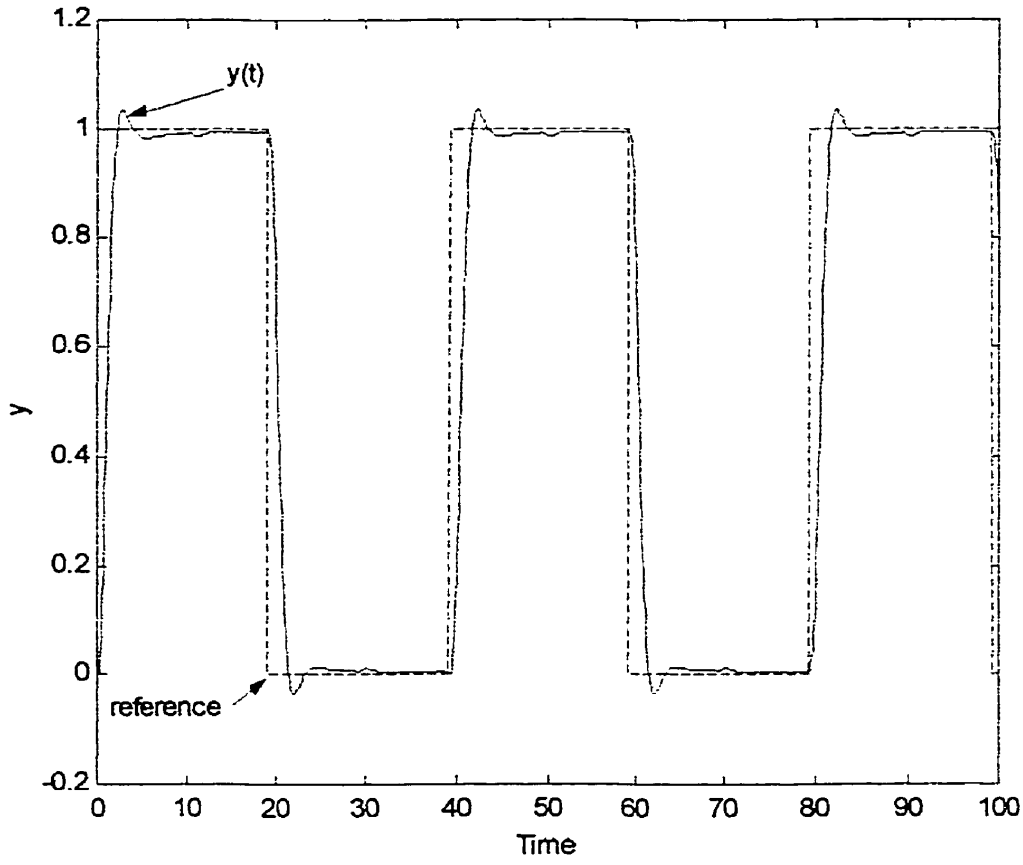

Figure. 6.14: Predictive controller tracking for D_a=0.072.

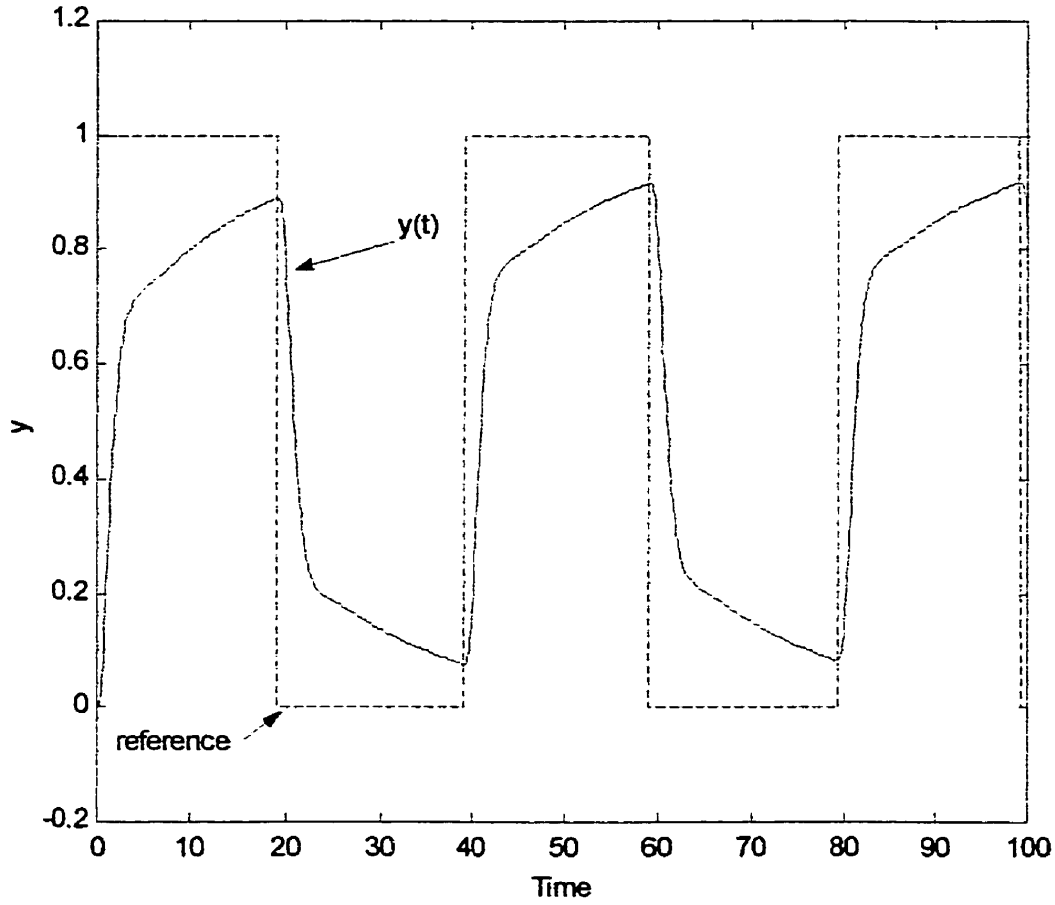

Figure 6.15: Predictive controller tracking for D_a=0.0576.

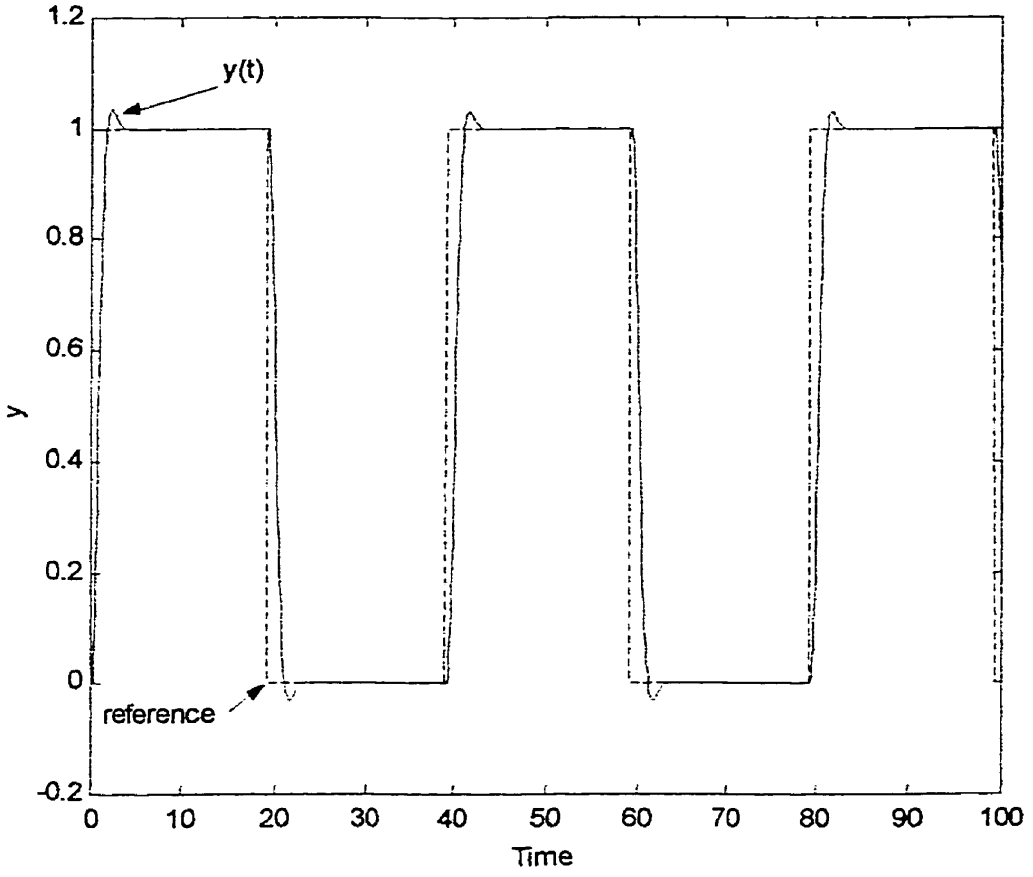

Figure 6.16: Predictive controller tracking for D_a=0.0576 and adaptive b-spline technique.

6.5.2 *Control of a process subject to multirate sampling*

The performance of the predictive controller under a variable sampling environment is tested in this simulation. A classical NPM and a b-spline model are used as the controller's internal model.

The predictive controller described in the previous subsection is used to track a train of step signals. When the controller sampling time matches the design sampling time, both internal models perform adequately as shown in Figure 6.17. When the sampling time is set to 1.5 *To*, the performance of the predictive controller based on the NPM is poorer than the b-spline model. The tracking response shown in Figure 6.18. The performance of the controller based on the NPM is degrading as the sampling time deviates from *To* as shown in Figure 6.19.

The poorer performance of the NPMs is explained by the analysis of the convolution Expression (4.1). When a change in the sampling rate occurs, the sequence of control actions $u(t)$ are not longer following the sequence of weighting coefficients of the FIR. As the sampling rate deviates more and more from the nominal (design sampling rate), the mismatch increases.

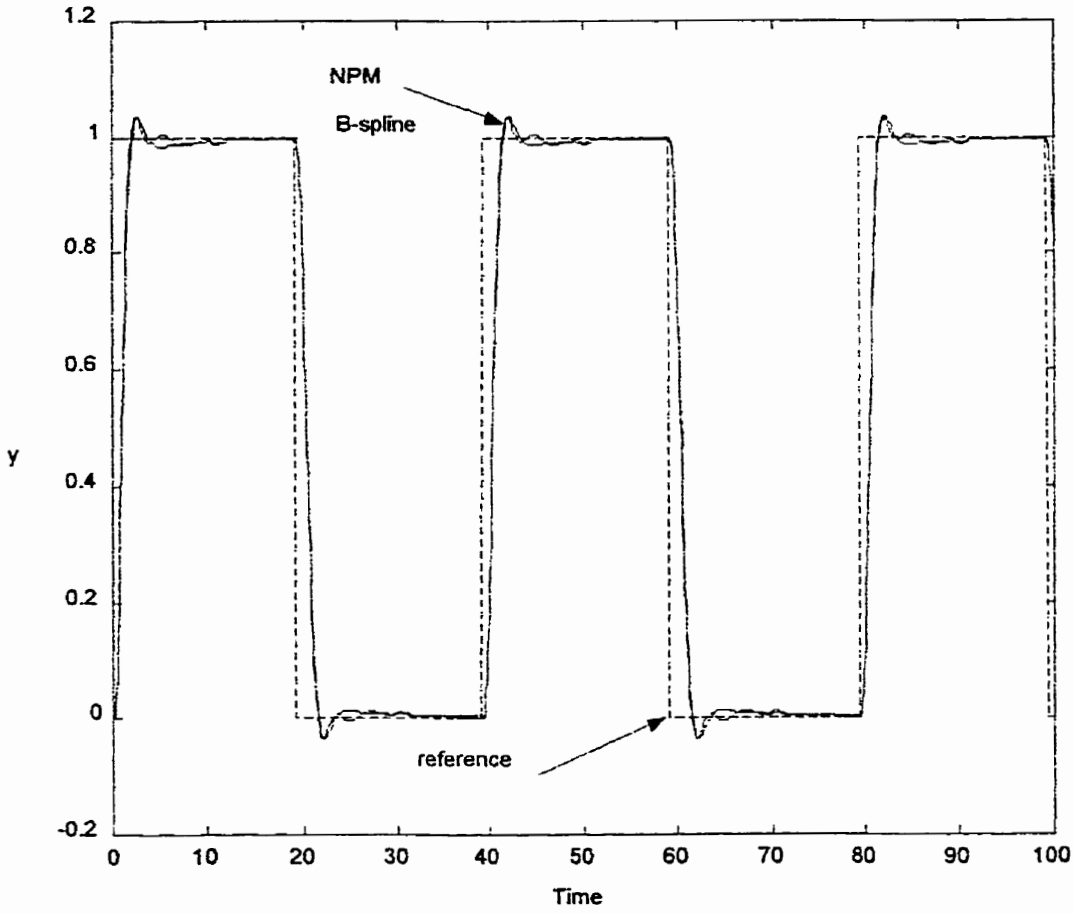

Figure 6.17: Predictive controller tracking for sampling time *To*.

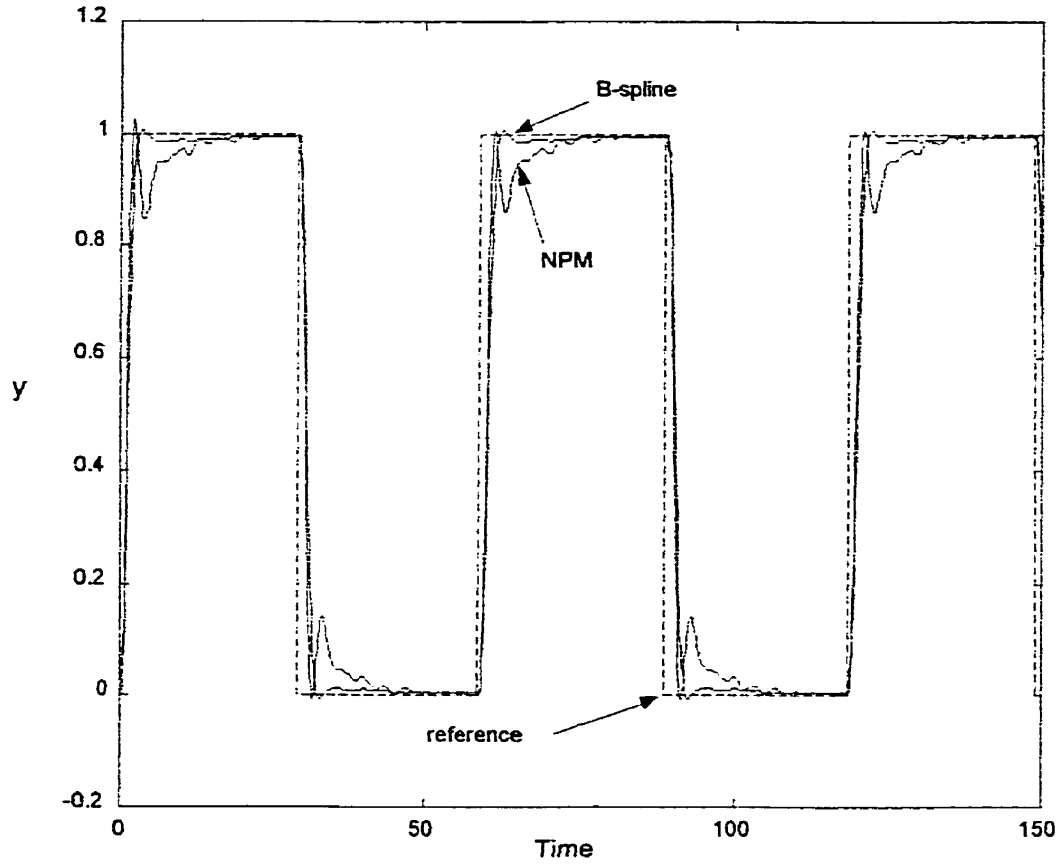

Figure 6.18: Predictive controller tracking for sampling time $1.5To$.

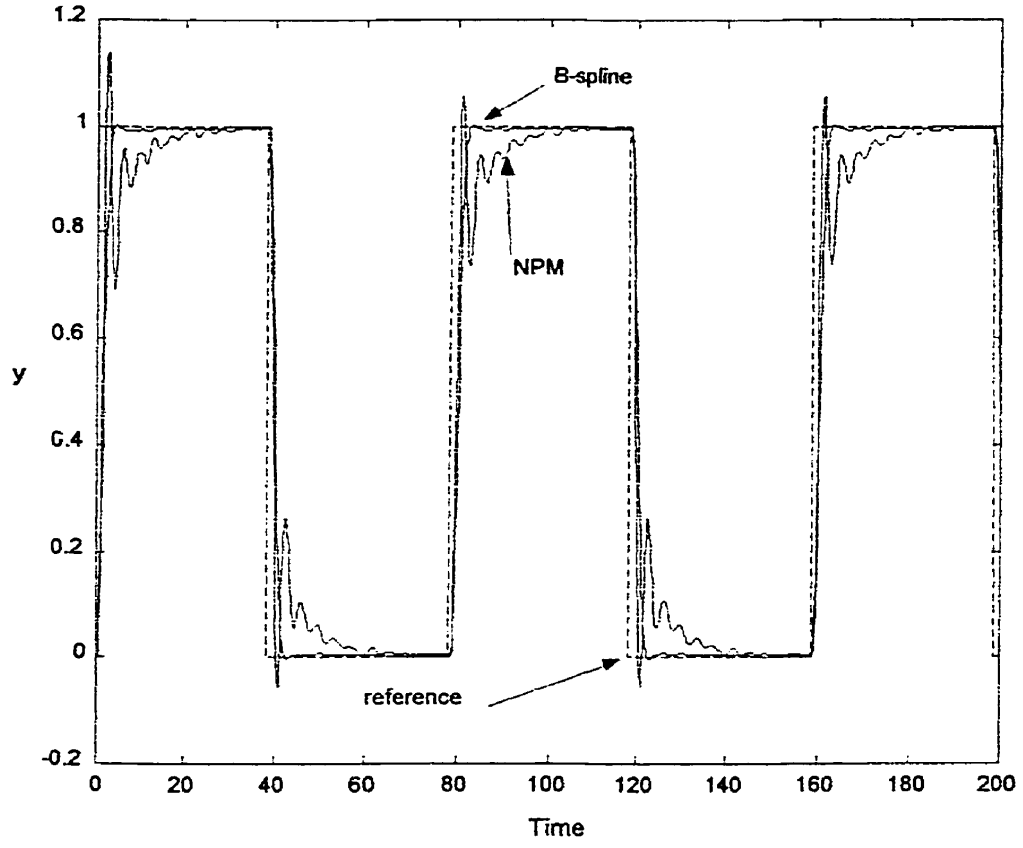

Figure 6.19: Predictive controller tracking for sampling time $2To$.

6.5.3 Generalized weighting matrix adaptation

A more precise result is obtained when the adaptation of the weighting matrix W_E is computed using the generalized version of the weighting matrix adaptation described in Chapter 5. The result is $W_E = 4.96\ I$, as compared to $4.8\ I$ obtained earlier.

Chapter 7

7. SPLINE FUNCTIONS FOR THE ANALYSIS OF ELECTRIC ARC FURNACES

In this chapter, the classical analysis for the optimal operation of electric arc furnaces (EAFs) is reviewed and the problem of waveforms distortion is presented. The concept of instantaneous phasors described by Nabae and Tanaka (1996) is used to verity the waveform shape preserving property. This property is the starting point for the reconstruction of voltage and current signals using the spline functions technique. The optimal operation of EAFs based on spline functions is proposed. A hybrid technique that combines instantaneous phasors and spline functions is developed at the end of the chapter.

7.1 Introduction

In classical circuit theory, voltage and current signals are often related to the ideal sinusoidal waveforms. In the presence of signal distortions, Fourier analysis is used to determine harmonics content, that is, the non-sinusoidal signal is expressed as a linear combination of an infinite set of sinusoidal signals each one with distinct frequency. The Fourier series can describe any periodic function that is well behaved to an arbitrary precision. However, the Fourier series have no predictive value because they are a representation of the signals at a specific time (Ochs *et al.*, 1986).

Voltage and current waveforms can be mathematically approximated by mean of spline functions. Once a mathematical expression of the signals is obtained, it is possible to

predict the performance of the circuit at a different operating point. This is particularly important for the optimization of circuits with nonlinear components.

In this chapter, the operation of electric arc furnaces (EAF) is analyzed based on the spline approximation of the phase voltage and current waves. With the signals represented in spline form, an optimal operating point of the EAF is predicted.

7.1.1 Description of EAFs

The electric arc furnace may be described as a process machine in which materials can be submitted to high temperature by the dissipation of energy from an electric arc. Figure 7.1 shows a schematic representation of a three phase EAF. A single line diagram of the electrical circuit is shown in Figure 7.2.

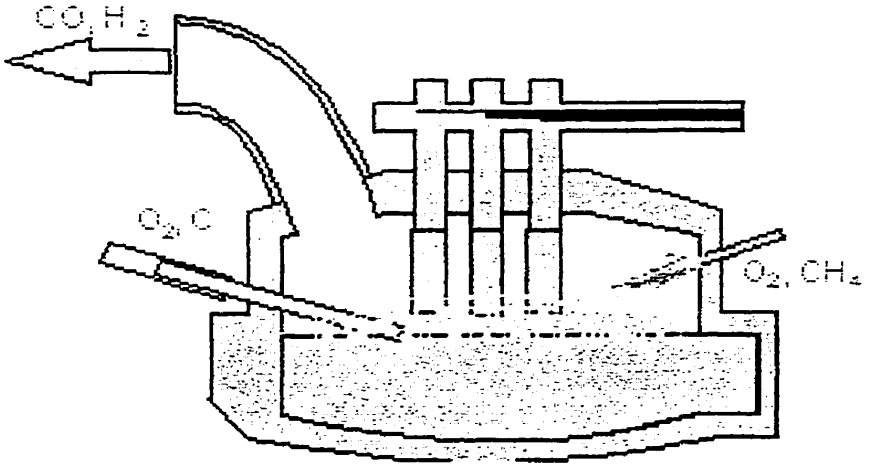

Figure 7.1: Schematic representation of a three phase EAF.

The design of the EAF has remained almost unchanged since it was introduced at the end of the nineteen century (Stansfield, 1914, Sims, 1963 and Layt, 1981). Although in recent years, a DC version of the furnace has been introduced (Vervacke and Fehn, 1994) where the arc is generated by a single electrode excited with DC voltage.

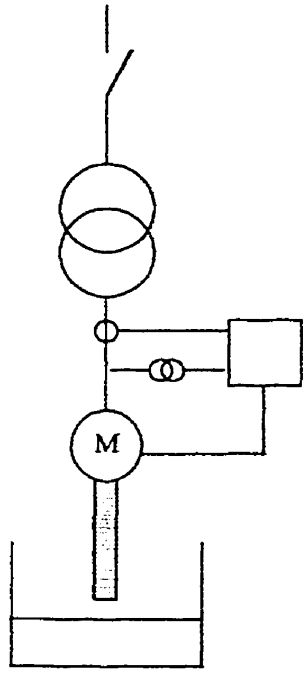

Figure 7.2: Single line diagram of the EAF electrical circuit.

The operating characteristics of an EAF are determined by the design of its secondary circuit, which consists of a transformer, bus bars connecting the transformer to flexible cables, the flexible cables, bus tubes mounted on the electrodes arms, electrode contacts pads and the electrodes. Some EAFs are equipped with a series reactor to improve regulation. The electrode regulator, or electrode position control system maintains the average secondary current, voltage and power at predetermined values. At the same time,

it controls the instantaneous current during scrap melting in order to limit the size and duration of current surges.

Traditionally, the arc furnace control is based upon phase impedance whereby the phase secondary current and voltage are measured either directly or indirectly and the two compared. Any variation produces an error signal which initiates movement of the electrode driven mechanism such that the ratio between voltage and current is restored by varying the arc length. The measured secondary voltage approximates the arc voltage and thus the term arc impedance control can also be applied to this system. Some manufacturers have introduced additional algorithms into their regulators to compensate for the effects of secondary circuit impedance on the voltage when measured at the transformers, and have thus come closer to a true arc impedance control. Other systems of control are current control, arc power control and power factor control. Recently, neural networks and fuzzy logic techniques have been used to control electrode positioning.

7.1.2 Electric arc characteristic

Due to its nonlinear nature, an accurate mathematical model of an electric arc is complex (Persson and Bliss, 1994; Knoop, 1998) and, in general, no attempt is made to use it for electrode positioning. However, there are some important properties of the electric arc that should not be overlooked as indicated by Bellido and Gómez (1996). In the first place, the voltage-current characteristic of the arc is negative (Sims, 1963). This is particularly important for the selection of the EAF operating point. Even though there is a theoretical optimal point (maximum active power deployed at the tips of the electrides), it may not be feasible to operate the furnace at that optimal because the stability of the arc could be compromised. Secondly, there are mechanical constraints not addressed in this

work such as heat transfer and refractory wear. The heat delivered by the arc may damage the furnace shield because the limited capabilities of the cooling system to control the temperature of the jacket (Celada, 1995). This effect is taken into consideration when limits to the length of the arc are imposed as process constraints.

The main objective of this work is the optimization of the electrical operation of arc furnaces. The results obtained from the electrical analysis of the furnace should be considered as a building block in the optimization of the furnace from an overall point of view.

7.1.3 Furnace equivalent circuit

In this work, a simplified electrical model of the EAF is used. The single phase model shown in Figure 7.3 is excited with the supply voltage e at the point of common coupling (PCC). This voltage is considered fixed and perfectly sinusoidal. The voltage v is applied to the load side of the transformer. The system transformer-reactor is modeled as a lumped reactance X_t, the furnace reactance (included connection cables and busses) is modeled by X_f and the arc is modeled by a variable nonlinear resistance R_a. The furnace current is represented by i.

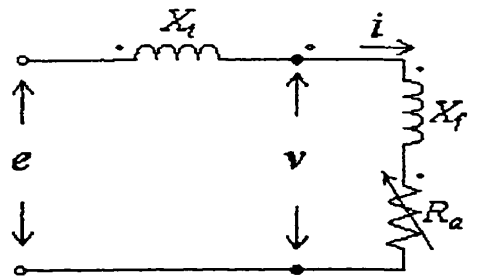

Figure 7.3: EAF per phase electrical model .

7.2 Classical analysis of EAFs

The classical analysis of EAFs is added to the present chapter for reference purposes. Traditionally, the optimal operation of an EAF is determined based on the rms value of the voltages and currents measured at the PCC. With the classical approach, the simplified electrical model of the EAF shown in Figure 7.3 is excited with sinusoidal signals, that is, $e(t)$, $v(t)$ and $i(t)$ are perfectly sinusoidal and their instantaneous values are given by

$$e(t) = \sqrt{2}E\sin(\varpi t) \tag{7.1}$$

$$v(t) = \sqrt{2}V\sin(\varpi t - \Phi + \phi) \tag{7.2}$$

$$i(t) = \sqrt{2}I\sin(\varpi t - \Phi) \tag{7.3}$$

with Φ the phase angle between $e(t)$ and $i(t)$; ϕ the phase angle between $v(t)$ and $i(t)$; ω the wave frequency scaled by 2π. E, V and I are the rms. values of $e(t)$, $v(t)$ and $i(t)$ respectively, given by

$$E = \sqrt{\frac{1}{T}\int_0^T e_m{}^2(t)dt} \tag{7.4}$$

$$V = \sqrt{\frac{1}{T}\int_0^T v_m{}^2(t)dt} \tag{7.5}$$

$$I = \sqrt{\frac{1}{T}\int_0^T i_m{}^2(t)dt} \qquad (7.6)$$

T is the voltage and current wave length measured in degrees and m stands for measured value.

7.2.1 *Maximum active power*

The main objective in the operation of an EAF is to maximize the active power delivered to the load at the lowest operating cost. Losses in the furnace occur at the transformer and series reactor windings and the connecting cables. They are proportionally related to the square of the furnace load current. This explains the need to maximise the active power deployed at the tips of the electrodes.

By definition, the active power P supplied to a load (Ramshaw, 1993) is given by

$$P = \frac{1}{T}\int_0^T vi\, d\alpha \qquad (7.7)$$

When the analysis of the operation of the EAF assumes sinusoidal signals, a maximum active power at the tips of the electrodes is found by matching the arc resistance R_a to the furnace total reactance X (maximum power transfer theorem [†]). Then

$$X = R_a \qquad (7.8)$$

[†] see for instance Paul et al., 1992

with

$$X = X_t + X_f \tag{7.9}$$

In this ideal sinusoidal environment, the arc resistance R_a is linear and given by the arc length, that is, the larger the arc is, the larger the resistance imposed to the furnace circuit.

To determine the furnace power factor, the following expression is used:

$$PF = \cos\Phi = \frac{R_a}{\sqrt{R_a{}^2 + X^2}} \tag{7.10}$$

Therefore, the given by Expression (7.8) implies that

$$PF = 70.71\,\% \quad or \quad \Phi = 45\ \text{deg} \tag{7.11}$$

Typically, EAFs are operated with a power factor close to 71%. A power factor instrument is used to operate at this theoretical optimal. The rms current is adjusted accordingly by positioning the electrodes with respect to the surface of the bath, thereby making R_a approximately equal to X.

7.2.2 EAF active power characteristic

The active power characteristic of an EAF is given by the complete range of theoretically achievable furnace currents. The active power characteristic of an EAF with linear components and sinusoidal signals is shown in Figure 7.4 (Taylor and Custer, 1985).

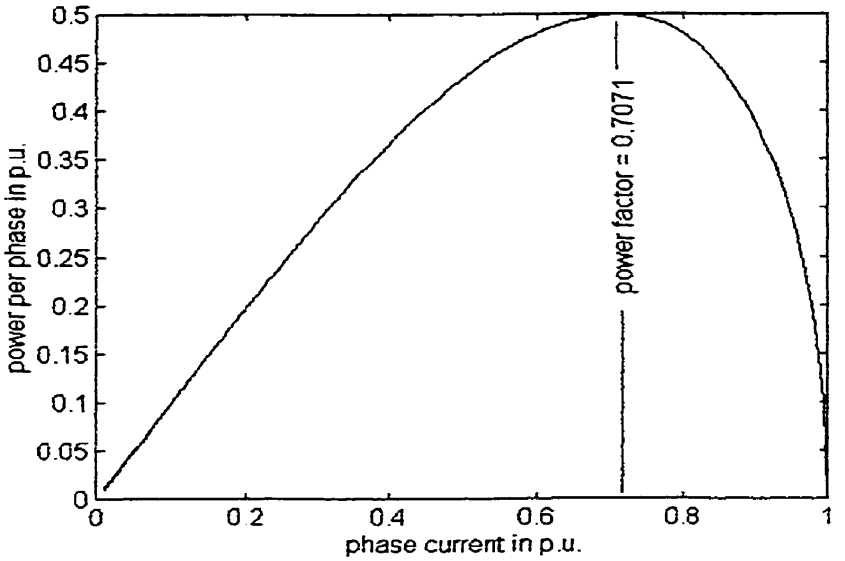

Figure 7.4: EAF active power characteristic in p.u.

The diagram is obtained by solving simultaneously the following elementary expressions:

$$I = \frac{V}{\sqrt{R_a{}^2 + X^2}} \qquad (7.12)$$

$$\cos\Phi = \frac{R_a}{\sqrt{R_a^2 + X^2}} \qquad (7.13)$$

$$P = 3V\,I\cos\Phi \qquad (7.14)$$

and

$$0 < R_a < \infty \qquad (7.15)$$

The diagram clearly shows the current value needed to obtain maximum active power, that in terms, corresponds to the optimal power factor.

7.3 Non-sinusoidal waveforms

A considerable error arises in the analysis of EAF because arc voltages and currents are non-sinusoidal, whereas the traditional techniques are based upon sinusoidal quantities (Schwabe, 1954). During melt down, the wave shape of the voltage and current is constantly varying. Figure 7.5 shows the voltage and current trajectories taken at the PCC on a 30 MW, 3 phase EAF. With the highly-distorted current and voltage wave shapes shown, the heat delivered to the arc furnace is appreciably less than the calculated from the equations developed in the previous section.

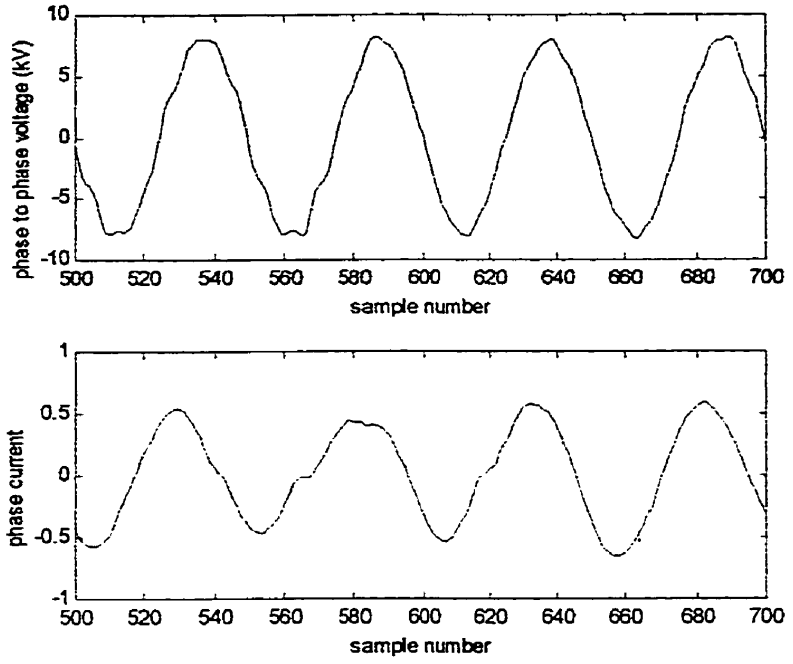

Figure 7.5: Voltage and current waves taken from a 30 MW, 3 phase EAF

The arcs also give some rectification, so the two halves of the voltage and current waves are not identical. This produces an effect equivalent to a DC component which may not be considered in the traditional analysis. To limit the reflection of the current distortions to the primary side, the transformers for EAFs are chosen with the load side windings in delta connection. Due to the unbalance characteristics of the load, the use of a transformer with windings in delta connection is required.

A different view of the distortions found in the voltage and current wave shapes is shown in Figure 7.6, where the measurements have been taken at the secondary side of a 58 MW, 3 phase EAF at Slater Steel in Hamilton, Ontario.

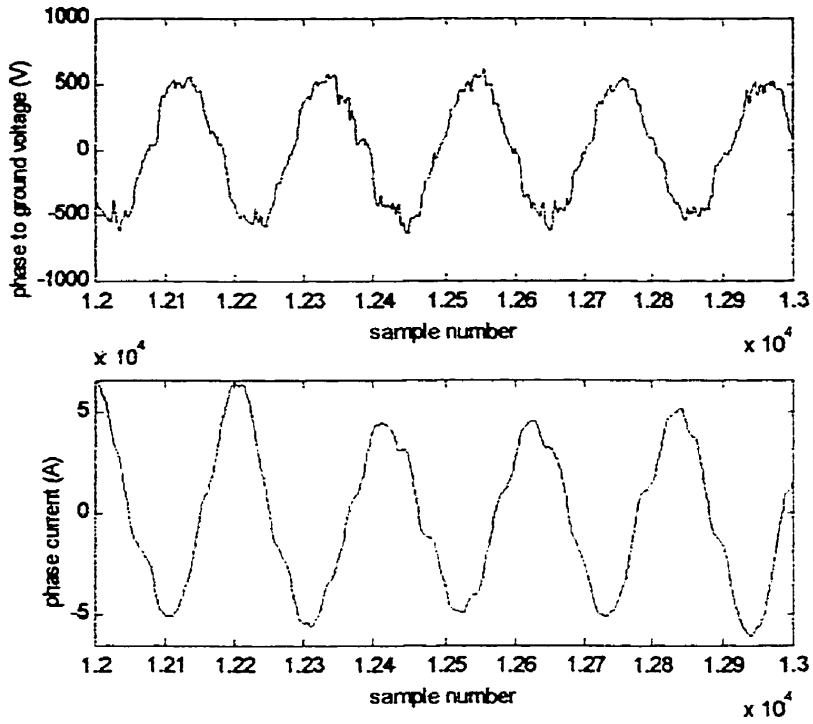

Figure 7.6: Voltage and current waves taken from a 58 MW, 3 phase EAF.

As the measurement are taken closer to the electric arc, the wave distortions are more evident.

7.3.1 Instantaneous phasors

Recently, instantaneous phasors have been introduced for power quality monitoring and diagnostics (Nabae and Tanaka, 1996). The trajectory of the instantaneous phasors indicates how close the signals are to the ideal sinusoidal waveforms. The roundness of the trajectory is an indication of the power quality. This roundness is a function of the circuit parameters, therefore, the trajectory of the instantaneous phasors has a repetitive pattern for circuits with constant parameters. According to Nabae and Tanaka, the

instantaneous voltage phasor V_{phasor}ent phasor I_{phasor}ve power phasor P_{phasor}, apparent power phasor S_{phasor} and power factor $cos\ \phi$ for a three-phase system are given by

$$V_{phasor} = \sqrt{\frac{2}{9}\left[(v_a - v_b)^2 + (v_b - v_c)^2 + (v_c - v_a)^2\right]} \qquad (7.16)$$

$$I_{phasor} = \sqrt{\frac{2}{9}\left[(i_a - i_b)^2 + (i_b - i_c)^2 + (i_c - i_a)^2\right]} \qquad (7.17)$$

$$P_{phasor} = \frac{3}{2} V\ I \cos\phi \qquad (7.18)$$

$$S_{phasor} = \frac{3}{2} V\ I \qquad (7.19)$$

$$\cos\phi = \frac{P_{phasor}}{S_{phasor}} \qquad (7.20)$$

where v_a, v_b and v_c are the instantaneous phase voltages from phase A, B and C, respectively; and i_a, i_b and i_c are the instantaneous load currents from phase A, B and C, respectively.

7.3.2 Wave-preserving property of the voltage and current signals

The spline approximation technique that is developed in this chapter relies on the assumption that the optimal phase angle is constant throughout the melting and refining

stages. This assumption implies the existence of a wave-preserving property, that is, the amplitude of the waves change but their shape remain approximately constant for small changes in the phase angle. The assumption is based on the fact that the components of the furnace do not change during the heat except for the resistance of the arc. It also assumes that the furnace load does not suffer significant alteration, from the electrical point of view, when the charges are made during the refining process.

7.3.2.1 Time series based analysis

Although this technique is not used in this work, the time series analysis of the data samples is a more rigorous approach to prove the wave-preserving property of the voltage and current signals. When the data samples (called time series) exhibit some sort of regularity over time, the series is called stationary. When the probabilistic behavior of a time series $i_{t_1}, i_{t_2}, \cdots, i_{t_k}$ is identical to that of the shifted set $i_{t_{1+h}}, i_{t_{2+h}}, \cdots, i_{t_{k+h}}$ for any collection of time points t_1, t_2, ..., t_k, for any number $k = 1, 2, \ldots$, and any shift $h = 0, 1, 2, \ldots$, we say that the series is strictly stationary.

In the time series context, the measure of the wave-preserving property of the voltage and current signals is given by the auto-correlation function, as shown in Shumway and Stoffer (2000).

7.3.2.2 Instantaneous phasors based analysis

Although the use of instantaneous phasors to show the wave-preserving property of the voltage and current signals is not as rigorous as the time series based analysis, it provides additional information regarding the power quality characteristics of the EAF. Therefore, we have chosen to pursue the instantaneous phasors based analysis to verify the repetitiveness of the signals.

To test this repetitiveness hypothesis, we set up a field test with two different units: a 3 phase - 40 MW furnace and a 3 - phase 58 MW unit. Samples of the phase voltages and currents are obtained at a sampling rate of 0.08ms. The samples are taken at different stages of the heat, thereby all possible states of the arc are captured. With the sampled data, the instantaneous phase voltages and currents are computed using the expressions given in the previous subsection. The instantaneous phasors are plotted in polar diagrams as a function of the electrical angle of the fundamental component of the waveforms.

7.3.3 Field test 7.1

7.3.3.1 Trajectory of the instantaneous phasors

Figures 7.7 a, b and c show the results of the test performed at the PCC of a 3 phase - 40 MW EAF to determine the quality of the voltage and current signals as well as the shape preserving characteristics of the waveforms.

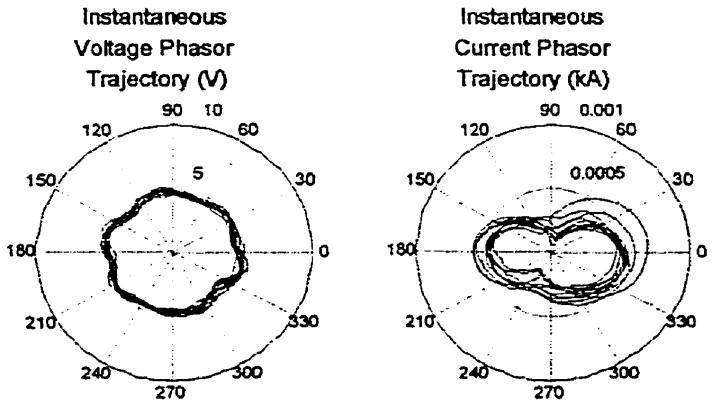

Figure 7.7a: Trajectory of the current and voltage instantaneous phasors during the meltdown process.

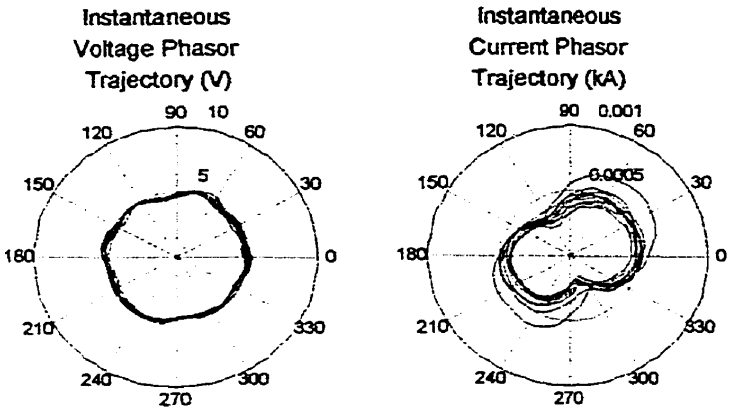

Figure 7.7b: Trajectory of the current and voltage instantaneous phasors at the end of the meltdown process.

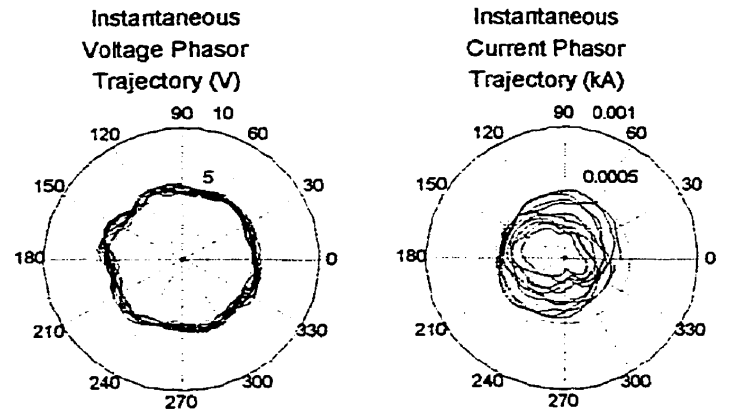

Figure 7.7c: Trajectory of the current and voltage instantaneous phasors during the charging process.

7.3.3.2 Analysis of the Trajectory of the instantaneous phasors

The trajectory of the instantaneous phasors shown in Figures 7.7a and b depict a very repetitive pattern from cycle to cycle. Both, the voltage and current instantaneous phasors present a predictable trajectory even though the electric arc is a highly nonlinear load. The trajectory of the voltage instantaneous phasor presents a more circular shape, suggesting the lower content of harmonics in its waveform compared to the current waveform.

When a charge is made (for the refining of the bath), the distortion of the current waveform is higher as suggested by the diagram shown in Figure 7.7c. The assumption of shape preserving property does not hold during this part of the heat.

7.3.4 Field test 7.2

Figure 7.8 to 7.10 show the results of the test performed at the load side of a 3 phase - 58 MW EAF to determine the quality of the voltage and current signals as well as the shape preserving characteristics of the waveforms.

7.3.4.1 Trajectory of the instantaneous phasors during the melt down stage

Samples were taken at the end of the melt down stage and time stamped for comparison purposes.

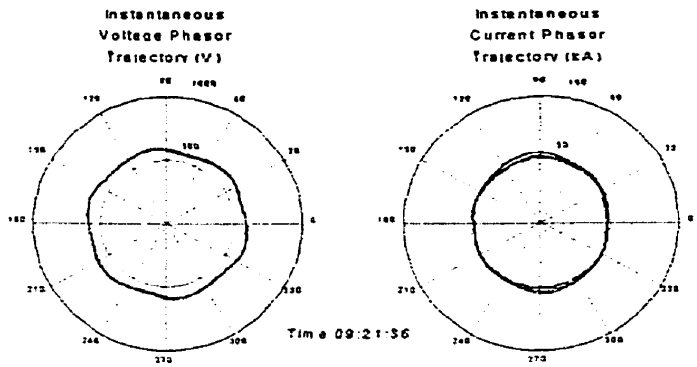

Figure 7.8a: Trajectory of the current and voltage instantaneous phasors at the end of the meltdown process (Time 9:21:36).

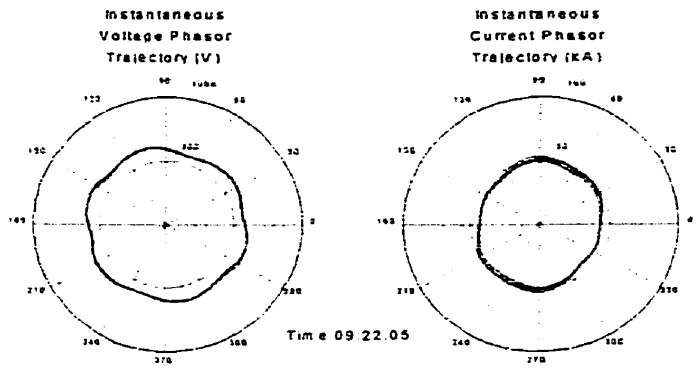

Figure 7.8b: Trajectory of the current and voltage instantaneous phasors at the end of the meltdown process (Time 9:22:05).

7.3.4.2 Analysis of the trajectory of the instantaneous phasors during the meltdown process

The trajectories of the voltage and current instantaneous phasors shown in Figures 7.8a and b are more repetitive than the trajectories shown in Figures 7.7a and b for the same part of the heat stage. One of the reasons that explain the improved repeatability of the trajectories is the well known fact that the larger the furnace the more stable is the arc. The other reason is the less harmonics content that the waveforms have compared to the trajectories of the furnace studied in the previous test. The lower harmonics content of the waveforms is made evident by the more circular trajectory shown in Figures 7.8.a and b as compared to Figures 7.7a and b.

7.3.4.3 Trajectory of the instantaneous phasors during the first charge

Samples were taken at the time of the first charge and time stamped for comparison purposes.

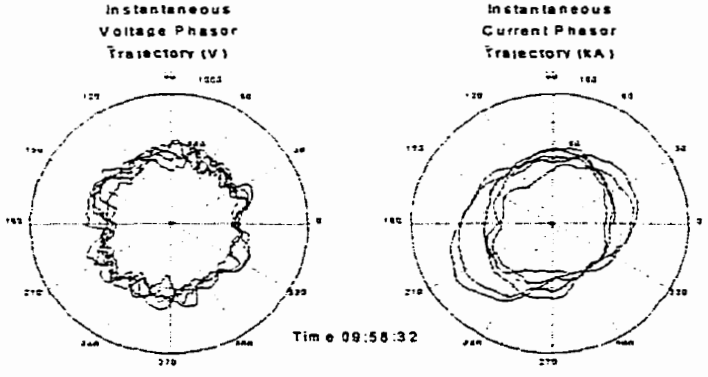

Figure 7.9a: Trajectory of the current and voltage instantaneous phasors at the time of the first charge (Time 9:58:32).

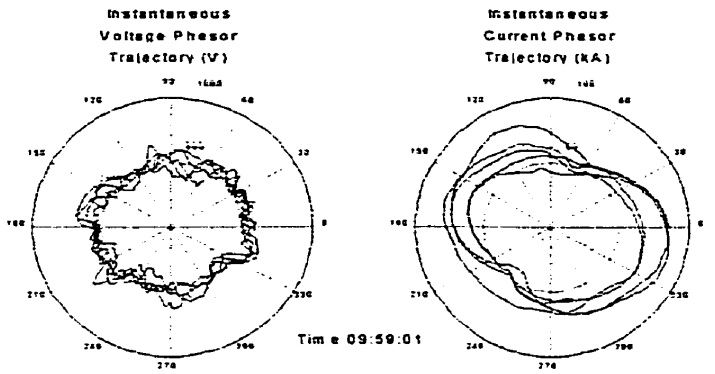

Figure 7.9b: Trajectory of the current and voltage instantaneous phasors during the first charge (Time 9:59:01).

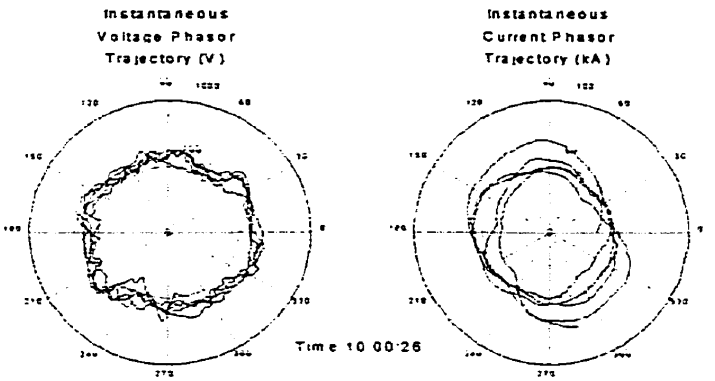

Figure 7.9c: Trajectory of the current and voltage instantaneous phasors after the first charge (Time 10:00:26).

7.3.4.4 Analysis of the trajectory of the instantaneous phasors during the first charge

The trajectories of both, the voltage and current instantaneous phasors are affected by the charging process. Figures 7.9a, b and c show evidence of the increased harmonic component as well as an on-going chaotic behavior of the electric arc. However, as it is made evident from the analysis of the time stamps along the samples, the shape preserving property of the waveforms is recovered soon after the transient (Figure 7.9c).

7.3.4.5 Trajectory of the instantaneous phasors during the second charge

Finally, samples were taken at the time of the second charge and time stamped for comparison purposes.

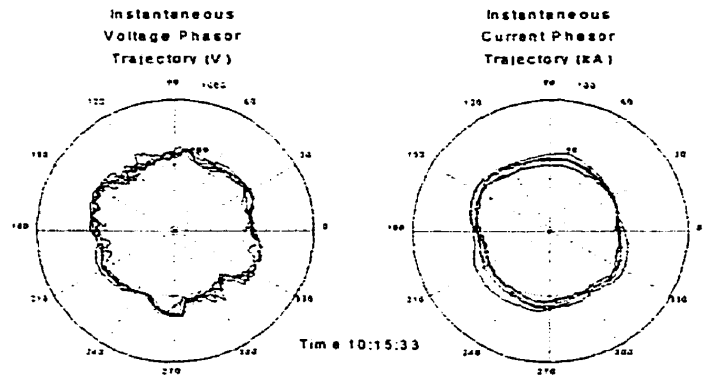

Figure 7.10a: Trajectory of the current and voltage instantaneous phasors at the time of the second charge (Time 10:15:33).

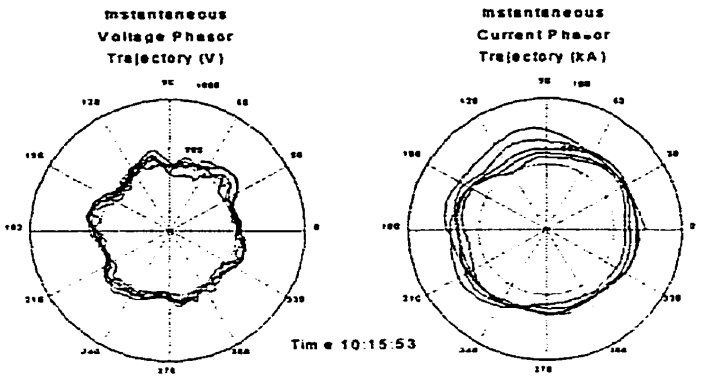

Figure 7.10b: Trajectory of the current and voltage instantaneous phasors during the second charge (Time 10:15:53).

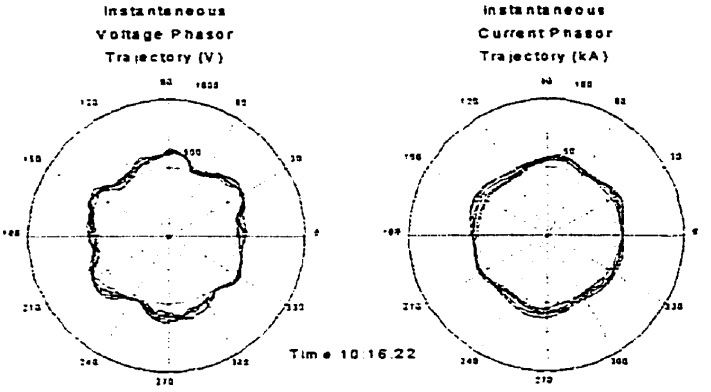

Figure 7.11c: Trajectory of the current and voltage instantaneous phasors after the second charge (Time 10:16:22).

7.3.4.6 Analysis of the trajectory of the instantaneous phasors during the second charge

Similarly to the case of the first charge, the trajectories the voltage and current instantaneous phasors are affected by the charging process. However, Figures 7.10a, b and c show a less severe transient probably due to the smaller volume of the charge (the second charge is a fine adjustment of the refining initiated with the first charge).

7.4 Spline approximation of current and voltage waveforms

7.4.1 Determination of the optimal number of knots per cycle and their location

7.4.1.1 Selection of the optimal number of knots

The larger the number of knots per cycle, the better the reconstruction of the original signal is. There is no limitation on the maximum number of knot apart from the fact that the complexity of the computations increases with the total number of samples. Additionally, there is a limitation imposed by the sampling device. Although it is common to find sampling devices that have high sampling rate (>100 kHz), they are, in general, stand alone units that require integration with the controller.

In order to develop a technique that can be used in the lower-end range of controllers (for instance PLCs), there exists the need to limit the number of samples per cycle, that is, the number of knots per cycle. Then, a low sampling rate reduces the computation effort and, at the same time, makes the spline functions an attractive technique for low cost optimization.

To determine the number of knots per cycle, the Shannon's theorem (Taub and Schilling, 1991) is used. The decision to use the Shannos's theorem is, however, a conservative approach. Ostrander (1971) has shown that the transform from a spline-function approximation to continuous data (called a spline transform), reduces errors introduced by the discrete Fourier transform. Additionally, Ostrander has shown that the spline transform alleviates noise problems when the sampling rate is limited due to experimental method or hardware constraints.

7.4.1.2 Optimal knots placement

The theory of spline functions provides a series of tools to determine the optimal location of the knots. This optimal location is determined by the degree of the interpolating polynomials. Micchelli *et al.*(1976) and Gaffney and Powell (1976) have developed the tools to determine a knot sequence that is optimal in the sense that it provides the center function in the band formed by all interpolants to the given data.

The draw back with these theoretical tools is that the resulting knot sequence is not regular, that is, the intervals are not equal. The irregular intervals are a limitation for an on-line application of the spline techniques developed in this chapter. The samples of the field signals are obtained at regular intervals. Therefore, the technical limitations imposed by the sampling device indicates that the knots must be located at regular intervals.

7.4.2 Signal reconstruction

Let us consider the phase voltage signal from an EAF shown in Figure 7.11. Samples are obtained at selected knots and these samples are the starting point of the signal reconstruction process. The voltages sampled at the knots are obtained by a measurement

device, sampling at regular intervals. Preferably, the sampling rate is a sub-multiple of the signals wave length. In this particular case, the samples are taken every 36 degrees for a total of ten knots per cycle.

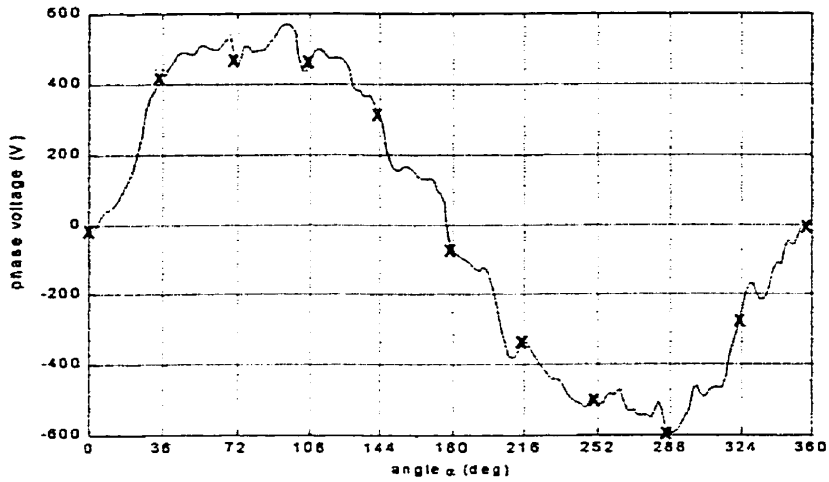

Figure 7.12: Samples at the knots of a voltage signal.

When the interpolating splines are cubic functions, the approximation of the instantaneous phase voltage has the form

$$v(\alpha) \approx a_0 + a_1\alpha + a_2\alpha^2 + a_3\alpha^3 \qquad (7.21)$$

Similarly, the approximation of the instantaneous phase current has the form

$$i(\alpha) \approx b_0 + b_1\alpha + b_2\alpha^2 + b_3\alpha^3 \qquad (7.22)$$

The interpolating polynomial coefficients a_i and b_i are obtained by the recursive algorithm described in the Chapter 2. There are as many expressions of the type given by Equations (7.21) and (7.22) as number of knots per cycle minus one. They differ only on the polynomial coefficients.

7.4.3 Computation of active power

When non-sinusoidal signals are considered in the simplified EAF electrical model shown in Figure 7.3, the optimal operation condition given by Expression (7.8) does not apply. Instead, the optimal operating condition is derive from the definition of active power given by Expression (7.7).

The computation of the active power for non-sinusoidal waves requires the use of Expression (7.14) for each harmonic component or, alternatively, by combining Expressions (7.7), (7.21) and (7.22). Then, when the voltage and current waves are expressed in terms of interpolating splines, the approximated expression for the active power is given by

$$P \approx \frac{1}{T}\sum_{k=1}^{n} \int_{0}^{T/n} v_k(\alpha)\, i_k(\alpha)\, d\alpha \qquad (7.23)$$

where k represents the knot number n represents the total number of intervals per cycle.

7.4.3.1 Active power as a function of arc length

When the arc length is modified to achieve optimal operation of the furnace, the phase angle ϕ between the load voltage and current changes (Figure 7.12). The consequence of changing the phase angle between $v(\alpha)$ and $i(\alpha)$ is two fold: at one end, a change in the

phase angle affects explicitly the electrical angle α, at the other end, the signals amplitude are affected.

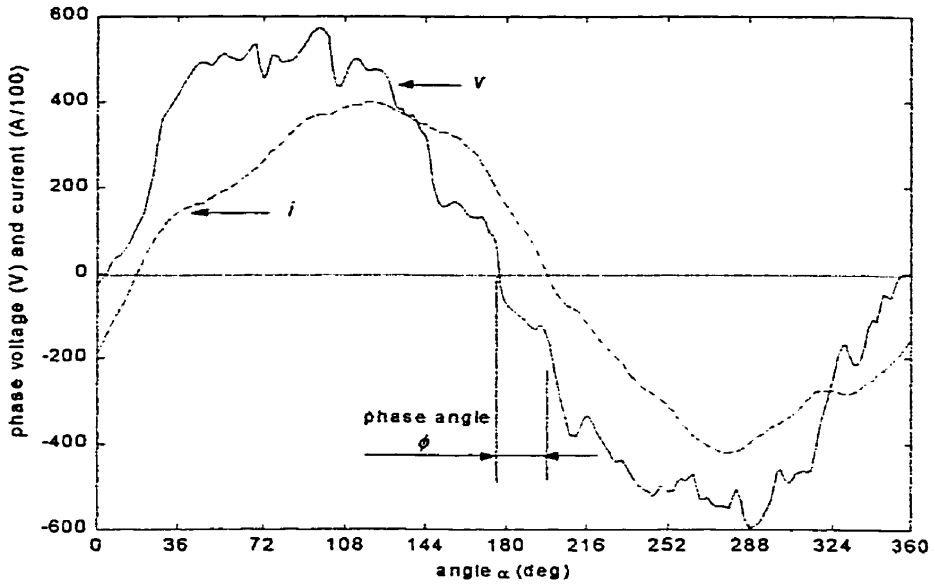

Figure 7.13: Phase angle ϕ between phase voltage and current.

7.4.3.2 Shifting of the electrical angle α

Changes in the phase angle are expressed by increasing ϕ by φ. The net effect of a phase angle increase on the interpolating spline polynomial is a shift of the independent variable α by φ. The shift effect is applied either to the voltage or the current spline polynomials or spliced between them. For the voltage, the resultant expression is

$$v(\alpha,\varphi) \cong v(\alpha+\varphi) \qquad (7.24)$$

or in expanded form

$$v(\alpha,\varphi) \approx a_0 + a_1(\alpha+\varphi) + a_2(\alpha+\varphi)^2 + a_3(\alpha+\varphi)^3 \qquad (7.25)$$

In Expression (7.25) the sliding knots technique introduced in Chapter 3 has been used.

7.4.3.3 Sensitivity of the signals amplitude w.r.t. the phase angle

Changes on the signals amplitude due to changes on the phase angle can be analytically approximated by a sensitivity analysis of the coefficients a_i and b_i. To this end, the circuit theory for sinusoidal waveforms is used. The phasor diagram of the EAF equivalent circuit shown in Figure 7.13 is used to investigate the effect that a change on ϕ has over the amplitude of the voltage v and current i.

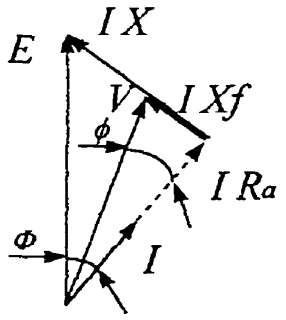

Figure 7.14: EAF phasor diagram.

Based on Figure 7.13, the following expressions are obtained:

$$V\cos\phi = E\cos\Phi \tag{7.26}$$

$$I\ X = E\sin\Phi \tag{7.27}$$

$$\tan\phi = \frac{X_f}{X}\tan\Phi \tag{7.28}$$

The interactions between the amplitude of the voltage $\hat{v}$ and current $\hat{i}$ is evaluated by a sensitivity expression given by

$$sensitivity\ of\ \hat{v}\ and\ \hat{i}\ w.r.t.\ \phi\ = \frac{\frac{d(\hat{v}\,\hat{i})}{d\phi}}{\hat{v}\,\hat{i}} \tag{7.29}$$

An approximation of the expression of the sensitivity s_s is made by considering the fundamental components of the voltage and current signals. Then, Expression (7.9) is approximated to

$$sensitivity\ of\ \hat{v}\ and\ \hat{i}\ w.r.t.\ \phi = \frac{\frac{d(V\ I)}{d\phi}}{V\ I} \tag{7.30}$$

The voltage at the PCC (E), and the reactance of the EAF circuit (X) are considered unchanged throughout the analysis. Then, the load voltage and current are referred to these two parameters. Form Expressions (7.26) and (7.27), the following equation is obtained:

$$I V = \frac{E^2}{2X} \frac{\sin 2\Phi}{\cos \phi} \tag{7.31}$$

In order to have the same angle reference, the following approximation is used:

$$\frac{\Phi}{\phi} \approx \frac{\Phi_m}{\phi_m} = r \tag{7.32}$$

where sub-index m indicates measured value at the point of analysis. The sensitivity Expression (7.30) is combined with Expressions (7.31) and (7.32) as follows:

$$sensitivit\ of\ \hat{v}\ and\ \hat{i}\ w.r.t.\ \phi \approx \frac{\frac{d}{d\phi}\left(\frac{\sin 2r\phi}{\cos \phi}\right)}{\left(\frac{\sin 2r\phi}{\cos \phi}\right)} \tag{7.33}$$

giving the following approximation for the sensitivity coefficient:

$$sensitivity\ of\ \hat{v}\ and\ \hat{i}\ w.r.t.\ \phi \approx s_s = \frac{2r \cos 2r\phi \cos \phi + \sin 2r\phi \sin \phi}{\cos \phi \sin 2r\phi} \tag{7.34}$$

7.4.3.4 Active power expression

Based on Expressions (7.22), (7.23), (7.25) and (7.34), the active power P per phase is approximated by

$$P(\varphi) \approx \frac{1}{T} \sum_{k=1}^{n} \int_{0}^{T/n} v_k(\alpha, \varphi)\, i_k(\alpha)\, (1 + s_s \varphi)\, d\alpha \qquad (7.35)$$

Expression (7.35) is analytically solved using Maple software (Redfern, 1993),

7.4.4 Optimal phase angle

The solution of Equation (7.35) is a polynomial in φ of order 4^{th}. The value of φ for which P becomes maximum is given by

$$\frac{dP}{d\varphi} = 0 \rightarrow \varphi_O \qquad (7.36)$$

where φ_o is the deviation from the operating phase angle to achieve maximum power transfer to the furnace bath. Finally, the phase angle for maximum power at the tips of the electrodes is given by

$$\phi_O = \phi_m + \varphi_O \qquad (7.37)$$

with ϕ_o the optimal phase angle and ϕ_m the measured phase angle at the load. In terms of the furnace power factor PF (Ramshaw, 1993), we have

$$\cos\phi_m \approx PF = \frac{P}{S} \qquad (7.38)$$

where the power factor PF is measured or computed by measuring the active power P and the apparent power S.

7.4.5 Controller design

An alternative implementation of the technique presented in this work is the computation of the optimal operating phase angle with an on-line controller. Once a decision is made on the number of samples per cycle, Equation (7.36) is solved analytically. The derivative (7.36) is solved off line and the result is expressed (using relative reference of the spline knots) as

$$\frac{dP}{d\varphi} = \sum_{k=1}^{n}\sum_{h=0}^{3} A_k^T (M_h + s_s N_h) B_k \varphi^h \qquad (7.39)$$

where

$$A_k^T = [\ a_0\ \ a_1\ \ a_2\ \ a_3\ ]_k \qquad (7.40)$$

is a vector of coefficients of the voltage interpolating spline for the interval k,

$$B_k^T = [\quad b_0 \quad b_1 \quad b_2 \quad b_3 \quad]_k \tag{7.41}$$

is a vector of coefficients of the current interpolating spline for the interval k, and

$$M_h \text{ and } N_h \in \Re^{4x4} \tag{7.42}$$

are a matrices of constant coefficients. Matrices M_h and N_h are independent of the sampled data and the interval k. Therefore, they remain unchanged throughout the optimization process. Only A_k , B_k and s_s need to be updated. Equation (7.39) is made equal to 0 and the optimal φo is computed. The spline coefficients of the vectors A_k and B_k are obtained recursively from the algorithm described in Chapter 2.

The proposed optimal controller is recommended for use in a supervisory mode due to the fact that the waveforms are contaminated with environmental noise and, therefore, filtering procedures of the samples based on the history of the waveforms are recommended.

7.4.5.1 Conjecture on the decrease of the phase angle with increasing arc length

The operation at optimal phase angle requires the positioning of the electrodes with respect to the surface of the bath. So far, it has been assumed that the phase angle at the load was inversely related to the arc length. This assumption stems from the combined

analysis of the EAF approximated electrical model shown in Figure 7.3 and the Expression (7.13) derived from the classical circuit theory. The assumption is reinforced by the fact that the arc resistance is a monotone non-decreasing function of the arc length (Sims, 1963).

With respect to the case of non-sinusoidal waveforms, the analysis of relationship between the phase angle at the load side of the EAF and the arc length is complex. In this work, it is assumed that the relationship between these two variables corresponds in some degree to the results derived from the ideal linear furnace.

In order to formalize the concepts mentioned in this subsection, the following conjecture is enunciated:

7.4.5.1.1 Conjecture 7.1

The phase angle at the load side of an EAF is a monotone non-increasing function of the arc length.

Points of coincidence

There are two conditions where the above conjecture coincides with field data: the EAF operating in open circuit and short circuit. In order to test the conjecture at these operating points, the following expression of the phase angle is used:

$$\phi = a\cos\frac{P}{S} \qquad (7.43)$$

When the furnace operates in short circuit mode, the arc resistance Ra is very small. Mathematically, this condition is described as

$$\lim_{R_a \to 0} \phi = \lim_{R_a \to 0} a\cos\frac{\bar{P}}{S} = \lim_{R_a \to 0} a\cos\frac{\bar{I}R_a}{V} = \frac{\pi}{2} \qquad (7.44)$$

with I and V rms. values. When the furnace operates in open circuit mode, the arc resistance Ra is very large. Mathematically, this condition is described as

$$\lim_{R_a \to \infty} \phi = \lim_{R_a \to \infty} a\cos\frac{P}{S} = \lim_{R_a \to \infty} a\cos\frac{R_a}{Z} = 0 \qquad (7.45)$$

where Z is an equivalent impedance made up of the arc resistance R_a and the reactance to all harmonic components.

Between these extreme points the conjecture is loosely supported by the classical analysis of the ideal EAF and the field data.

7.5 Spline representation of instantaneous phasors

In this section, a different approach for the optimization of EAFs is presented. It is based on the concept of instantaneous phasors used earlier in this chapter for the analysis of the furnace signals.

The instantaneous phasors are represented in spline form as described earlier in this chapter for the voltage and current signals. The instantaneous voltage phasor V_{phasor} current phasor I_{phasor}, are approximated by spline polynomials in α

$$V_{phasor}(\alpha) \cong a_0 + a_1\alpha + a_2\alpha^2 + a_3\alpha^3 \qquad (7.46)$$

$$I_{phasor}(\alpha) \cong b_0 + b_1\alpha + b_2\alpha^2 + b_3\alpha^3 \qquad (7.47)$$

where polynomial coefficients a_i and b_i are obtained by the recursive algorithm described in Chapter 2, and α is the signals electrical angle.

7.5.1 Sensitivity analysis

Similarly to the method described earlier for spline functions, the hybrid technique presented in this section makes used of the polynomial splines. The expression for the sensitivity of the amplitudes of V_{phasor} and I_{phasor} w.r.t. the phase angle is different that the one given in (7.34).

7.5.1.1 Sensitivity of V_{phasor} and I_{phasor} w.r.t. the phase angle.

The objective is to determine the impact that a change in the phase angle has over the Expression (7.18). The sensitivity coefficient s_p is determined by

$$sensitivity\ of\ V_{phasor}\ and\ I_{phasor}\ w.r.t\ \phi = \frac{\frac{d(V_{phasor}\ I_{phasor}\cos\phi)}{d\phi}}{V_{phasor}\ I_{phasor}\cos\phi} \qquad (7.48)$$

Recalling that

$$V = \frac{E\cos\Phi}{\cos\phi} \qquad (7.49)$$

and

$$I = \frac{E\sin\Phi}{X} \qquad (7.50)$$

Then,

$$sensitivity\ of\ V_{phasor}\ and\ I_{phasor}\ w.r.t.\ \phi \approx \frac{\frac{d(\sin 2\Phi)}{d\phi}}{\sin 2\Phi} \qquad (7.51)$$

Finally,

$$sensitivity\ of\ V_{phasor}\ and\ I_{phasor}\ w.r.t.\ \phi \approx s_p = 2r\frac{\cos 2\Phi}{\sin 2\Phi} \qquad (7.52)$$

where the approximation given by (7.32) has been used.

7.5.2 *Active power expression*

The active power is obtained by computing the average value of the instantaneous active power (7.18). The expression of the active power is

$$P = \frac{1}{T}\int_0^T \frac{3}{2} V_{phasor}\, I_{phasor} \cos\phi \, d\alpha \qquad (7.53)$$

Using the spline approximations (7.46) and (7.47), the sliding knots technique for the expression of V_{phasor} and the sensitivity coefficient s_p, (7.53) is approximated as follows:

$$P(\varphi) \approx \frac{3}{2T} \sum_{k=1}^{n} \int_0^{T/n} V_{phasor}(\alpha, \varphi)\, I_{phasor}(\alpha)\, (1 + s_p \varphi) \cos\phi_m \, d\alpha \qquad (7.54)$$

Chapter 8

8. EAF CASE STUDY

In this chapter, the spline function techniques described in Chapter 7 are applied to data sampled from an EAF. A circuit model of the EAF and a simulator are developed to compare the results obtained from the sampled data to those derived from the classical circuit theory.

8.1 Description of the EAF

The EAF under study has been selected mainly due to unit availability and accessibility to phase voltage and current recording instruments already installed at the load side of the step-down transformer. The furnace has the ratings given in Table 8.1.

Table 8.1: EAF data

Description	*Ratings*
Furnace type	3 phase - AC
Step-down transformer rated power	58 MVA
Step-down transformer secondary line voltage	812 V
Transformer impedance	6%
Series reactor	2.40 mΩ

From the ratings given in Table 8.1 the following circuit components are identified:

Table 8.2: EAF data

Components	*Ratings*
Series reactor X_r	j 2.40 mΩ
Step down transformer impedance X_t	j 0.682 mΩ
Load-side circuit reactance (average)† X_f	j 3.60 mΩ
Load resistance R_a	0 Ω<R_a<∞ Ω

† This value is considered equal for all three phases.

8.2 Classical analysis

As shown in Chapter 7, the classical analysis of the EAFs is based on the assumption that all the signals are sinusoidal, therefore, the maximum power transfer theorem applies. With these hypothesis, the furnace is regulated at an power factor equal to 0.7071. This corresponds to an input phase angle of 45 degrees. Considering the ratings given in Table 8.2, the optimal phase angle computed at the load side of the transformer is given by

$$\phi_o = \arctan\frac{X_f}{X_f + X_t + X_r} = 28.3 \text{ deg.} \qquad (8.1)$$

8.3 EAF circuit model

A single phase model is developed using Matlab 5.3 based on the parameters given in Tables 8.1 and 8.2. The circuit model used for simulation is shown in Figure 8.1.

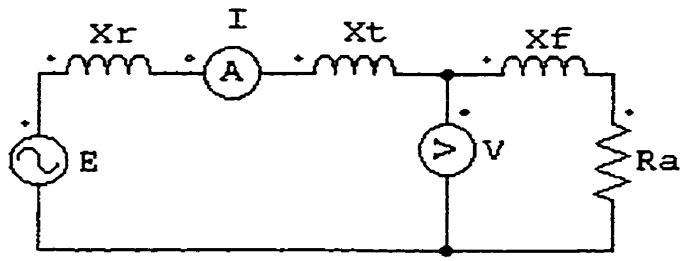

Figure 8.1: Schematic of the EAF single phase circuit model.

8.3.1 Harmonics

The model shown in Figure 8.1 is excited with a set of voltage signals with harmonics. In order to reflect the conditions in the actual EAF, the harmonic components of the voltage signal in the model should approximately match those found in the actual EAF. Samples of the phase voltages and currents at the load side of the EAF are obtain, and a spectral analysis is performed with a fast Fourier transform using Matlab. Figures 8.2 to 8.4 show the diagrams of the power spectral density of the products of each voltage and current harmonic component as a function of the frequency. The fundamental component has been removed from the diagrams to highlight the contribution of higher harmonics.

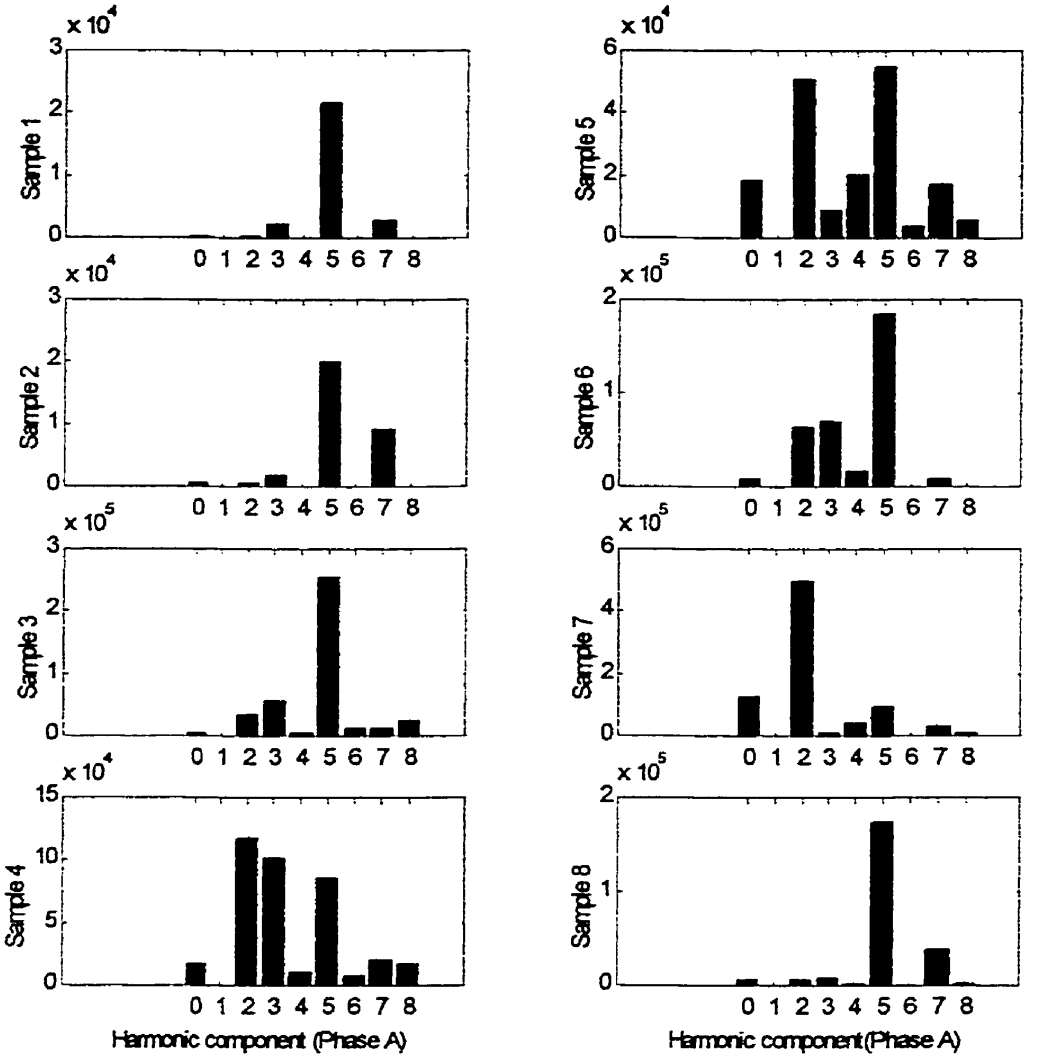

Figure 8.2: Power spectral density of the EAF apparent power for phase A.

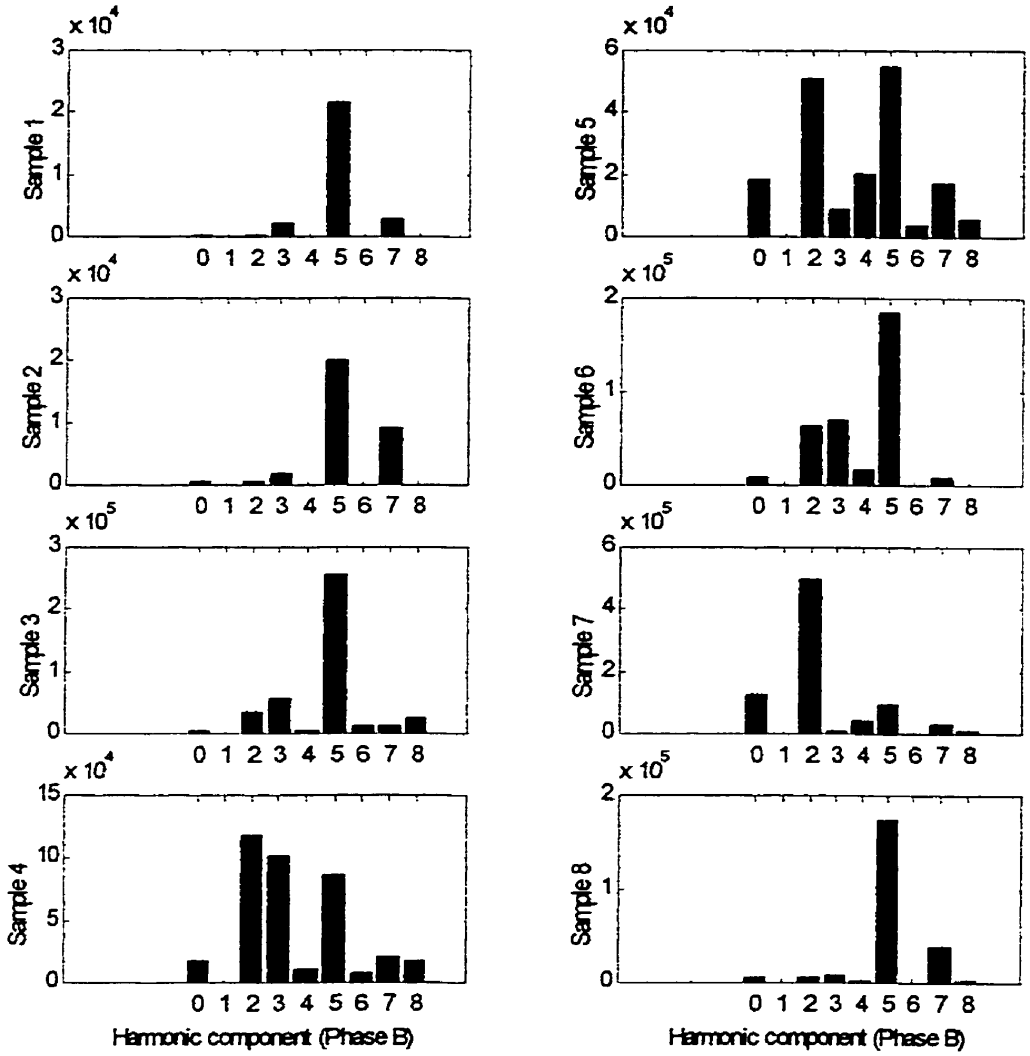

Figure 8.3: Power spectral density of the EAF apparent power for phase B.

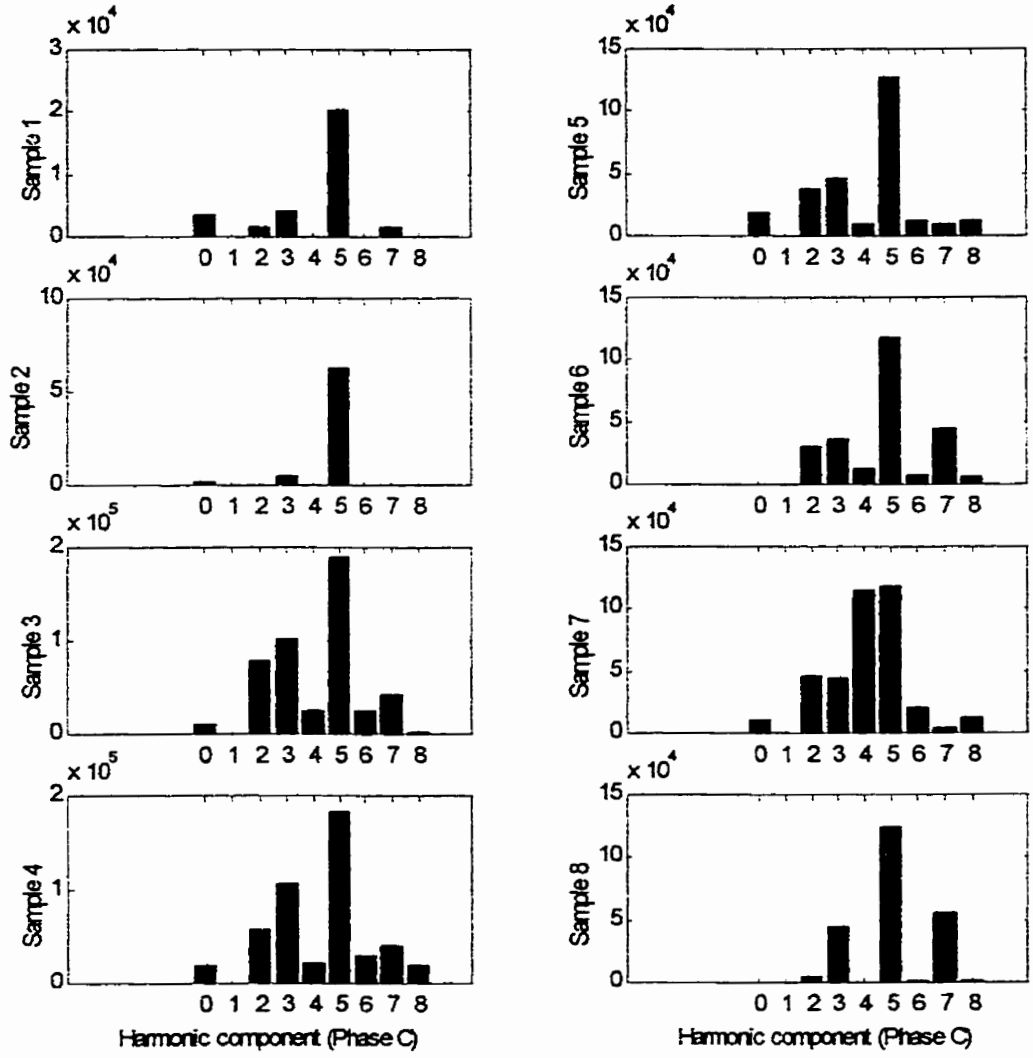

Figure 8.4: Power spectral density of the EAF apparent power for phase C.

From the spectral analysis of the figures shown above, it is clear that the harmonics components present in the sampled signals are the 1st (or fundamental), 3rd, 5th and 7th. There is also a small DC component on the voltage signal.

The tool of choice for the analysis of the harmonic components is the total harmonic distortion (THD). The expression of the THD is given by (see for instance Ramshaw, 1993)

$$THD = \sqrt{\frac{E^2_{rms} - E^2_{1\,rms}}{E^2_{1\,rms}}} \qquad (8.2)$$

The total harmonic distortion (THD) is variable along the test, however it is estimated to be 0.2 pu < THD < 0.7 pu.

8.3.2 Power supply synthesis

The expression of the active power in the presence of harmonic is used to determine which components need to be included in the model of the EAF. The expression of the active power is

$$P = E_1 I_1 \cos\phi_1 + E_3 I_3 \cos\phi_3 + E_5 I_5 \cos\phi_5 + E_7 I_7 \cos\phi_7 + \cdots \qquad (8.3)$$

From Expression (8.3) it is clear that only those components of the same frequency between the voltage and the current make contribution to the average power. Therefore, the power source used for the simulation only supply a voltage with harmonics up to 5th harmonic. From the spectral analysis shown in Figures 8.2, 8.3 and 8.4 it is determined that the 3rd and 5th harmonics have a power spectral density of approximately the same

order of magnitude compared to the fundamental component which make the largest contribution. Then, the simulation is carried out by equally increasing the presence of the 3rd and 5th harmonics from 0 to 1.2 % of the total voltage signal.

8.3.3 Circuit expressions

Finally, the expressions used to complete the circuit model are

$$E_{rms} = \sqrt{\sum_{i=1}^{n} E_{i\,rms}^2} \qquad (8.4)$$

$$I_{rms} = \sqrt{\sum_{i=1}^{n} I_{i\,rms}^2} \qquad (8.5)$$

$$X_i = i\,X_1 \qquad (8.6)$$

$$Zi = \sqrt{R^2 + X_i^{\,2}} \qquad (8.7)$$

$$\cos\phi_i = \frac{R}{Z_i} \qquad (8.8)$$

$$S = \sum_{i=1}^{n} V_i\,I_i \qquad (8.9)$$

$$\cos\phi = \frac{P}{S} \qquad (8.10)$$

with sub-index i indicating the variable associated to the corresponding harmonic component order.

8.3.4 Simulation

For a wide range of arc resistance, the active power P is computed using Expression (8.3). Once the maximum active power is located, the phase angle at the load side of the transformer is recorded. Following, the contribution of the 3rd and 5th harmonics to the voltage signal is increased and a new maximum for the active power P is found. The phase angle is recorded and the simulation proceeds until THD reaches a maximum of 1.2. The results of the phase angles at the load side of the transformer as a function of the total harmonic distortion THD is shown in Figure 8.5. for completeness, the simulation is repeated first, with only the presence of the fundamental and the 5th harmonic and then, with only the presence of the fundamental and the 3rd harmonic. The results are included in Figure 8.5.

From Figure 8.5 it is clear that the traditional optimal operation is only valid at for ideal sinusoidal signals. It also indicates that the order of the harmonic components of the waveforms affect the optimal phase angle.

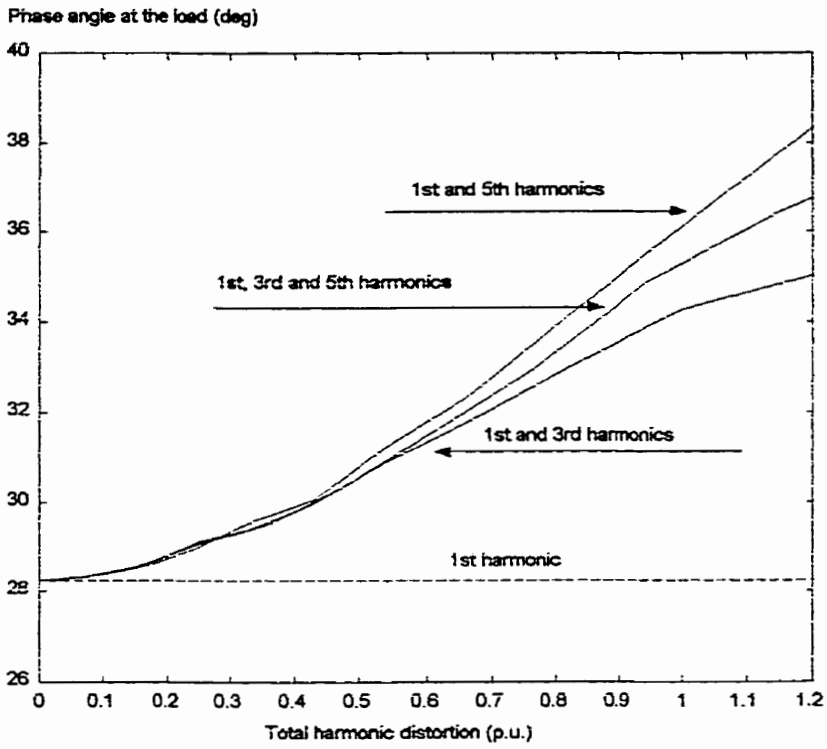

Figure 8.5: Optimal phase angle as a function of the THD.

8.4 Spline functions technique

The spline function technique developed in the previous chapter is now used to determine the EAF optimal operating phase angle.

8.4.1 EAF simulator

The spline technique is first applied to data samples from a single phase simulator of an ideal EAF. This simulator is developed using SIMCAD demo version 4.1a. The circuit model is shown in Figure 8.6.

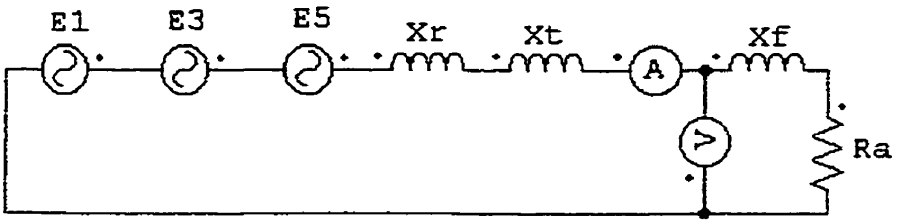

Figure 8.6: Single phase, EAF simulator developed in SIMCAD

Changes of the EAF load are simulated by changing the simulator resistance according to the values given in the following table:

Table 8.3: Variations of the arc resistance

Load	*1*	*2*	*3*	*4*	*5*	*6*	*7*	*8*
Ra (mΩ)	6	7	7.5	8	9	10	11	12

For each load given in Table 8.3, the simulator generates a data file with samples of the phase voltages and currents. The waveforms are reconstructed using the spline technique described in Chapter 7. The number of knots required for the reconstruction of the non-sinusoidal signals depend on their harmonics content. In the previous subsection, it was determined that the harmonic components up to order 5^{th} are significant in the contribution to the active power. Then, according to Shannon's theorem, the number of knots per cycle is set to ten.

8.4.2 Simulation results

8.4.2.1 Optimal phase angle

Once a decision on the number of knots per cycle is made, the proposed spline technique is applied to the sampled data and the optimal phase angle is computed for each load given in Table 8.3. Three different THD are selected for the simulation: 0, 0.5 and 1 p.u. The results are shown in Figures 8.7 to 8.9.

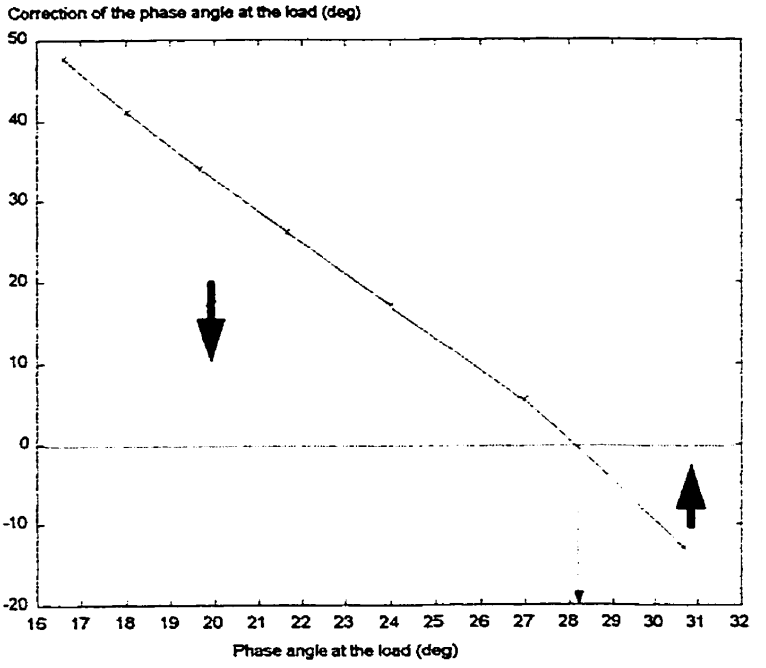

Figure 8.7: Optimal phase angle at the load for THD = 0.

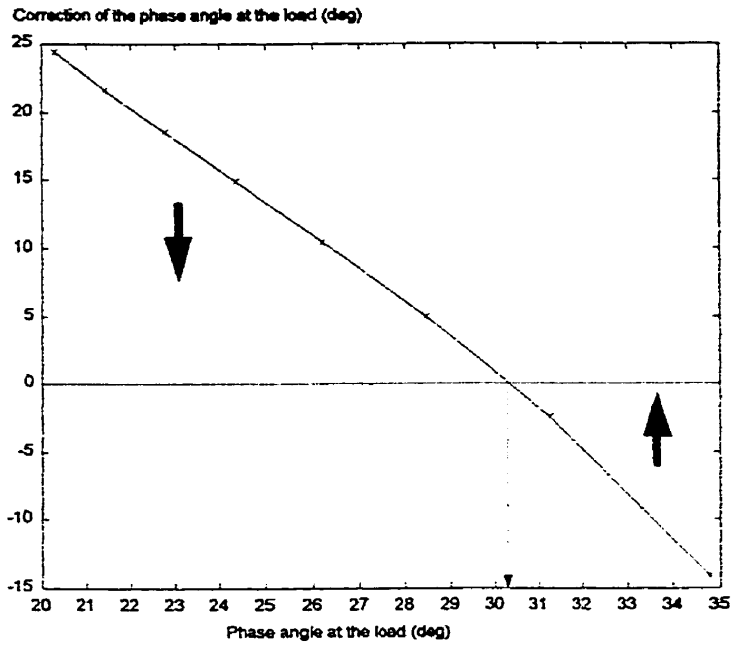

Figure 8.8: Optimal phase angle at the load for THD = 0.5.

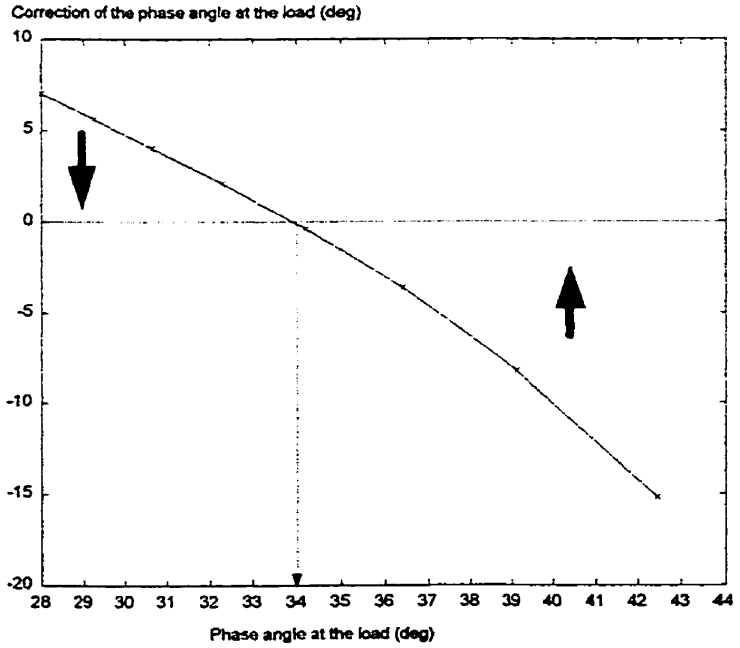

Figure 8.9: Optimal phase angle at the load for THD = 1.

The results obtained from Figures 8.7 to 8.9 are summarized in Table 8.4.

Table 8.4: Optimal phase angles at the load.

THD (pu)	0	0.5	1
ϕ (deg)	28.2	30.5	34

8.4.2.2 Maximum active power

In order to verify the findings summarized in Table 8.4, the active power computed at different phase angles is plotted as shown in Figures 8.10 and 8.11.

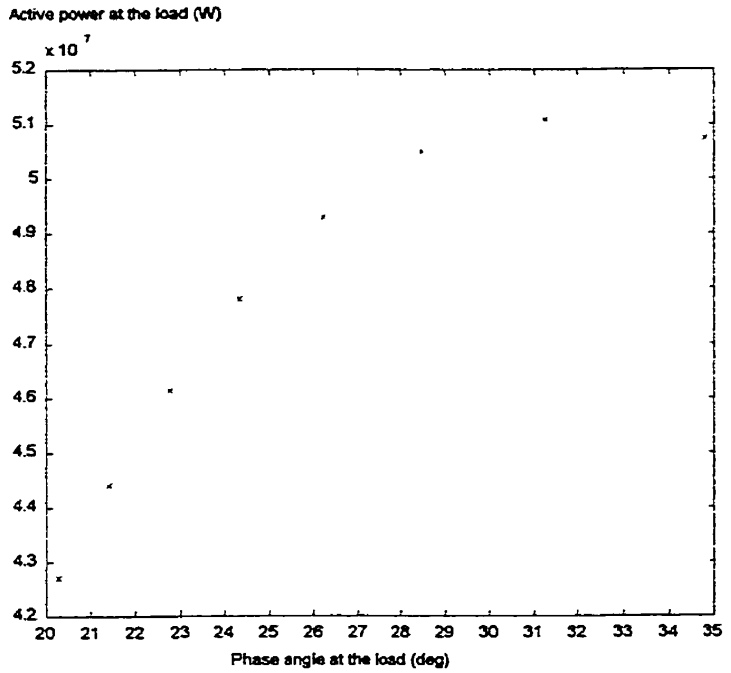

Figure 8.10: Active power at the load for THD = 0.5.

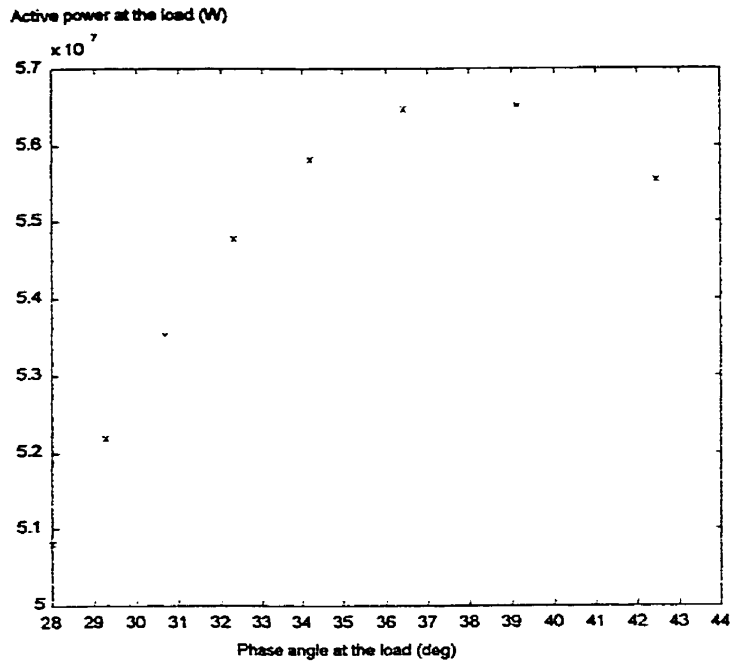

Figure 8.11: Active power at the load for THD = 1.

The analysis of Figure 8.10 and 8.11 reveal that the optimal angles are slightly larger than those obtained from the spline approximation method.

8.4.3 EAF field measurements

The spline function technique is applied to data sampled from the actual EAF. At eight different stages of the melting and refining process, the furnace phase voltages and line currents are measured and recorded. The results given by the spline functions technique for each of the three phases are shown in Figures 8.10 to 8.12.

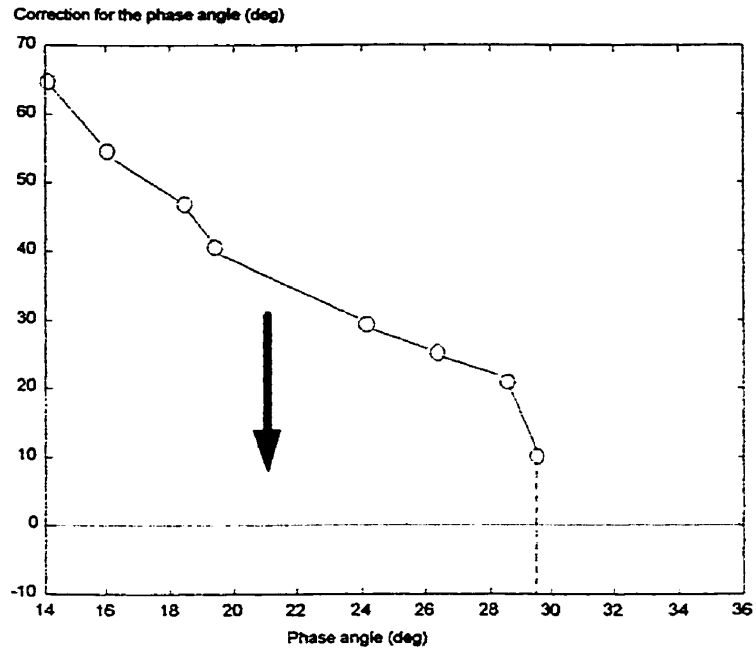

Figure 8.12: Phase A optimal angle at the load of the EAF.

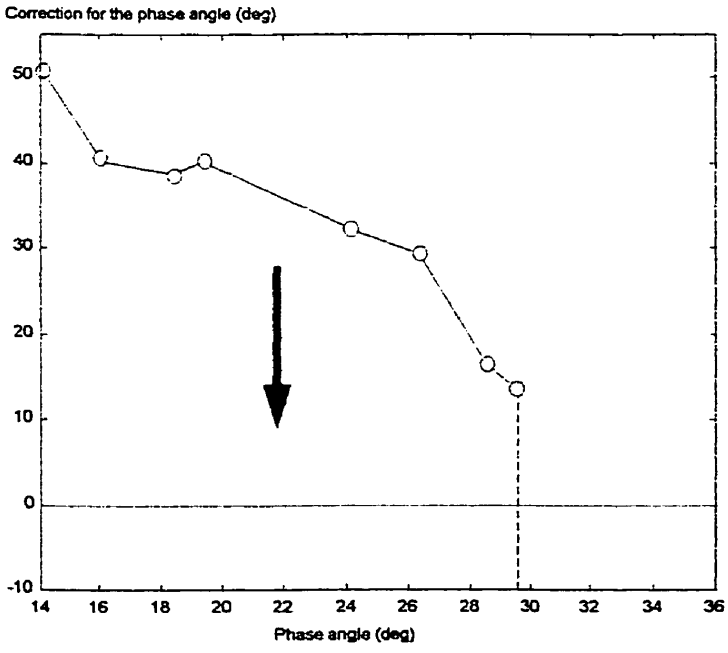

Figure 8.13: Phase B optimal angle at the load of the EAF.

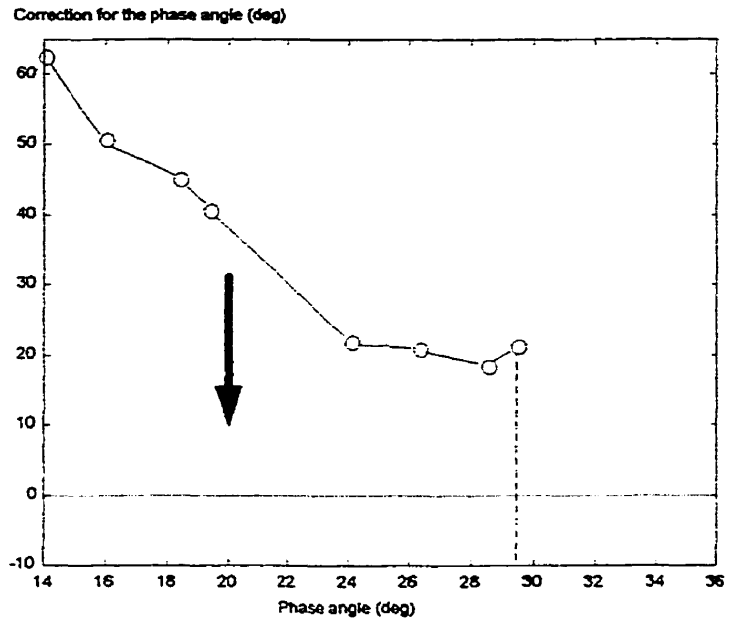

Figure 8.14: Phase C optimal angle at the load of the EAF.

Figures 8.10 to 8.12 show a trend instead of a clear phase angle cross-over point. All three phases have been included to account for discrepancies on the phases parameters. A projection of the trend in any of the three diagrams suggests that the optimal phase angle may be found at a location beyond the 30 degrees.

8.4.3.1 Maximum active power

The active power computed at different phase angles is plotted as shown in Figure 8.15.

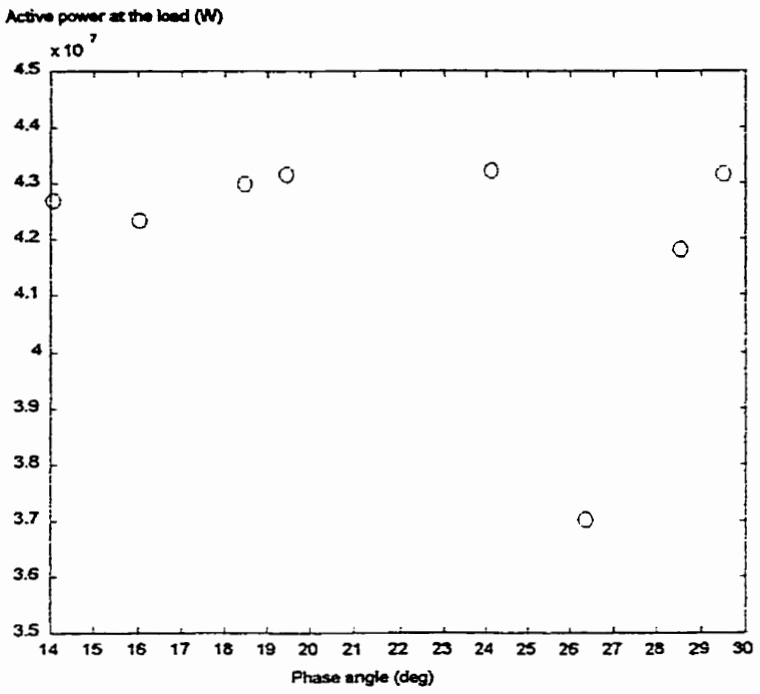

Figure 8.15: Active power at the load of the EAF.

According to Figure 8.15, there is no well defined active power maximum. This may be explained by the fact that the furnace is not operating near a maximum phase angle as shown in Figures 8.12 to 8.14. Another possible source of errors is the fluctuation of the voltage at the PCC. This fluctuation affects the power output of the furnace.

8.5 Instantaneous phasors - spline functions technique

The instantaneous phasors - spline function technique developed in the previous chapter is used to determine the EAF optimal operating phase angle.

8.5.1 EAF Simulator

Similar to the procedure followed for the spline technique, the instantaneous phasors - spline function technique is first applied to data samples from a simulator of an ideal

EAF. The simulator developed using SIMCAD shown in Figure 8.6 is adapted to generate samples for a symmetrical 3 - phase system. Due to the limitation of the number of sources allowed by the program per circuit, the experiment is run in separated program files and the results are merged in a single file.

Changes of the EAF load are simulated by changing the simulator resistance according to the values given in Table 8.3. As opposed to the spline function technique, the Instantaneous phasors - spline functions technique cannot be used for perfectly sinusoidal waveform (THD = 0). The reason behind this limitation is given by the fact that, for THD = 0, the instantaneous phasors for the voltage and the current have a circular trajectory. Therefore, their linear profile is flat. Knowing that the optimization techniques based on spline functions relay on the sensitivity of the active power due to changes in the relative position of the waveform, no improvement can be made in the active power when the profiles are flat.

8.5.2 Simulation results

The results are shown in Figures 8.16 and 8.17 and listed in Table 8.5.

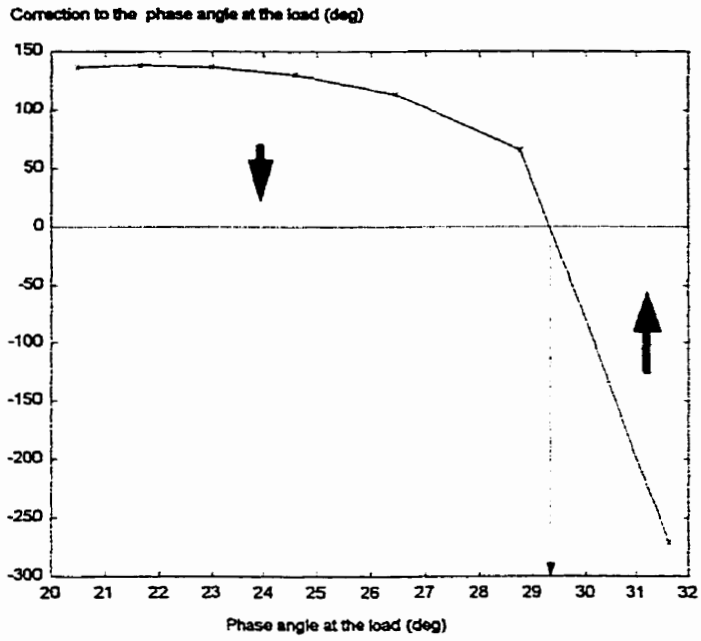

Figure 8.16: Optimal phase angle at the load for THD = 0.5.

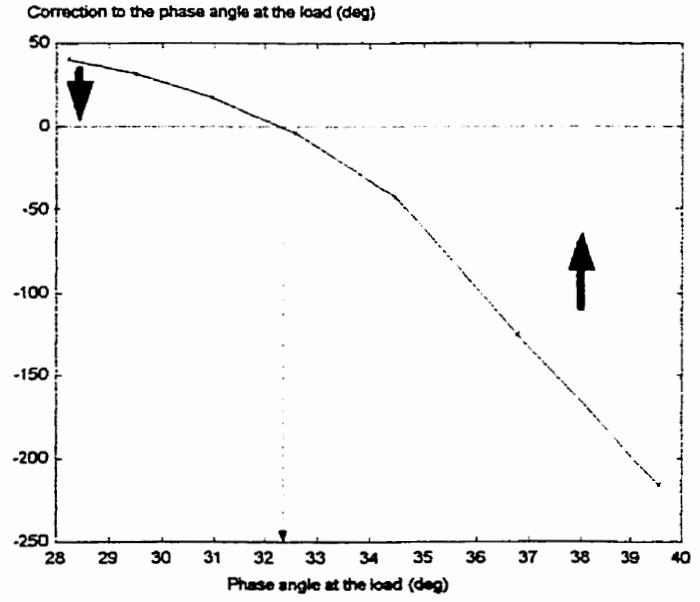

Figure 8.17: Optimal phase angle at the load for THD = 1.

Table 8.5: Optimal phase angles at the load.

THD (pu)	0	0.5	1
ϕ (deg)	---	29.5	32.7

8.5.3 EAF field measurements

The Instantaneous phasors - spline functions technique is applied to data sampled from the actual EAF. The results are shown in Figure 8.18.

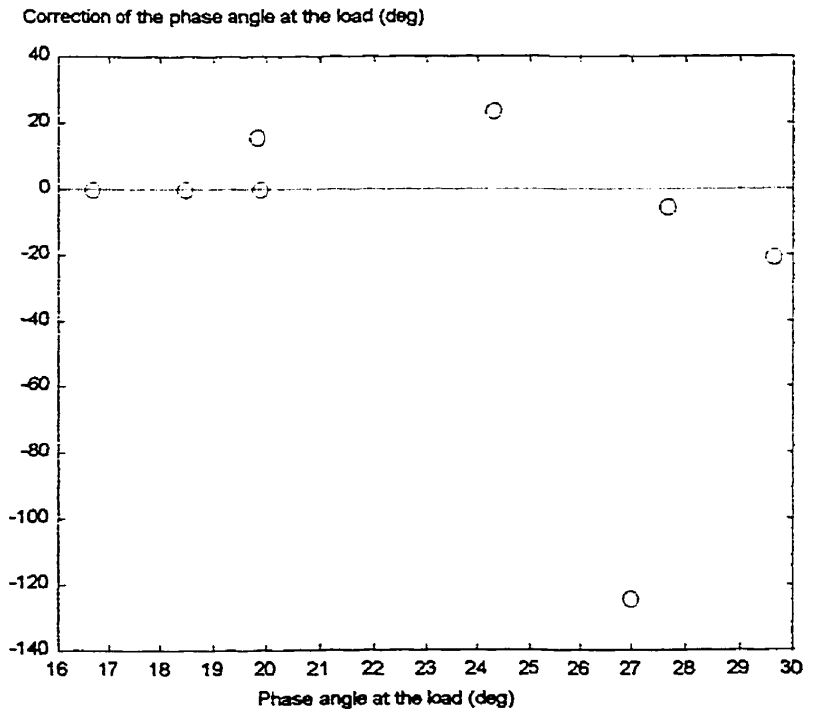

Figure 8.18: Optimal phase angle at the load of the EAF.

The instantaneous phasor - spline function approach failed to show a trend in Figure 8.18, therefore, an optimal operating phase angle cannot be determine when the samples of the actual EAF are used. The poorer performance of the instantaneous phasor - spline function compared to the spline function approach for samples from the EAF may indicate that the method is not recommended for waveforms with high harmonic content. This conclusion agrees with the fact that the instantaneous phasors - spline functions technique performs relatively well in the case of sampled data from the simulator where the number of harmonics is limited. In the presence of DC components and even harmonics, the technique seems to reach a local minimum. Due to the potential benefit of having an alternative technique to validate the results of the spline function technique, further investigation of the performance of the instantaneous phasors - spline functions technique for phase angles closer to the optimal is a topic for future research.

8.6 Summary of test results

Finally, a comparative analysis of the simulations and fields test is made. The following figure shows the results:

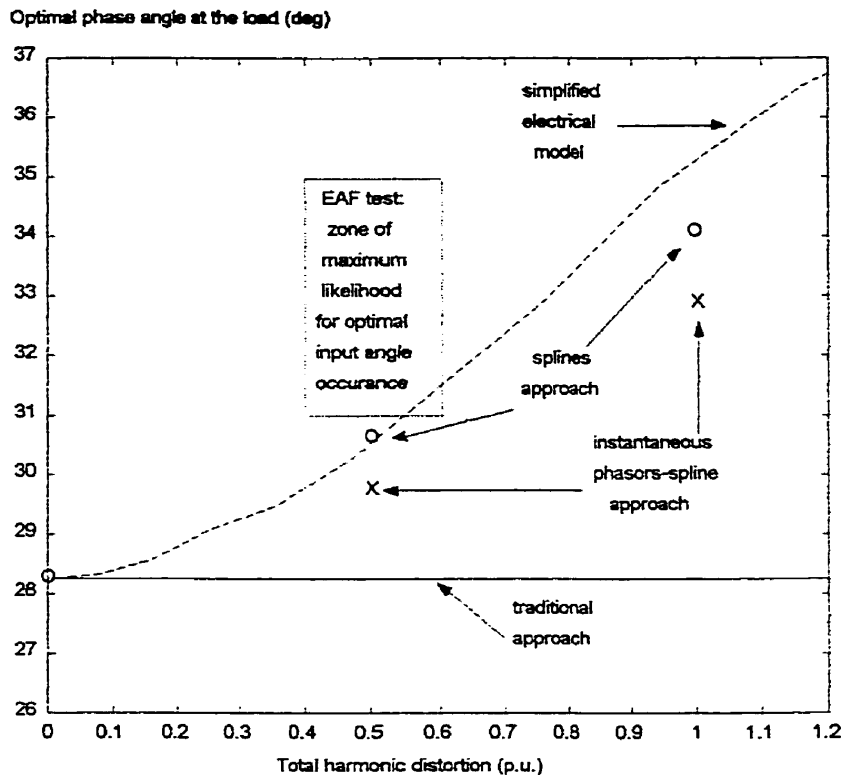

Figure 8.19: Summary of results.

The results displayed in Figure 8.19 show that the circuit theory model and the spline methods give a higher optimal phase angle than the classical techniques used today in industry (sinusoidal waveforms). With low signal distortion, the instantaneous phasors - spline functions method does not perform properly due to the proximity to the ideal sinusoidal case. The spline function technique performs closer to the circuit theory model than the instantaneous phasor - spline function technique for all THD and, in particular, when the distortion becomes higher. The spline technique applied to real field data gives an optimal phase angle higher than the predicted with the approximated electrical model. This discrepancy may be explained by the fact that the electrical model uses a reduced set of harmonic components. As depicted in Figure 8.5, not only the THD determines the

deviation from the ideal sinusoidal case but also the order of the harmonic components. Another cause for errors is the assumption of constant furnace reactance. This reactance of the furnace may change due to load configuration or composition of the bath. Finally, the sensitivity coefficient used in the spline function technique introduces errors that do not vanish when the optimal phase angle is reached.

Chapter 9

9. CONCLUSIONS

In this work, the application of spline and b-spline functions to process modeling and power systems analysis have been studied. In process control, the mathematical representation of nonparametric models allows the application of the well known adaptive control techniques. Splines and b-spline functions are the tools of choice for this task since they are both based on sampled data.

In this thesis, the representation of nonparametric models (NPM) based on the process impulse response is reviewed. The weighing factors are replaced by samples at the knots. The result is a model with reduced dimension called adaptive spline model (ASM). The reduced dimension allows the application of traditional model identification techniques, in particular, the projection algorithm (PA) that is thoroughly used in this work. Simulation of a continuous stirred tank reactor (CSTR) is used to compare the performance of the ASM versus the NPM. The results show the superior prediction performance of the ASM, particularly, in the presence of time variant processes. The ASM is used to update the weighing coefficients of the NPM in a supervisory mode so that the changes on the plant dynamics are incorporated in the model. The weighing coefficients are recovered by the spline transform method at each sample.

The evaluation of model uncertainties is presented in the form of a theorem, following the guidelines of global uncertainties for NPM. The development of the ASM is extended to address the particular case of multirate sampling time control.

The analytical representation of NPM by means of b-splines is also addressed in this work. The resulting model, called adaptive b-spline model (ABM), has a simpler formulation than the ASM with the added advantage of a reduced number of parameters (dimension). An additional advantage resulting from the use of ABM is the simpler formulation of models with deadtime. This is one of the most important features of the ABM due to its unique capability for the identification of deadtime compared to the rest of the NPM used in control systems today. Model uncertainties are evaluated in the same manner as in the case of ASM. The extension of the ABM to multivariable models is also presented in this work. Future research should address the optimal location of the knots as well as their number.

The problem of adaptive controller tuning is also addressed in this thesis. For changes in the process dynamics and in the sampling time, the tuning of the weighting coefficients of the optimal control law have been determined using two interesting methods developed in this work. These methods are based on the controller - plant system equal performance criterion.

For power systems analysis, two methods have been developed in this work: the spline function approximation technique and the instantaneous phasor - spline function hybrid technique. It has been shown that the two techniques have powerful capabilities for power quality monitoring and analysis. The voltages and currents non-sinusoidal waveforms are approximated by means of spline polynomial, resulting in the analytical expressions of the signals. These expressions are used in the computation of active power and power factor. They are also used for the optimization of circuits. The formulation makes use of the sliding knots technique introduced for the first time in this work. The error introduced by the application of the sliding knots technique is evaluated and presented in the form of a

theorem. The theory is applied to data samples from a simulator and an EAF presently in operation. The objective is to evaluate its operation conditions and potential improvements. The results show that the technique is computationally stable, in particular the spline functions method. These results are compatible with those obtained from circuit theory. The application of the analytical techniques presented in this work have shown that the EAF chosen as the test process is operating in sub-optimal conditions, probably due to process constraints. Nevertheless, the method is an attractive tool for the optimization of smaller furnaces which in practice have less constraints and where the presence of harmonics is more pronounced. As shown in this work, the technique can be used for the optimization of EAF in off line mode or, optionally, can be used in an on-line controller. The two methods, the spline function approximation technique and the instantaneous phasor - spline function hybrid technique have given consistent results when the data samples from the simulator are used. The spline function approximation performs closer to the results given by the circuit theory on signals with low harmonics content. The spline functions method is particularly suitable for furnaces with asymmetry among phases because the technique is applied in a per phase basis. The instantaneous phasor - spline function hybrid technique have performed poorly when samples from an EAF are used, therefore, the applicability of the technique is limited. Another limiting factor of the instantaneous phasor - spline function hybrid technique is that the analysis is performed globally for the whole furnace. Therefore, the technique ignores the asymmetries that are present among phases.

9.1 Directions for future research

The theoretical question of how to select the optimal number and location of the knots may be considered as a topic for future research. The optimal number and location of the knots minimizes the errors introduced by the sliding knots technique and, at the same time, minimizes the errors in the approximation by spline functions. As proven in Chapter 3, the sliding knots technique, introduced in this thesis, is a source of errors. These errors are a function of the coefficients of the spline polynomials, specifically, the coefficient associated to the variable of highest degree. Minimizing the sliding knots errors requires the strategic location of the knots. On the other hand, the location of the knots affects the approximation of functions as described by Gaffney and Powell (1976). A trade off should exists such that the overall error is minimized.

As expressed in Chapter 1, this thesis focuses on deterministic dynamical systems. The concepts developed in this work could be extended to stochastic models to include random components defined on some probability space (see for instance Goodwin and Sin, 1984).

Future research in the area of EAF optimization based on spline functions should address the improvement of the sensitivity analysis for the amplitude of the signals with respect to the phase angle. The sensitivity expression is the main sources of errors in the estimation of the optimal operating point. In the proximity of the optimal input phase angle, these errors do not vanish, as in the case of the sliding knots technique. Future research should also include the analysis of the errors when the sensitivity of the amplitude is computed.

As shown in Chapter 8, the instantaneous phasor - spline function approach failed to show a trend in the estimation of the optimal operating input phase angle when samples

from the EAF are used. The poorer performance of this technique compared to the spline function technique can be attributed to the existence of a local minimum. Future research should address the analysis of the performance of this technique when the EAF is operating at input phase angles close to the optimal. The success of the instantaneous phasor - spline function approach is critical given the fact that the technique can be used as a verification tool for the spline function technique.

A more exact electrical model of the EAF is an important topic for future research. By including the resistance of the winding of the transformer, series reactor and connection cables, a more precise optimal can be estimated. The losses of these devises need to be taken into account in order to improve the furnace efficiency.

The analysis of EAFs carried out in this work is limited to AC type furnaces. In recent years, a DC version of the furnace has been introduced. It is expected that the AC to DC conversion generate distortion to the voltage and current waves. Therefore, the concepts developed in this thesis are useful for the optimization of DC type furnaces.

There are important difference to consider when the spline techniques developed in this thesis are applied to the analysis of DC furnaces. The first one is that the three phases in the AC side of the furnace are balanced, therefore, the analysis does not required to be repeated for each phase. On the other hand, the arc resistance needs to be reflected to the AC side of the converter. This may pose a problem because the relationship between the are resistance and the load phase angle is not straight forward as in the case of the AC type of furnace. Therefore, the formulation requires the development of a more complex sensitivity coefficient. Finally, the electrical model of the furnace must include the losses of the transformer core and windings due to the increased distortion of the waveforms.

An important topic for future research is the analysis of the errors introduced by the measurements of the voltage and current signals. There are two main sources of errors: the primary elements and the recording devices. The primary elements are the measuring transformers and sensors. They are classified according to their class (maximum error in ratio and angle shift). This classification, however, is only approximated when signals with distortions are measured. With respect to the recording devices, they impose a delay between channels that translates directly into a delay or shift in the angle between signals. At the same time, these recording devices have a frequency response that must be compensated to obtain more accurate measurements. A thorough analysis of the effect of the signal distortion on the measurements can be found in Boulet *et al.* (1997).

The approximation of signals by spline functions can be applied to the analysis of circuits with nonlinear elements in general. The analysis of the EAF detailed in this thesis can be extended to other electric machines subject to voltage and current waves with distortions.

REFERENCES

Boulet, B., Wikston, J. and Kadar L., 1997, The effects of measuring system accuracy on power quality measuremants in electrical arc furnaces. IEEE Industrial Applications Society Annual Meeting, New Orleans, Louisiana, October 5 - 9.

Camacho, E. F. and Bordoms, C., 1999, *Model predictive control.* Springer-Verlag, London.

Celada, J., 1995, Electric analysis of the low Current, high reactance arc furnace. *Iron and Steel Engineer*, No 11.

Cheney, W. and Kincaid, D., 1994, Approximation by spline functions. In *Numerical Mathematics and Computing*, 3rd ed. Pacific Grove, CA: Brooks/Cole, pp 258-302.

Collantes-Bellido, R. C. and Gómez, T., 1996, Identification and modelling of a three phase arc furnace for voltage disturbance simulation. *IEEE Transactions on Power Delivery*, PE-519-PWRD-0-12.

Cutler, C. R., Hawkins, R. B., 1988, Application of a large predictive multivariable controller to a hydrocracker second stage reactor (oil refining). *Proceedings of the 1988 American Control Conference.*

Cutler C. R., and Ramaker B. L., 1979, Dynamic matrix control: a computer algorithm. *Proceedings of the American Institute of Chemical Engineers 86th National Meeting*, USA.

Gaffney, P. W. and Powell, M. J. D., 1976, Optimal interpolation, *Proceedings of the Dundee Conference on Numerical Analysis*, Springer - Verlag, Heidelberg, Berlin.

Goodwin, G. C. and Sin, K. S., 1984, *Adaptive filtering prediction and control.* Prentice-Hall, Englewood Cliffs, N.J.

Guy, T. V. and Karny, M., 2000, Design of an adaptive controller of LQG type: spline-based approach, *Kybernetika*, Institute of information theory and automation, Czech Republic.

Henderson, M. A. and Seborg, D. E., 1997, *Nonlinear process control*. Prentice Hall.

Isaksson, A. J. and Kaul, V., 1996, Identifying process models when some data are missing. *Pulp and Paper Canada*, vol 8, pp 48-51.

Isermann, R., 1981, *Digital control systems* (Heidelberg , Berlin: Springer-Verlag).

Isermann, R., Lachmann, K. H., and Matko, D., 1992, *Adaptive control systems*. (Prentice Hall International).

Knoop, M. K. F., 1998, Electrical design of high voltage, high reactance AC arc furnaces. *Iron and Steel Engineer*, Vol. 75, No. 3.

Kraus, J. D., 1987, *Electromagnetics*. (Singapore: McGraw-Hill international).

Layt, G. H. G., 1981, The electric arc furnace. *International Iron and Steel Institute*, Brussels.

Mantha, D., 1998, Parsimonious identification of discrete Volterra models using wavelets compression. Master Thesis, Department of Chemical Engineering, University of Houston.

Micchelli, C. A. and Rivlin, T. J., 1976, *Optimal estimation in approximation theory*. (IBM, Yorktown Heights, New York).

Miller,D., 1997, Adaptive control. Lecture notes, Electrical and Computer Engineering, University of Waterloo, Canada.

Morari, M. and Zafiriou, E., 1989, Robust process control. Prentice-Hall, Inc.

Muske, E. S. and Rawlings, J., 1993, Model predictive control with linear models. *AIChE Journal*, 39:262-287.

Nabae, A. and Tanaka, T., 1996, A new definition of instantaneous active-reactive current and power based on instantaneous space vectors on polar co-ordinates in three-phase circuits, *IEEE/PES Winter Meeting*, Paper 96WM227-9 PWRD.

Nikolaou, M. and Vuthandam, P., 1998, FIR model identification: parsimony through kernel compression with wavelets. *AIChE Journal*, 44(1), 141-150.

Ochs, T. L., Hartman, A. D., and Witkowski, S. L., 1986, Waveform analysis of electric furnace arcs as a diagnostic tool. United States Department of Interior, Bureau of Mines Report of Investigations.

Ostrander, L. E., 1971, The Fourier transform of spline-function approximation to continuous data, *IEEE Transactions on audio and electroacustics*.

Owens, D. H., 1986 First-oder models for slow sampled data multivariable systems: an asymptotic analysis. *IEEE Transactions on Automatic Control*, vol AC-31, No 6.

Owens, D. H., 1996, Adaptive stabilisation using variable sampling rate. *International Journal of Control*, **63**, 107-119.

Owens, D. H. and Hong, G. S., 1986, Frequency domain robust stability conditions for multi-rate predictor control schemes. *Proceedings of the 25th conference on Decision and Control*, Athens, Greece.

Owens, D. H. and Wang, L., 1987, Robust adaptive controllers using first order models under slow sampling speed. *Proceedings of the 26th conference on Decision and Control*, Los Angeles, California.

Paul, C. R., Nasar, S. A. and Unnewehr, L. E., 1992, *Introduction to electrical engineering*. Second edition, (USA: McGraw-Hill, Inc.).

Penrose, R., 1956, On best approximate solutions of linear matrix equations, *Cambridge Philos. Soc.*, 52, 17.

Persson, J. and Bliss, N., 1994, The state of the arc in electric furnaces. *Electric Furnace Conference Proceedings*, pp. 211-213, 1994.

Piovoso, M. J., Kosanovich, K. A., Rokhlenko, V. and Guez, A., 1992, A comparison of three nonlinear controller designs applied to a non-adiabatic first-order exothermic reaction in a CSTR. *Proceedings of American Control conference*, pp 490-494, June. Chicago, IL.

Prett, D. M., Garcia, C. E., 1988, Design of robust process controllers. *IFAC*, Selected Papers from the 10th Triennial World Congress.

Prett, D. M., and García, C. E., 1986, Advances in industrial model predictive control. *Chemical Process Control*, Vol. III, Elsevier, New York.

Qin, S. J. and Badgwell, T. A., 1997, An overview of industrial model predictive control technology in chemical process control: an assessment and new directions for research. In *AIChE Symposiums series316, 93.* Jeffery C. Kantor, Carlos E. García and Brice Carnaham Editors.

Ramshaw, R., 1993, Energy processing. Lecture notes, University of Waterloo, Canada.

Redfern, D., 1993, *The Maple Handbook.* Springer-Verlag, New York.

Richalet, J., Rault, A., Testud, J. L., Papon, J., 1978, Model predictive heuristic control: applications to industrial processes. *Automatica*, Vol 14.

Ricker, N. L., Sim, T. and Cheng, C. M., 1986, Predictive control of a multieffect evaporation system. *Proceedings of the 1986 American Control Conference*, Cat. No.86CH2336-6.

Rohal - Ilkiv, B., 1998, One approach to continuous-time predictive control, *2nd IFAC workshop on new trends in design of control systems*, 107-14, Kidlington, UK.

Rouhani, R. K., and Mehra, R. K., 1982, Model algorithmic control (MAC): basic theoretical properties. *Automatica* **18**, 4, 401 - 414.

Sarshar, A., 1996, Analyses of harmonic and transient phenomena due to operation of an AC arc furnace. *Iron and Steel Engineer*, No 4.

Sheen, I. E. and Tsai, J. S. H., 1997, Optimal digital redesign of continuous-time systems with input time delay and/or asynchronous sampling. *Journal of the Franklin Institute*, Elsevier Science Ltd., Great Britain.

Sims, C. E., 1963, *Electric furnace steelmaking.* American Institute of Mining, Metallurgical., and Petroleum Engineers, Iron and Steel Division, Vol II.

Seborg, D. E., Edgard, T. F., and Mellichamp D. A., 1989, *Process dynamics and control.* (John Wiley & Sons).

Stansfield, A., 1914, *The electric arc furnace.* Second edition, McGraw-Hill, New York.

Schumann, R., Lachmann, K. H. and Isermann, R., 1981, Towards applicability of parameter adaptive control algorithms. *IFAC* Control Science and Technology, 8th Triennial World Congress, Kyoto, Japan.

Shumway, R. H. and Stroffer, D. S., 2000, *Time series analysis and its applications.* Springer-Verlag, New York.

Schwave, W. E., 1954, Problems and techniques at A-C furnaces arcs. *Journal of the Electrochemical Society*, v. 101, No. 11, p. 554.

Taub, H. and Schilling, D.L., 1991, *Principles of communication systems.* Second edition, McGraw-Hill, Inc.

Taylor, C. R. and Custer. C. C., 1985, *Electric furnace steelmaking*, AIME, Iron & Steel Society.

Uppal, A., Ray, W., and Poore, A. B., 1974, On the dynamic behaviour of continuous stirred tank reactors. *Chemical Engineering Science*, **29**, 967-985.

Vervacke, J. and Fehn, U., 1994, development of DC-electric arc furnaces with arc control. *Metallurgical Plant and Technology International*, No 4.

Voulgaris, P., 1994, Control of asynchronous sampled data systems. *IEEE Transactions on Automatic Control*, Vol. 39, No. 7.

GLOSSARY

Nomenclature for process control

b	b-spline model
c	prediction correction
Da	Damköhler number
$\boldsymbol{E}$	vector of predicted errors
g	plant impulse response
$\boldsymbol{G}$	matrix of b-spline coefficients
$\boldsymbol{\Gamma}$	augmented matrix of $\boldsymbol{Gs}$
J	performance criterion
k	time step
M	number of knots
n	disturbance signal
N	horizon
$\boldsymbol{R}$	vector of reference trajectory
To	sampling time
$\boldsymbol{\theta}$	model uncertainty
u	plant input (control action)
$\boldsymbol{U}$	vector of plant inputs (control actions)
$\boldsymbol{W}$	weighting coefficient matrix
x	state variable

Nomenclature for process control (cont.)

y	plant output
$\hat{y}$	predicted plant output

Acronyms for process control

ABM	adaptive b-spline model
CSTR	continuously stirred tank reactor
FIR	finite-impulse response
LS	least squares
NDE	non-linear differential equation
NPM	non-parametric model
DMC	dynamic matrix control
MAC	model algorithmic control
MIMO	multiple input - multiple output
PA	projection algorithm

Nomenclature for power systems

A_h	vector of voltage spline coefficients
B_h	vector of current spline coefficients
E	rms value of e
e	instantaneous voltage at PCC
f	frequency
I	rms value of i
i	instantaneous current
$\hat{i}$	current amplitude
I_{phasor}	current instantaneous phasor
M_h	matrix of fixed coefficients
N_h	matrix of fixed coefficients
P	average active power
P_{phasor}	active power phasor
r	phase angle ratio
R_a	arc resistance
S	apparent power
s_p	instantaneous phasor-spline sensitivity coefficient
S_{phasor}	apparent power phasor
s_s	spline sensitivity coefficient
T	waveform period
V	rms value of v

Nomenclature for power systems (cont.)

v	instantaneous voltage at the load
$\hat{v}$	voltage amplitude
V_{phasor}	voltage instantaneous phasor
X	reactance
Z	circuit impedance
α	electrical angle
φ	phase angle shift
Φ	phase angle at PCC
ϕ	phase angle at the load
ω	$2\pi f$

Acronyms for power systems

AC	alternating current
DC	direct current
EAF	electric arc furnace
PCC	point of common coupling
PF	power factor
rms	root mean square
THD	total harmonic distortion